University of Alberta

PENALTY OF HYBRID DIVERSITY IN RAYLEIGH FADING

by

Sasan Haghani ©

A thesis submitted to the Faculty of Graduate Studies and Research in partial fulfillment

of the requirements for the degree of Master of Science

Department of Electrical and Computer Engineering

Edmonton, Alberta

Fall 2002

The author has granted a non-exclusive licence allowing the National Library of Canada to reproduce, loan, distribute or sell copies of this thesis in microform, paper or electronic formats.

The author retains ownership of the copyright in this thesis. Neither the thesis nor substantial extracts from it may be printed or otherwise reproduced without the author's permission.

L'auteur a accordé une licence non exclusive permettant à la Bibliothèque nationale du Canada de reproduire, prêter, distribuer ou vendre des copies de cette thèse sous la forme de microfiche/film, de reproduction sur papier ou sur format électronique.

L'auteur conserve la propriété du droit d'auteur qui protège cette thèse. Ni la thèse ni des extraits substantiels de celle-ci ne doivent être imprimés ou autrement reproduits sans son autorisation.

0-612-81404-1

Canada

University of Alberta

Library Release Form

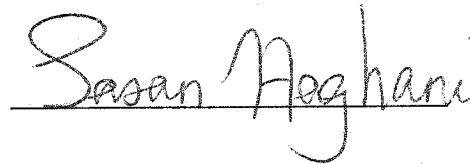**Name of Author:** Sasan Haghani

Title of Thesis: Penalty of Hybrid Diversity in Rayleigh Fading

Degree: Master of Science

Year This Degree Granted: 2002

Permission is hereby granted to the University of Alberta Library to reproduce single copies of this thesis and to lend or sell such copies for private, scholarly or scientific research purposes only.

The author reserves all other publication and other rights in association with the copyright in the thesis, and except as herein before provided, neither the thesis nor any substantial portion thereof may be printed or otherwise reproduced in any material form whatever without the author's prior written permission.
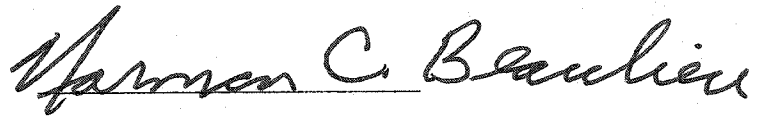
Sasan Haghani

44 Shahzadeh Ebrahim Avenue
Shamsabadi Street
Isfahan, IRAN, 81347

July 29, 2002

University of Alberta

Faculty of Graduate Studies and Research

The undersigned certify that they have read, and recommended to the Faculty of Graduate Studies and Research for acceptance, a thesis titled **Penalty of Hybrid Diversity in Rayleigh Fading** submitted by **Sasan Haghani** in partial fulfillment of the degree of Master of Science.

Dr. Norman C. Beaulieu

Dr. Douglas P. Wiens

Dr. Xiaodai Dong

July 7, 2002

Abstract

The wireless propagation environment is a complex and harsh environment which places fundamental limitations on the performance of mobile communication systems. Multipath propagation in a wireless system causes fading which severely degrades the performance of the system. To mitigate the effect of fading, diversity methods are employed. Linear diversity techniques such as maximal ratio combining (MRC) and selection combining (SC) are employed to reduce the effects of fading in wireless systems. MRC is known to be the optimal linear combining technique, however, the complexity of the MRC receiver is directly proportional to the number of resolvable paths, which might be quite high in some applications. Also MRC is sensitive to channel estimation error especially for the paths with small signal-to-noise ratios (SNR's). Selection combining, on the other hand does not exploit the full amount of diversity offered by the channel. These has given impetus to the study of systems in which only a subset of branches are considered. Hybrid-selection/maximal ratio combining (H-S/MRC) is one such system in which L paths, from the available N paths, having the largest SNR's are selected and combined at each instant of time. Hybrid diversity is thus desirable since it reduces the complexity of the system and also is less sensitive to the channel estimation errors. However, in hybrid diversity a loss or penalty is incurred compared to that of MRC where all the paths are combined. This penalty is defined as the increase in the SNR in a hybrid diversity system to achieve the same target symbol error probability as that of MRC.

In this Thesis, we find bounds to the SNR penalty of H-S/MRC relative to MRC in Rayleigh fading. We show that the bounds are valid for any two-dimensional signalling constellation with polygonal decision regions. We show that the bounds are independent of constellation and the SNR and only depend on L and N. We also find, asymptotes to the SNR penalty of H-S/MRC with *arbitrary* modulation. Using these asymptotes, the symbol error probability (SEP) of H-S/MRC can be approximated using the SEP of MRC to a high degree of accuracy.

Acknowledgments

I would like to express my sincere thanks to my supervisor Dr. Norman Beaulieu for his valuable guidance, encouragement, technical advice and financial support. I would also like to thank my lab mates David, Siva, Julian and Tim for their help on technical issues and documentation.

I am indebted to my parents for their continuous love and moral support. They have been a continuous source of support and encouragement. I always feel the warmth of their love, even now that we are thousands of kilometers apart. Also many thanks to Parisa and Sina for being such a wonderful sister and brother to me. Last but not least, I wish to thank my loving wife, Laleh, whose patience, love and support has made my studies both possible and enjoyable. Her smile has been a continuous source of comfort and happiness to me. This thesis is dedicated to all of them.

Contents

List of Tables

List of Figures

Acronyms

AGC	automatic gain control
AWGN	additive white Gaussian noise
CDMA	code division multiple access
FDMA	frequency division multiple access
GDC	general diversity combining
H-S/MRC	hybrid-selection/maximal ratio combining
ISI	inter symbol interference
MPSK	M-ary phase shift keying
MQAM	M-ary quadrature amplitude modulation
MRC	maximal ratio combining
PDF	probability density function
RV	random variable
SEP	symbol error probability
SC	selection combining
SNR	signal-to-noise ratio
TDMA	time division multiple access

List of Symbols

A_k	The integral defined in (4.43)
a_n	As defined in (4.39)
c_i	Weight of the envelope of the ith diversity branch in a linear combiner or coefficients in an asymptotic expansion
c_{MQAM}	A coefficient defined in the SEP of MQAM in AWGN.
$c_{n,\text{MRC}}$	The coefficients of the asymptotic expansion of SEP of MRC with two-dimensional signaling
$c_{n,\text{H-S/MRC}}$	The coefficients of the asymptotic expansion of the SEP of H-S/MRC with two-dimensional signaling
$E_0 C_n$	Real amplitude of the nth wave of the electrical field
E_s	Average received signal energy per symbol
E_z	The electrical field
$\mathbb{E}[\cdot]$	Expectation operation
$e_i(t), i = 1, 2$	Orthonormal functions
erfc(x)	The complementary error function
f_c	Carrier frequency
$f_{\mathbf{n}}(n_1, n_2)$	The bivariate pdf of Gaussian noise in Cartesian coordinates
$f_{\mathbf{n}}(r, \theta)$	The bivariate pdf of Gaussian noise in polar coordinates
$f_{X_{(1)},\cdots,X_{(n)}}(x_1,\cdots,x_n)$	The joint pdf of the order statistic $X_{(1)},\cdots,X_{(n)}$

G_k	The integral defined in (4.41)
$g_k(\theta)$	As defined in (2.17b)
$I_1(x1,\cdots,x_N)$	The multidimensional integral defined in (B.21)
$I_2(x1,\cdots,x_N)$	The multidimensional integral defined in (B.22)
$I_3(x1,\cdots,x_N)$	The multidimensional integral defined in (B.30)
$(i_1,\cdots,i_n$	Any permutation of $(1,\cdots,n)$
J	The Jacobian matrix of a transformation
J_π	The set defined in (4.5a)
$\bar{J}_\pi$	The set defined in (4.5b)
K_i	The total number of erroneous subregions given symbol s_i is transmitted
K	The total nyumber of erroneous subregions for all the signal points in the constellation
L	Number of selected diversity branches in hybrid diversity
M	Number of signals in a modulation format
m_i	The ith transmitted message
N	Total number of diversity branches
N_0	One-sided power spectral density of white Gaussian noise
N_{tot}	Total noise power in N diversity branches
N_i	One-sided noise power spectral density of the ith diversity branch
$\mathbf{n_i} = (n_{i1}, n_{i2})$	The vector representation of noise in two-dimensional signalling
$P(C)$	The probability of correct decision
$P(m_i)$	The a priori probability that message m_i is transmitted
$P(C|m_i)$	The conditional probability that the ith message was transmitted
$P(C|s_i)$	The conditional probability that the ith signal was transmitted

$P_{s_{i,j}}$	The probability of error that transmitted signal s_i falls in subregion j
$P_{e,\text{AWGN}}$	Probability of two-dimensional signalling in AWGN channel
$Pr(e\|x)$	The probability of error conditioned on x
$P_{e,\text{AWGN}}^{\text{MPSK}}$	Probability of MPSK in AWGN channel
$P_{e,\text{AWGN}}^{\text{MQAM}}$	Probability of MQAM in AWGN channel
$P_{e,\text{AWGN}}^{\text{16-star QAM}}$	Probability of 16-star QAM in AWGN channel
$P_{e,\text{AWGN}}^{M\text{-orth}}$	Probability of M-ary orthogonal signalling in AWGN channels
$P_{e,\text{AWGN}}^{M\text{-biorth}}$	Probability of M-ary biorthogonal signalling in AWGN channels
$P_{e,\text{AWGN}}^{3\text{-orth}}$	SEP of 3-ary orthogonal signalling in AWGN channel
$P_{e,\text{AWGN}}^{4\text{-orth}}$	SEP of 4-ary orthogonal signalling in AWGN channel
$P_{e,\text{AWGN}}^{6\text{-biorth}}$	SEP of 6-ary biorthogonal signalling in AWGN channel
$P_{e,\text{AWGN}}^{8\text{-biorth}}$	SEP of 8-ary biorthogonal signalling in AWGN channel
$P_{e,\text{GDC}}$	SEP of GDC in Rayleigh Fading
$P_{e,\text{GDC}}^{3\text{-orth}}$	SEP of GDC with 3-ary orthogonal signalling
$P_{e,\text{GDC}}^{4\text{-orth}}$	SEP of GDC with 4-ary orthogonal signalling
$P_{e,\text{GDC}}^{6\text{-biorth}}$	SEP of GDC with 6-ary biorthogonal signalling
$P_{e,\text{GDC}}^{8\text{-biorth}}$	SEP of GDC with 8-ary biorthogonal signalling
$P_{e,\text{asy}}^{\text{GDC}}$	Asymptotic SEP of GDC in Rayleigh Fading
$P_{e,\text{H-S/MRC}}$	SEP of H-S/MRC in Rayleigh Fading
$P_{e,\text{H-S/MRC}}^{-1}$	The inverse H-S/MRC SEP function
$P_{e,\text{asy}}^{\text{H-S/MRC}}$	Asymptotic SEP of H-S/MRC in Rayleigh Fading
$P_{e,\text{MRC}}$	SEP of MRC in Rayleigh Fading
$P_{e,\text{asy}}^{\text{MRC}}$	Asymptotic SEP of MRC in Rayleigh Fading
$P_{e,\text{SC}}$	SEP of SC in Rayleigh Fading
$\mathbb{P}(x)$	Probability of event x

$P_k(\Gamma)$	The integral defined in (4.38)
p	The probability that a single sample is below a threshold
$\mathbf{p} = \{p_1, p_2, \cdots, p_N\}$	A probability vector
$p(r)$	pdf of the received signal, r
$p(t)$	Any pulse shape such as the Nyquist pulse
$p_{\mathbf{X}}$	The joint pdf of the vector $\mathbf{X}$
$Q(x)$	Gaussian tail integral
q_i	Weight of the ith diversity branch in GDC or as defined in (4.38)
$R(\theta)$	As defined in Eqn. (2.13)
r	The envelope of the transmitted signal
$r_i(t)$	The envelope of the ith received faded signal
$\mathbf{r_i} = (r_1, r_2)$	The vector representation of the ith received signal in two-dimensional signalling
r_{MRC}	The envelope of the received signal at the output of MRC
s_i	The ith transmitted signal
$\mathbf{s_i} = (s_{i1}, s_{i2})$	The vector representation of the ith transmitted signal in two-dimensional signalling
$T_c(t)$	In-phase component of the electrical field
$T_s(t)$	Quadrature component of the electrical field
T_s	Time duration of the transmission of a symbol
T_0	Coherence time of the channel
$t_i, i = 1, \cdots, 4$	Parameters to evaluate the SEP of 16-star QAM in AWGN.
$V_i, i = 1, \cdots, N$	The set of virtual branches
v	Velocity of a mobile station
w_k	a priori probability of the symbol to which subregion k corresponds.

w_n	Doppler shift
x'	Distance shown in Figure 2.1
$\mathbf{x} = \{x_1, x_2, \cdots, x_N\}$	A vector with non-negative elements
$\mathbf{y} = \{y_1, y_2, \cdots, y_N\}$	A vector with non-negative elements
$y(t)$	The output of the linear combiner
$y_i(t)$	The envelope of the ith diversity branch
$\mathfrak{A}(\mathbf{x}, \mathbf{y})$	The arithmetic mean of $\mathbf{x}$ and $\mathbf{p}$
$\mathfrak{G}(\mathbf{x}, \mathbf{p})$	The geometric mean of $\mathbf{x}$ and $\mathbf{p}$
α_n	Azimuthal angle of arrival of the nth wave
β	SNR penalty
β_L	Lower Bound to the SNR penalty
β_U	Upper Bound to the SNR penalty
β_L^A	Asymptotic SNR penalty for small SNR
β_U^A	Asymptotic SNR penalty for large SNR
Γ_i	The average SNR of the ith diversity branch
Γ	The average SNR in any diversity branch
γ	instantaneous signal-to-noise ratio
γ_i	The instantaneous SNR of the ith diversity branch
γ_{GDC}	The instantaneous SNR of GDC
$\gamma_{H\text{-}S/MRC}$	The instantaneous SNR of H-S/MRC
γ_{MRC}	The instantaneous SNR of MRC
γ_{SC}	The instantaneous SNR of SC
$\{\gamma_{[1]}, \cdots, \gamma_{[N]}\}$	The set of ordered diversity branches
λ	Ring ratio for a circular signal constellation or the wavelength of the carrier frequency

ϕ_n	Random phase in the nth wave
$\theta_i, i = 1, 2$	Integration variables
σ	Variance of the in-phase and quadrature components of the electrical field
δ	Integration variable
ρ	Integration variable

Chapter 1

Introduction

1.1 Radio Propagation Environment

The wireless propagation environment is a complex and harsh environment since it is not fixed and changes continuously. This places fundamental limitations on the performances of mobile communication systems. The transmission paths between the transmitter and the receiver can vary from simple line-of-sights to ones that are severely obstructed by buildings, mountains and foliage.

The transmission in a radio propagation environment is subjected to many sources of degradation. Some are fading, shadowing and co-channel interference. Fading is due to multipath propagation, when the transmitted signal reaches the mobile receiver through different paths. Shadowing occurs because of the topographical variations that happen along the transmission path. Finally, co-channel interference is due to frequency reuse in communication systems which increases the spectrum efficiency of these systems.

Many methods such as diversity, equalization and spread spectrum techniques have been proposed in the literature to overcome the effects of fading, shadowing and co-channel interference. Among these methods, diversity combining has a great potential to overcome

the effects of fading since it is achieved with no increase in the transmission power or bandwidth. However, the system complexity will increase.

1.2 Fading Channels

When a steady-state, single-frequency, radio wave is transmitted over a long path, the envelope amplitude of the received signal is observed to fluctuate in time. This phenomenon is known as fading [1] and its existence constitutes one of the limitations of mobile communication design. Fading channels can be categorized as fast fading or slow fading channels [2]- [6]. The terminology fast fading is used to describe channels in which the channel coherence time, T_0, is less than the time duration of a transmission symbol, T_s. The coherence time is a measure of the expected time duration over which the channels response is essentially invariant [2]. In fast fading channels $T_0 < T_s$, and the time in which the channel behaves in a correlated manner is shorter than the time duration of the symbol. So it can be expected that the fading characteristics of the channel will change several times within the duration of one symbol transmission. In contrast under slow fading $T_0 > T_s$, and so the channel state will virtually remain unchanged during the time in which the symbol is transmitted.

Another categorization of fading channels is large scale and small scale fading [2]-[6]. Large scale fading represents the average signal power attenuation or path loss due to motion of the signal over large areas. The statistics of large-scale fading provide a way of comparing an estimate of the path loss as a function of distance, where path loss is defined as the received power expressed in the terms of transmitted power. Small scale fading refers to dramatic changes in signal amplitude and phase that can be experienced as a result of small changes (as small as one-half wavelength) in the spatial separation between the

2

receiver and the transmitter. Small scale fading is further categorized as frequency selective and frequency non-selective fading.

1.2.1 Frequency Non-Selective Fading Channels

The fading is frequency non-selective if all the frequencies are affected in the same manner. This kind of fading occurs in narrow-band systems where the transmission bandwidth is usually less than the coherence bandwidth [4]. Coherence bandwidth is defined as the range of frequencies over which the fading effect introduced by the channel is highly correlated [3]. In other words, the coherence bandwidth represents a range of frequency over which the channel passes all spectral components with approximately equal gain and linear phase. In a frequency non-selective channel the phase and the amplitude of the signal are affected. For the envelope of the transmitted signal many different distribution models have been proposed in the literature. The most well known distributions are the Rayleigh, Ricean and Nakagami-m distributions. In this thesis, we will focus on the Rayleigh distribution. In Rayleigh fading the phase is usually assumed to have a uniform distribution in $[0, 2\pi)$.

The amplitude variation of a signal transmitted over a mobile radio propagation path when the mobile moves from one location to another has been recorded by many workers. These measurements show that the envelope of the mobile signal is Rayleigh distributed for a wide range of frequencies from 50Hz to 11,200 MHz [7]. These measurements are carried out over distances of a few tens of wavelengths when the mean signal is almost constant. Based on these measurements, Gans [8], suggested that at any instant of time the received signal envelope is made up of a number of horizontally plane waves with random amplitudes and angles of arrival. The phases of these waves are assumed to be uniformly distributed in $[0, 2\pi)$ and also are assumed to be independent. Because the receiver is a

3

mobile, a Doppler shift is introduced in every wave as [7]

$$w_n = \frac{2\pi}{\lambda} v \cos(\alpha_n) \qquad (1.1)$$

where λ is the wavelength of the carrier frequency, v is the speed of the mobile and α_n is the azimuthal angle of arrival. Assuming field components are vertically polarized the electrical field component can be expressed as

$$E_z = E_0 \sum_{n=1}^{N} C_n \cos\left((w_c + w_n)t + \phi_n\right) \qquad (1.2)$$

where $E_0 C_n$ is the amplitude of the nth wave of the E_z field, and ϕ_n is a random phase angle which is uniformly distributed in $[0, 2\pi)$. Rice has showed that the electrical field, E_z, can be expressed as [9]

$$E_z = T_c(t) \cos(w_c t) - T_s(t) \sin(w_c t) \qquad (1.3)$$

where

$$T_c(t) = E_0 \sum_{n=1}^{N} C_n \cos(w_n t + \phi_n) \qquad (1.4a)$$

$$T_s(t) = E_0 \sum_{n=1}^{N} C_n \sin(w_n t + \phi_n) \qquad (1.4b)$$

are the in-phase and the quadrature components of the electrical field, respectively. As a consequence of the central limit theorem, $T_c(t)$ and $T_s(t)$ can be considered as Gaussian random processes with zero means and equal variances, for large values of N. Since $T_c(t)$ and $T_s(t)$ are Gaussian processes, at any given time t, the probability density function (pdf) of the random variables (rv's) T_c and T_s can be written as

$$p(x) = \frac{1}{\sqrt{2\pi}\sigma} e^{-\frac{x^2}{2\sigma^2}} \qquad (1.5)$$

where $x = T_c$ or $x = T_s$ and $\sigma = \frac{E_0^2}{2}$. Further more $T_c(t)$ and $T_s(t)$ are uncorrelated [7] and hence, they are independent. The envelope of the transmitted signal in terms of T_c and T_s is

4

given by

$$r = \sqrt{T_c^2 + T_s^2}.$$ (1.6)

It is shown in [9] that the PDF r is

$$p(r) = \begin{cases} \frac{r}{\sigma} e^{-\frac{r^2}{2\sigma}} & , \quad r \geq 0 \\ 0 & , \quad r < 0, \end{cases}$$ (1.7)

which is a Rayleigh pdf.

1.2.2 Frequency Selective Fading Channels

In frequency selective fading, as the name suggests, the frequency components of the transmitted signal are not treated equally by the channel. Frequency selective fading is found in wide-band systems where the bandwidth is greater than the coherence bandwidth. One of the consequences of frequency selective channels is the time dispersion in the transmitted signal which limits the system performance by causing inter symbol interference (ISI) in the detection process.

1.3 Diversity Methods

In general, the term diversity refers to a system in which one has available two or more closely similar copies of the desired signal [1]. The basic idea underlying diversity is to obtain two or more samples of the incoming signal which have low, ideally zero, cross-correlation [5]. If the N diversity branches are independent, then it follows from elementary statistics that the probability of all of them having signal-to-noise ratio (SNR) below a certain level is p^N, where p is the probability that a single sample is below the threshold value. Therefore, using diversity methods, one can increase the reliability of the communication

system. There are many methods by which diversity can be achieved [4]. Some are angle, polarization, field, time, frequency and space. These methods are introduced briefly below.

Angle diversity, also known as directional diversity, is implemented using directional antennas. Polarization diversity exploits the fact that in normal ionospheric transmission at frequencies of a few megahertz, the received signal includes both horizontally and vertically polarized components which undergo approximately independent fading. Field diversity uses the fact that the electrical and magnetic field are uncorrelated at any receiving point. Polarization and field diversity methods have their difficulties because depolarization is not always available along the transmission path and design of antennas suitable for field diversity is difficult. Time diversity is achieved by sending the same data after a suitable time interval which has attractions in digital systems where storage facilities exist. Examples of time diversity are automatic repeat request systems which have been available in conventional radio mobile systems for some years [5]. In frequency diversity the data is transmitted on two or more carrier frequencies. It is however, space diversity, also known as antenna diversity, which seems by far the most attractive diversity method. For mobile communication systems, space diversity is achieved by using multiple transmit and receive antennas. Space diversity uses the fact that signals received from spatially separated antennas on the mobile would have essentially uncorrelated envelopes for antenna separations of one-half wavelength or more.

In the sequel, we will focus on linear diversity combining techniques. In these methods, the various signal inputs are weighted individually and then summed. If the addition takes place after the detection of the individual branches, the system is called a post-detection combiner. If the addition is performed before the detection process, the system is called

a predetection combiner. For coherent modulations, both systems have identical performances. The output of a linear combiner consisting of N diversity branches is given by [5]

$$y(t) = \sum_{i=1}^{N} c_i y_i(t) \tag{1.8}$$

where $y_i(t)$ is the envelope of the ith signal to which a weight c_i is applied and can be expressed as

$$y_i(t) = r_i(t)e^{j\theta_i(t)} + n_i(t). \tag{1.9}$$

In (1.9), $r_i(t)$ is the envelope of the ith received faded signal, $n_i(t)$ is an additive white Gaussian noise and $\theta_i(t)$ is a random phase. We further assume that the noise in each branch is independent of the signal and independent of the noises in other branches.

1.3.1 Maximal Ratio Combining

In maximal ratio combining (MRC), first proposed by Kahn [10], the signals from N branches are weighted proportionally to their signal-amplitude-to-noise-power ratios (SNR's), co-phased and then summed. Brennan [1] has proved that MRC is the optimum linear combiner.

Assuming that co-phasing has been performed, the envelope of the combined signal, at each instant of time, can be written as

$$r_{MRC} = \sum_{i=1}^{N} c_i r_i \tag{1.10a}$$

$$c_i = r_i/N_i \tag{1.10b}$$

where r_i is the envelope of the ith received faded signal and N_i is the average noise power in the ith branch. Assuming the average noise powers are equal in all N branches, the total noise power can be expressed as

$$N_{tot} = N \sum_{i=1}^{N} c_i^2. \tag{1.11}$$

Hence, the SNR of MRC is

$$\gamma_{MRC} = \frac{r_{MRC}^2}{N_{tot}} \qquad (1.12)$$

which can be simplified as [7]

$$\gamma_{MRC} = \sum_{i=1}^{N} \gamma_i \qquad (1.13)$$

where γ_i is the instantaneous SNR of the ith diversity branch.

1.3.2 Selection Combining

In selection combining (SC) the input having the largest SNR among N possible branches is connected to the output [7]. The output SNR of SC can be expressed as

$$\gamma_{SC} \triangleq \max_i \{\gamma_i\} = \gamma_{(1)} \qquad (1.14)$$

where $\{\gamma_{(1)}, \cdots, \gamma_{(N)}\}$ are the ordered diversity branches, i.e., $\gamma_{(1)} > \cdots > \gamma_{(N)}$.

1.3.3 Hybrid-Selection/Maximal Ratio Combining

Although MRC is known as the optimum linear combining technique [1], it may not be cost efficient in some systems, because the receiver complexity is directly proportional to the number of resolvable paths, N. This is an undesirable feature from operation and implementation points of view because N may vary with location and time. This imposes a limitation on the number of rays which can be processed; so in practical implementations of the RAKE receiver, only a subset of rays will be considered. Typically, a RAKE receiver will select, at each instant of time, L rays with the maximum instantaneous SNR's among the available N paths and performs MRC [11]. This is known as hybrid-selection/maximal ratio combining (H-S/MRC). The instantaneous output SNR of H-S/MRC can be written as [12]

$$\gamma_{H\text{-}S/MRC} = \sum_{i=1}^{L} \gamma_{(i)} \qquad (1.15)$$

8

1.3.4 General Diversity Combining System

To analyze the performance of MRC, SC and H-S/MRC using a unified approach, a general diversity combining (GDC) technique is introduced in [12] with the instantaneous output SNR of the form

$$\gamma_{GDC} = \sum_{i=1}^{N} q_i \gamma_{(i)} \tag{1.16}$$

where $q_i \in \{0, 1\}$. Note that MRC, SC and H-S/MRC are all special cases of the GDC system defined above. The output SNR of the SC can be obtained from (1.16) by substituting $q_1 = 1$ and $q_i = 0, i = 2, \cdots, N$. Setting $a_i = 1$, for all $i = 1, \cdots, N$ in (1.16) yields the output SNR for MRC. For H-S/MRC where L branches are selected out of maximum N branches, $q_i = 1$ for $i = 1, \cdots, L$ and $q_i = 0$ for $i = L + 1, \cdots, N$.

1.4 Thesis Outline and Contributions

In Chapter 2 we calculate the symbol error probability (SEP) of coherent modulation of two-dimensional signalling in additive white Gaussian noise (AWGN) channels, using Craig's approach [13]. Craig's formula for the SEP of two-dimensional signalling is expressed as a weighted summation of single integrals with finite integration intervals and elementary function integrands. We also present new analytical expressions for a class of orthogonal signaling in AWGN channels, derived by Dong and Beaulieu [14], by extending Craig's method to higher dimension modulations.

A general expression for the SEP of GDC in Rayleigh fading is derived in Chapter 3. Using this expression, the SEP of GDC is derived for arbitrary two-dimensional modulations with polygonal decision regions in Rayleigh fading. The SEP expression is expressed as a weighted summation of single integrals with finite limits. Previously, only results for M-ary phase shift keying (MPSK) and M-ary quadrature amplitude modulation (MQAM)

9

were available [12]. Next, the SEP of SC, MRC and H-S/MRC are derived from the SEP of GDC for two-dimensional signalling constellations. Finally, the SEP of GDC with classes of orthogonal signalling is derived using the results in Chapter 2.

In H-S/MRC only a subset of available paths are combined. This incurs a loss or penalty compared to MRC where all the N paths are combined. In Chapter 4, we define the penalty of H-S/MRC with respect to MRC and derive simple lower and upper bounds to the SEP of hybrid diversity with two-dimensional signalling in Rayleigh fading. Previously, only results for MPSK were available [15]. The bounds are simple closed-form expressions and are valid for arbitrary SNR. We will show that the analytical expressions for the bounds are only dependent on L and N, and are independent of the two-dimensional modulation format used. We also derive asymptotic SNR penalties of H-S/MRC for small and large values of SNR for any two-dimensional signalling constellation with polygonal decision regions.

In Chapter 5, we establish that the asymptotic SNR penalties of H-S/MRC relative to MRC exist for *arbitrary* modulations. Analytical expressions for the asymptotes are derived in closed-form. The results in this chapter generalize and confirm the results in Chapter 4. Based on several examples, we also conjecture that the penalty bounds valid for two-dimensional signalling with polygonal decision regions are also valid for other modulation formats.

Finally, the conclusions and a summary of the Thesis are given in Chapter 6.

Chapter 2

Symbol Error Probability of Two-Dimensional and Orthogonal Signalling in AWGN Channels

In this chapter, we elaborate Craig's method for computing the SEP of two-dimensional signalling constellations in AWGN channels. Craig's method can be applied to any two-dimensional signalling sets whose decision region boundaries are polygons surrounding each of the signal points in the constellation. The symbol error probability is expressed as a weighted summation of single integrals with finite limits and the integrands are exponentials of elementary trigonometric functions.

New expression for the SEP of classes of orthogonal signalling are also presented. The new expressions were derived by Dong and Beaulieu by extending Craig's method to M-ary constellations. In the new expressions, the SEP of 3-ary and 4-ary orthogonal signalling as well as 6-ary and 8-ary biorthogonal signalling are expressed as single or double integrals with finite intervals and elementary function integrands.

2.1 Symbol Error Probability of Two-Dimensional Signalling in AWGN Channels

In an AWGN channel the received signal can be expressed as

$$r(t) = \alpha s(t) + n(t), \quad 0 \le t \le T \tag{2.1}$$

where $\alpha = \sqrt{E_s}$ denotes the square root of the average received signal energy per symbol, $s(t) = s_i(t), i = 1, \cdots, M$ is a known deterministic time function, of duration T seconds and unit average energy, used to transmit the message $m_i, i = 1, \cdots, M$ and $n(t)$ is the additive white Gaussian noise with one-sided spectral density of N_0. For two-dimensional signalling systems it is well known that the transmitted signal can be expressed as a linear combination of two orthonormal functions, $e_1(t)$ and $e_2(t)$ given by [16]

$$e_1(t) = \sqrt{2}p(t)\cos(2\pi f_c t) \tag{2.2}$$

$$e_2(t) = \sqrt{2}p(t)\sin(2\pi f_c t) \tag{2.3}$$

where $p(t)$ denotes a pulse shape such as the Nyquist pulse. However $n(t)$ can only be represented by an infinite dimension signal space. Using the Theory of Irrelevance [16], one can show that only the projection of the noise signal on the orthonormal functions mentioned above is needed to make the optimum decision. Therefore, the received signal can be written as

$$r(t) = r_1 e_1(t) + r_2 e_2(t) = (s_{i1} + n_{i1})e_1(t) + (s_{i2} + n_{i2})e_2(t) \tag{2.4}$$

where

$$s_{ij} = \int_0^T s(t)e_j(t)dt, j = 1, 2 \tag{2.5}$$

$$n_j = \int_0^T n(t)e_j(t)dt, j = 1, 2 \tag{2.6}$$

Thus, the received signal has the vector representation of the form

$$\mathbf{r_i} = \mathbf{s_i} + \mathbf{n_i} \tag{2.7}$$

where $\mathbf{r_i} = (r_1, r_2)$, $\mathbf{s_i} = (s_{i1}, s_{i2})$ and $\mathbf{n_i} = (n_1, n_2)$. To calculate the average symbol error probability, we need the pdf of $\mathbf{n_i}$. It is shown in [16] that the pdf of Gaussian noise in Cartesian and polar coordinates is given by

$$f_\mathbf{n}(n_1, n_2) = \frac{1}{N_0 \pi} e^{-\frac{n_1^2 + n_2^2}{N_0}} \tag{2.8}$$

and

$$f_\mathbf{n}(r, \theta) = \frac{r}{\pi N_0} e^{-\frac{r^2}{N_0}}, \quad r \geq 0, \quad 0 \leq \theta \leq 2\pi, \tag{2.9}$$

respectively, where N_0 is the one sided power spectral density of the additive white Gaussian noise. The traditional approach for evaluating the probability of correct decision for two-dimensional, M-ary vector receivers is to partition the observation space into M disjoint two-dimensional decision regions R_i surrounding the signal vectors [17]. The origin of the coordinates for defining these decision regions is assumed to be the same for each of these regions and is located in the two-dimensional space which is defined by the received vector $\mathbf{r}$. Assuming that the ith message was transmitted, the conditional probability of a correct decision is given by [17]

$$P(C|m_i) = P(C|s_i) = \int \int_{R_i} f_r(\rho|m_i) d\rho \tag{2.10a}$$

where

$$f_\mathbf{r}(\rho|m_i) = f_\mathbf{n}(\rho - s_i). \tag{2.10b}$$

Hence, the probability of correct decision can be evaluated using

$$P(C) = \sum_{i=0}^{M-1} P(m_i) P(C|m_i) \tag{2.11}$$

13
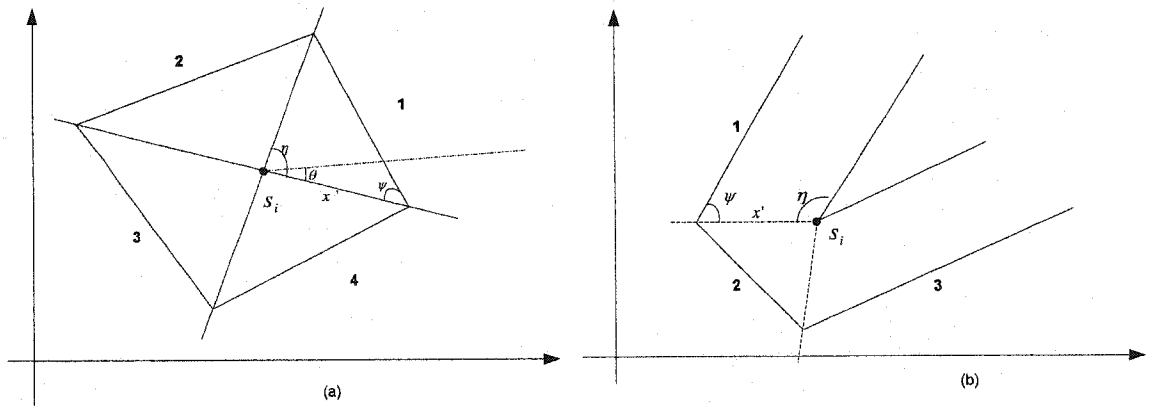
Figure 2.1. Two types of typical decision regions for a signal point; (a) closed region (b) open region (after [18, Fig. 1])

where $P(m_i)$ is the a priori probability of message m_i being transmitted. In some cases, the multidimensional integral in (2.10a) can be reduced to the product of one dimensional integrals, however, this is not true for the general case. In [13], Craig has shown that the evaluation of average error probability of two-dimensional signalling constellations with polygonal decision regions can be considerably simplified by choosing the origin of the coordinates for each decision region in the two-dimensional space defined by the corresponding signal vector. Fig. 2.1(after [18]) shows a symbol in two-dimensional space with it's decision boundaries and parameters η and ψ. In general, the decision boundaries form either a closed or open region. The correct decision regions given that s_i was sent can be divided into closed triangles or triangles with a vertex at infinity. If the signal s_i was sent and the received signal falls out of the correct decision boundaries an error will occur. In this case an error happens if the received signal falls in the disjoint subregions illustrated

in Fig. 2.1. The exact probability of error that $\mathbf{r}$ falls in subregion $j = 1, .., 4$ is given by

$$P_{s_{i,j}} = \int_0^{\eta_j} \int_{R_j(\theta)}^{\infty} f_n(r, \theta) dr d\theta \qquad (2.12a)$$

$$= \frac{1}{2\pi} \int_0^{\eta_j} e^{-\frac{R_j^2(\theta)}{N_0}} d\theta \qquad (2.12b)$$

where $R(\theta)$ can be derived, using the law of sines as [13]

$$R_j(\theta) = \frac{x' \sin(\psi_j)}{\sin(\theta + \psi_j)}. \qquad (2.13)$$

Assuming that $x' = \alpha\sqrt{x}$ in Fig.2.1 represents the distance when $\alpha = 1$, the average SNR per symbol can be expressed in the form of [18]

$$\gamma = \frac{\alpha^2}{N_0} = \frac{E_s}{N_0}. \qquad (2.14)$$

Combining the results in (2.12) and (2.13) yields

$$P_{s_{i,j}} = \frac{1}{2\pi} \int_0^{\eta_j} e^{-\frac{x\gamma \sin^2(\psi_j)}{\sin^2(\psi_j + \theta)}} d\theta. \qquad (2.15)$$

Let K_i denote the number of subregions for the signal s_i. Then the error probability given s_i was transmitted, is the sum of probabilities that the received signal falls into one of the K_i subregions. That is

$$P(C|s_i) = \sum_{j=1}^{K_i} P_{s_{i,j}}. \qquad (2.16)$$

The probability of error when another signal point in the constellation is transmitted is similar to (2.16) except that the sum will have a different number of terms and different parameters η and ψ. So the exact probability of symbol error in AWGN is the weighted sum of the probabilities for all subregions of all the constellation points and is expressed as [13], [18]

$$P_{e,\text{AWGN}}(\gamma) = \sum_{k=1}^{K} = \frac{1}{2\pi} \sum_{k=0}^{K} w_k \int_0^{\eta_k} \exp\left[-\frac{\gamma}{g_k(\theta)}\right] d\theta \qquad (2.17a)$$

15

where w_k is the a priori probability of the symbol to which subregion k corresponds, η_k and ψ_k are parameters corresponding to the kth subregion, K is the total number of erroneous subregions for all the signal points in the constellation and $g_k(\theta)$ is defined as

$$g_k(\theta) = \frac{\sin^2(\theta + \psi_k)}{x_k \sin^2(\psi_k)}. \tag{2.17b}$$

The symbol error probability (SEP) of MPSK, MQAM and 16-star QAM are given below as examples of the application of Craig's SEP expression:

(i) SEP of MPSK [13]

$$P_{e,\text{AWGN}}^{\text{MPSK}}(\gamma) = \frac{1}{\pi} \int_0^{\pi - \frac{\pi}{M}} e^{-\frac{\gamma \sin^2(\frac{\pi}{M})}{\sin^2(\theta)}} \, d\theta \tag{2.18}$$

(ii) SEP of MQAM [19]

$$P_{e,\text{AWGN}}^{\text{MQAM}}(\gamma) = \frac{1}{q} \int_0^{\frac{\pi}{2}} e^{-\frac{c_{\text{MQAM}}}{2\sin^2(\theta)}\gamma} \, d\theta - \frac{q^2}{4\pi} \int_0^{\frac{\pi}{4}} e^{-\frac{c_{\text{MQAM}}}{2\sin^2(\theta)}\gamma} \, d\theta, \tag{2.19}$$

where $q = 4(1 - \frac{1}{\sqrt{M}})$, and $c_{\text{MQAM}} = \frac{3}{2(M-1)}$.

(iii) SEP of 16-star QAM [20]

$$P_{e,\text{AWGN}}^{\text{16-star QAM}}(\gamma) = \frac{1}{2\pi} \sum_{k=1}^{4} \int_0^{\eta_k} e^{-\frac{t_k \sin^2(\Psi_k)\gamma}{\sin^2(\theta + \Psi_k)}} \, d\theta \tag{2.20a}$$

where

$$\eta_1 = \eta_3 = \tan^{-1}[(\sqrt{2} - 1)^2 \frac{\beta + 1}{\beta - 1}], \tag{2.20b}$$

$$\eta_2 = \pi - \eta_1, \quad \eta_4 = \frac{7\pi}{8} - \eta_1, \tag{2.20c}$$

$$\Psi_1 = \Psi_3 = \frac{\pi}{2} - \eta_1, \quad \Psi_2 = \frac{\pi}{8}, \quad \Psi_4 = \frac{\pi}{8} + \eta_1, \tag{2.20d}$$

$$t_1 = t_3 = \frac{1}{2(\beta^2 + 1)}[(\beta - 1)^2 + (\sqrt{2} - 1)^2(\beta + 1)^2] \tag{2.20e}$$

$$t_4 = \frac{1}{2(\beta^2 + 1)}[(\beta - 1)^2 + (\sqrt{2} - 1)^2(\beta + 1)^2], t_2 = \frac{2}{\beta^2 + 1}. \tag{2.20f}$$

2.2 Symbol Error Probability of Classes of Orthogonal Signalling Constellations in AWGN Channels

The M-ary orthogonal signalling constellations are important modulation schemes because they approach Shannon-limit performance as M approaches infinity [16]. The SEP's for M-ary orthogonal and biorthogonal signalling in AWGN are well known [17,19,21]. However because they are expressed as integrals with infinite intervals of integration they are difficult to compute. In [14], Dong and Beaulieu have generalized Craig's approach to derive new SEP's for the class of 3-ary and 4-ary orthogonal signalling, and six and eight biorthogonal signalling in AWGN channels. The new SEP expression are expressed as single or double integrals with finite limits and hence, are easy to compute. The SEP of M-ary orthogonal signalling is given by [21]

$$P_{e,\text{AWGN}}^{\text{M-orth}}(\gamma) = 1 - \int_{-\infty}^{\infty} \left[\frac{1}{2}\text{erfc}\left(-q - \sqrt{\gamma}\right) \right]^{M-1} \frac{e^{-q^2}}{\sqrt{\pi}} dq \qquad (2.21)$$

where $\text{erfc}(x)$ is the complementary error function and is defined as [22]

$$\text{erfc}(x) = \frac{2}{\sqrt{\pi}} \int_{x}^{\infty} e^{-t^2} dt. \qquad (2.22)$$

The new expressions for the SEP's of 3-ary and 4-ary orthogonal signalling are given by [14]

$$P_{e,\text{AWGN}}^{\text{3-orth}}(\gamma) = \frac{1}{\pi} \int_{0}^{\frac{2\pi}{3}} e^{-\frac{\gamma}{2\sin^2(\theta)}} d\theta \qquad (2.23)$$

and

$$P_{e,\text{AWGN}}^{\text{4-orth}}(\gamma) = Q\left(\sqrt{\frac{3\gamma}{2}}\right) + \int_{\frac{\pi}{6}}^{\frac{5\pi}{6}} \frac{3\sin(\theta)}{2\pi\sqrt{2+\sin^2(\theta)}} e^{-\frac{3\gamma}{4+2\sin^2(\theta)}} \left[1 - Q\left(\frac{\sqrt{3\gamma}\sin(\theta)}{\sqrt{4+2\sin^2(\theta)}} \right) \right] d\theta \qquad (2.24)$$

respectively. For biorthogonal signalling, the classical expression for SEP is given by [14]

$$P_{e,\text{AWGN}}^{\text{M-biorth}} = 1 - \int_{-\sqrt{\gamma}}^{\infty} \left[1 - \text{erfc}\left(q + \sqrt{\gamma}\right) \right]^{\frac{M}{2}-1} \frac{e^{-q^2}}{\sqrt{\pi}} dq \qquad (2.25)$$

17

which is difficult to compute because the region of integration is infinite. In [14], an alternative SEP expression is given for 6-ary and 8-ary biorthogonal signalling as

$$P_{e,\text{AWGN}}^{\text{6-biorth}}(\gamma) = Q(\sqrt{2\gamma}) + \frac{4}{\pi}\int_0^{\frac{\pi}{4}} \frac{\cos(\theta)}{\sqrt{1+\cos^2(\theta)}} e^{-\frac{\gamma}{1+\cos^2(\theta)}} \left[1 - Q\left(\frac{\sqrt{2\gamma}\cos(\theta)}{\sqrt{1+\cos^2(\theta)}}\right)\right] d\theta$$

(2.26)

and

$$P_{e,\text{AWGN}}^{\text{8-biorth}}(\gamma) = \frac{3}{\pi}\int_0^{\frac{3\pi}{4}} e^{-\frac{\gamma}{2\sin^2(\theta)}} - \frac{12}{\pi^2}\int_{\frac{\pi}{4}}^{\pi}\int_0^{\frac{\pi}{4}} \frac{\cos^2(\theta_2)}{\cos^2(\theta_2)+\sin^2(\theta_1)} e^{-\frac{(\cos^2(\theta_2)+\sin^2(\theta_1))\gamma}{2\cos^2(\theta_2)\sin^2(\theta_1-\frac{\pi}{4})}} d\theta_2 d\theta_1,$$

(2.27)

respectively.

2.3 Conclusions

In this chapter, Craig's method for calculating the SEP of two-dimensional signalling with polygonal decision regions, was elaborated. The SEP is expressed as a weighted summation of single integrals with finite limits and, hence, is easy to evaluate to a high degree of accuracy.

New expressions for a class of orthogonal signalling in AWGN channels were presented. The SEP of 3-ary and 4-ary orthogonal signalling as well as 6-ary and 8-ary biorthogonal signalling were presented. The new SEP formulas are expressed as single or double integrals with finite limits and are easy to compute.

Chapter 3

Symbol Error Probability of General Diversity Combining with Two-Dimensional Signalling in Rayleigh Fading

The SEP of two-dimensional signalling with polygonal decision regions in AWGN channels was reviewed in Chapter 2. In this chapter, we recall a general expression for the SEP of GDC in Rayleigh fading. Then using the results of Chapter 2, the SEP's of GDC with two-dimensional signalling with polygonal decision regions and classes of orthogonal signalling are derived.

3.1 System Model

Let γ_i denote the instantaneous SNR of the ith diversity branch defined as

$$\gamma_i = \alpha_i^2 \frac{E_s}{N_i} \tag{3.1}$$

where E_s is the average symbol energy, N_i is the one-sided noise power spectral density of the ith branch and α_i is the instantaneous fading envelope. We assume that the channel is a

Rayleigh fading channel and hence, the pdf of the instantaneous branch SNR is given by

$$f_{\gamma_i}(x) = \begin{cases} \frac{1}{\Gamma_i}e^{-\frac{x}{\Gamma_i}} & , \quad 0 \le x < \infty \\ 0 & , \quad \text{otherwise} \end{cases} \tag{3.2}$$

where $\Gamma_i = \mathbb{E}[\gamma_i]$. We further assume that the diversity branches have equal average SNR, i.e., $\Gamma_i = \Gamma$ and so $f_{\gamma_i}(x) = f(x)$. The instantaneous SNR of the GDC system was defined in (1.16) as

$$\gamma_{\text{GDC}} = \sum_{i=1}^{N} q_i \gamma_{(i)} \tag{3.3}$$

where $q_i \in \{0, 1\}$. To calculate the joint pdf of $\gamma_{(1)}, \cdots, \gamma_{(N)}$ we first recall a theorem and its proof [23].

Theorem 1: *Let $X_1, \cdots, X_n$ be n independent and identically distributed random variables with a common density function f. Then the joint probability density function of the order statistic $X_{(1)}, \cdots, X_{(n)}$, $X_{(1)} \ge \cdots \ge X_{(N)}$ is given as*

$$f_{X_{(1)}, \cdots, X_{(n)}}(x_1, x_2, \cdots, x_n) = n! f(x_1) \cdots f(x_n), \quad x_1 > x_2 > \cdots > x_n. \tag{3.4}$$

Proof: The joint pdf of the order statistics $X_{(1)}, X_{(2)}, \cdots, X_{(N)}$ is obtained by noting that the order statistics $X_{(1)}, X_{(2)} \cdots, X_{(N)}$ will take on the values $x_1 \ge x_2 \ge \cdots \ge x_n$ if and only if for some permutation $(i_1, i_2, \cdots, i_n)$ of $(1, 2, \cdots, n)$

$$X_1 = x_{i_1}, \quad X_2 = x_{i_2}, \cdots, X_n = x_{i_n}. \tag{3.5}$$

For any permutation $(i_1, i_2, \cdots, i_n)$ of $(1, 2, \cdots, n)$ we have

$$P\{x_{i_1} - \frac{\varepsilon}{2} < X_1 \quad < \quad x_{i_1} + \frac{\varepsilon}{2}, \cdots, x_{i_n} - \frac{\varepsilon}{2} < X_n < x_{i_n} + \frac{\varepsilon}{2}\} \tag{3.6a}$$

$$\cong \quad \varepsilon^n f_{X_1, \cdots, X_n}(x_{i_1}, \cdots, x_{i_n}) \tag{3.6b}$$

$$= \quad \varepsilon^n f(x_{i_1}) \cdots f(x_{i_n}) \tag{3.6c}$$

$$= \quad \varepsilon^n f(x_1) \cdots f(x_n). \tag{3.6d}$$

21

Hence, for $x_1 > x_2 > \cdots > x_n$ one has

$$P\left\{x_{i_1} - \frac{\varepsilon}{2} < X_1 < x_{i_1} + \frac{\varepsilon}{2}, \cdots, x_{i_n} - \frac{\varepsilon}{2} < X_n < x_{i_n} + \frac{\varepsilon}{2}\right\} \cong n! \varepsilon^n f(x_1) \cdots f(x_n). \quad (3.7)$$

Dividing both sides of (3.7) by ε^n and letting $\varepsilon \to 0$ yields

$$f_{X_{(1)},\cdots,X_{(n)}}(x_1, x_2, \cdots, x_n) = n! f(x_1) \cdots f(x_n), \quad x_1 > x_2 > \cdots > x_n. \quad (3.8)$$

■

The joint pdf of $\Gamma_{(N)} = [\gamma_{(1)} \cdots \gamma_{(N)}]$ can be derived using Theorem 1 as

$$f_{\Gamma_{(N)}}(\{\gamma_{(i)}\}_{i=1}^N) = \begin{cases} N! (\frac{1}{\bar{\Gamma}})^N e^{-\frac{1}{\bar{\Gamma}} \sum_{i=1}^N \gamma_{(i)}} & , \quad \gamma_{(1)} > \cdots > \gamma_{(N)} \\ 0 & , \quad \text{otherwise.} \end{cases} \quad (3.9)$$

3.2 Symbol Error Probability for GDC in Rayleigh fading

In a slow fading channel the SEP for the GDC system can be obtained by averaging the SEP of the unfaded signal over the fading. In other words the SEP of GDC is obtained by averaging the conditional SEP (the symbol error probability in AWGN channel) over the pdf of γ_{GDC}. Thus, the SEP of GDC can be written as

$$P_{e,\text{GDC}} = \mathbb{E}_{\gamma_{\text{GDC}}}\{\Pr(e|\gamma_{\text{GDC}})\} = \int_0^\infty \Pr(e|\gamma_{\text{GDC}}) f_{\gamma_{\text{GDC}}}(\gamma) d\gamma. \quad (3.10)$$

Another approach to calculate the SEP of GDC is to substitute the expression of γ_{GDC} directly in terms of the physical branches [24], [25]. That is,

$$\begin{aligned} P_{e,\text{GDC}} &= \mathbb{E}_{\{[\gamma_i]\}}\{\Pr\{e|\gamma_{\text{GDC}}\}\} \\ &= \int_0^\infty \int_0^{\gamma_{(1)}} \cdots \int_0^{\gamma_{(N-1)}} \Pr\{e| \sum_{i=1}^N q_i \gamma_{(i)}\} f_{\Gamma_{(N)}}(\{\gamma_{(i)}\}_{i=1}^N) d\gamma_{(N)} \cdots d\gamma_{(1)} \quad (3.11) \\ &= \int_0^\infty \int_0^{\gamma_{(1)}} \cdots \int_0^{\gamma_{(N-1)}} \Pr\{e| \sum_{i=1}^N q_i \gamma_{(i)}\} N! (\frac{1}{\bar{\Gamma}})^N e^{-\frac{1}{\bar{\Gamma}} \sum_{i=1}^N \gamma_{(i)}} d\gamma_{(N)} \cdots d\gamma_{(1)}. \end{aligned}$$

One can see that evaluating the integral in (3.25) involves N-nested integrals because the ordered branches are no longer independent. This problem can be alleviated by transforming the branches into a set of independent "virtual branches" [12]. This can be achieved using Sukhatme's Theorem [26] as stated and proved below from [11].

Theorem 2: *Let* $\mathbf{X} = \{x_{(1)}, \cdots, x_{(N)}\}$ *be a set of ordered statistics with the joint pdf of the form*

$$f_{\mathbf{X}}(\{x_{(i)}\}_{i=1}^{N}) = \begin{cases} N!(\frac{1}{\Delta})^N e^{-\frac{1}{\Delta}\sum\limits_{i=1}^{N} x_{(i)}} & , \quad x_{(1)} > \cdots > x_{(N)} \\ 0 & , \quad otherwise. \end{cases} \qquad (3.12)$$

Consider the transformation

$$y_n = x_{(n)} - x_{(n+1)}, \quad n = 1, \cdots, N-1 \qquad (3.13a)$$

$$y_N = x_{(N)}. \qquad (3.13b)$$

Then $\mathbf{Y} = \{y_n\}_{n=1}^{N}$ *are independent random variables with the exponential distribution given by*

$$P_{y_n}(y_n) = \begin{cases} \frac{n}{\Delta} e^{-n\frac{y}{\Delta}} & , \quad 0 < y < \infty \\ 0 & , \quad otherwise. \end{cases} \qquad (3.14)$$

Proof: From (3.13) we have

$$\frac{\partial y_l}{\partial x_{(l)}} = 1, \quad l = 1, \cdots, N-1$$

$$\frac{\partial y_l}{\partial x_{(l+1)}} = -1, \quad l = 1, \cdots, N-1 \qquad (3.15)$$

$$\frac{\partial y_N}{\partial x_{(N)}} = 1.$$

Hence, the Jacobian of the transformation becomes

$$|J(y_1,\cdots,y_N)| = \left\| \begin{bmatrix} 1 & -1 & 0 & . & . & 0 \\ 0 & 1 & -1 & 0 & . & 0 \\ . & . & . & . & . & . \\ 0 & . & . & . & 1 & -1 \\ 0 & 0 & 0 & . & . & 1 \end{bmatrix} \right\|_{N\times N} = 1. \qquad (3.16)$$

So we have

$$p_\mathbf{Y} = \frac{p_\mathbf{X}}{J(y_1,\cdots,y_N)} = p_\mathbf{X}. \qquad (3.17)$$

The pdf of $p_\mathbf{X}$ is given in (3.9). Substituting (3.9) in (3.17) yields,

$$p_\mathbf{Y} = \frac{N!}{\Delta^N} e^{-\frac{1}{\Delta}\sum_{n=1}^{N} x_{(n)}}. \qquad (3.18)$$

However, the $x_{(n)}$'s can be expressed in terms of y_i's as

$$x_{(i)} = \sum_{k=i}^{N} y_k. \qquad (3.19)$$

Substituting (3.19) in (3.18) gives

$$p_\mathbf{Y} = \frac{N!}{\Delta^N} e^{-\frac{1}{\Delta}\sum_{n=1}^{N}\sum_{k=i}^{N} y_k}$$

$$= \prod_{n=1}^{N} \frac{n}{\Delta} e^{-\frac{n y_n}{\Delta}}. \qquad (3.20)$$

This completes the proof. ∎

Intuitively, the result of Theorem 2 is expected because the diversity branches are independent and the system is memoryless, meaning that the selection of one diversity branch will not affect the selection of another. Define

$$\gamma_{(i)} = \sum_{n=i}^{N} \frac{\Gamma V_n}{n} \qquad (3.21)$$

where V_i's are a new set of virtual branches. Then using the result of Theorem 2 the joint pdf of the virtual branches can be expressed as [12]

$$f_{\mathbf{V}_n}(\{v_n\}_{n=1}^N) = \prod_{n=1}^N f_{V_n}(v_n) \tag{3.22a}$$

where $\mathbf{V}_N = [V_1, \cdots, V_N]$ and

$$f_{V_n}(v_n) = \begin{cases} \exp(-v_n), & 0 < v_n < \infty \\ \\ 0, & \text{otherwise.} \end{cases} \tag{3.22b}$$

Substituting (3.21) in (3.3), γ_{GDC} can be written as a linear combination of V_i's as

$$\gamma_{\text{GDC}} = \sum_{i=1}^N q_i \gamma_{(i)} = \sum_{n=1}^N b_n V_n \tag{3.23}$$

where

$$b_n = \frac{\Gamma}{n} \sum_{i=1}^n q_i. \tag{3.24}$$

Now, by substituting (3.22) and (3.23) in (3.11), the N-fold nested integral is reduced to

$$P_{e,\text{GDC}} = \int_0^\infty \int_0^\infty \cdots \int_0^\infty \Pr(e| \sum_{n=1}^N b_n V_n) \prod_{n=1}^N f_{V_N}(v_n) dv_n. \tag{3.25}$$

3.3   SEP of GDC with Two-Dimensional Signalling

In this section, we derive the SEP of GDC with two-dimensional signalling. For many modulation formats $\Pr(e| \sum_{n=1}^N b_n V_n)$ factors into a product of N terms, where each term depends only on one of the V_n's. This is true for all two-dimensional modulation formats with polygonal decision boundaries. The conditional SEP of two-dimensional signalling constellations with polygonal decision regions was derived in (2.17). Substituting (2.17) in

25

(3.25), the SEP of the GDC system with two-dimensional signalling can be written as

$$P_{e,\text{GDC}}(\Gamma) = \int_0^\infty \int_0^\infty \cdots \int_0^\infty \Pr\left(e \mid \sum_{n=1}^N b_n V_n\right) \prod_{n=1}^N f_{V_n}(v_n)\, dv_n \qquad (3.26a)$$

$$= \frac{1}{2\pi} \sum_{k=1}^K w_k \int_0^{\eta_k} \prod_{n=1}^N \int_0^\infty \exp\left\{-\left(\frac{b_n}{g_k(\theta)}+1\right)v_n\right\} dv_n \qquad (3.26b)$$

$$= \frac{1}{2\pi} \sum_{k=1}^K w_k \int_0^{\eta_k} \prod_{n=1}^N \mathbb{E}_{V_n}\left(\exp\left(-\frac{b_n v_n}{g_k(\theta)}\right)\right) d\theta \qquad (3.26c)$$

$$= \frac{1}{2\pi} \sum_{k=1}^K w_k \int_0^{\eta_k} \left(\frac{g_k(\theta)}{g_k(\theta)+b_n}\right)^N d\theta. \qquad (3.26d)$$

The SEP of the GDC of two dimensional signalling constellations is also derived in [27] using moment generating functions. Using the SEP of the GDC system we can now evaluate the SEP of SC, MRC and H-S/MRC with two-dimensional signalling. In the case of SC (3.24) reduces to

$$b_n^{\text{SC}} = \frac{\Gamma}{n}, \quad ,n = 1,\cdots,N. \qquad (3.27)$$

Substituting (3.27) in (3.26) yields

$$P_{e,\text{SC}} = \frac{1}{2\pi} \sum_{k=1}^K w_k \int_0^{\eta_k} \left(\frac{g_k(\theta)}{g_k(\theta)+\frac{\Gamma}{n}}\right)^N d\theta. \qquad (3.28)$$

For MRC, (3.24) is simplified to

$$b_n^{\text{MRC}} = \Gamma, \quad i = 1,\cdots,N. \qquad (3.29)$$

Substituting (3.29) in (3.26) one obtains the SEP of MRC as

$$P_{e,\text{MRC}}(\Gamma) = \frac{1}{2\pi} \sum_{k=1}^K w_k \int_0^{\eta_k} \left(\frac{g_k(\theta)}{g_k(\theta)+\Gamma}\right)^N d\theta. \qquad (3.30)$$

For H-S/MRC the coefficients, b_n in (3.24) are defined as

$$b_n^{\text{H-S/MRC}} = \begin{cases} \Gamma & , \quad n = 1,\cdots,L \\[2mm] \frac{\Gamma L}{n} & , \quad n = L+1,\cdots,N. \end{cases} \qquad (3.31)$$

Substituting (3.31) in (3.26) the SEP of H-S/MRC can be written as

$$P_{e,\text{H-S/MRC}}(\Gamma) = \frac{1}{2\pi} \sum_{k=1}^K w_k \int_0^{\eta_k} \left(\frac{g_k(\theta)}{g_k(\theta)+\Gamma}\right)^L \prod_{n=L+1}^N \left(\frac{g_k(\theta)}{g_k(\theta)+\frac{\Gamma L}{n}}\right) d\theta. \qquad (3.32)$$

3.4 SEP of GDC with Classes of Orthogonal Signalling

In this section, we derive new analytical expressions for SEP of GDC with classes of orthogonal signalling. Using the SEP of 3-ary and 4-ary orthogonal signalling and 6-ary and 8-ary biorthogonal signalling presented in Chapter 2 it is feasible to derive, easy to compute analytical expressions for the SEP of GDC with these constellations. Substituting (2.23) in (3.25) gives the SEP of 3-ary orthogonal signalling in a GDC system as

$$P_{e,\text{GDC}}^{3\text{-orth}} = \frac{1}{\pi} \int_0^{\frac{2\pi}{3}} \prod_{n=1}^{N} \left(\frac{2\sin^2(\theta)}{2\sin^2(\theta) + b_n} \right) d\theta. \tag{3.33}$$

Using the alternative representation of the Gaussian tail integral [13]

$$Q(x) = \frac{1}{\pi} \int_0^{\frac{\pi}{2}} e^{-\frac{x^2}{2\sin^2(\delta)}} d\delta \tag{3.34}$$

and by substituting (2.24) in (3.25), after some mathematical manipulations, the SEP of the GDC system with 4-ary orthogonal signaling is derived as

$$\begin{aligned}
P_{e,\text{GDC}}^{4\text{-orth}} = {} & \frac{1}{\pi} \int_0^{\frac{\pi}{2}} \prod_{n=1}^{N} \left(\frac{4\sin^2(\delta)}{4\sin^2(\delta) + 3b_n} \right) d\delta \\
& + \int_{\frac{\pi}{6}}^{\frac{5\pi}{6}} \frac{3\sin(\theta)}{2\pi\sqrt{2 + \sin^2(\theta)}} \prod_{n=1}^{N} \left(\frac{4 + 2\sin^2(\theta)}{4 + 2\sin^2(\theta) + 3b_n} \right) d\theta - \frac{1}{\pi} \int_{\frac{\pi}{6}}^{\frac{5\pi}{6}} \int_0^{\frac{\pi}{2}} \frac{3\sin(\theta)}{2\pi\sqrt{2 + \sin^2(\theta)}} \\
& \times \prod_{n=1}^{N} \left(\frac{2\sin^2(\delta)(4 + 2\sin^2(\theta))}{2\sin^2(\delta)(4 + 2\sin^2(\theta)) + 3(\sin^2(\theta) + 2\sin^2(\delta))b_n} \right) d\delta d\theta.
\end{aligned} \tag{3.35}$$

The SEP of the GDC system with 6-ary and 8-ary biorthogonal signalling can be derived in a manner similar to that used for 4-ary orthogonal signalling as

$$\begin{aligned}
P_{e,\text{GDC}}^{6\text{-biorth}} = {} & \frac{1}{\pi} \int_0^{\frac{\pi}{2}} \prod_{n=1}^{N} \left(\frac{\sin^2(\delta)}{\sin^2(\delta) + b_n} \right) d\delta \\
& + \frac{4}{\pi} \int_0^{\frac{\pi}{4}} \frac{\cos(\theta)}{\sqrt{1 + \cos^2(\theta)}} \prod_{n=1}^{N} \left(\frac{1 + \cos^2(\theta)}{1 + \cos^2(\theta) + b_n} \right) d\theta \\
& - \frac{4}{\pi^2} \int_0^{\frac{\pi}{4}} \int_0^{\frac{\pi}{2}} \frac{\cos(\theta)}{\sqrt{1 + \cos^2(\theta)}} \prod_{n=1}^{N} \left(\frac{\sin^2(\delta)(1 + \cos^2(\theta))}{\sin^2(\delta)(1 + \cos^2(\theta)) + \cos^2(\theta)b_n} \right) d\delta d\theta
\end{aligned} \tag{3.36}$$

and

$$P_{e,\text{GDC}}^{\text{8-biorth}} = \frac{3}{\pi} \int_0^{\frac{3\pi}{4}} \prod_{n=1}^{N} \left(\frac{2\sin^2(\theta)}{2\sin^2(\theta) + b_n} \right) d\theta$$
$$- \frac{12}{\pi^2} \int_{\frac{\pi}{4}}^{\pi} \int_0^{\frac{\pi}{4}} \frac{\cos^2(\theta_2)}{\cos^2(\theta_2) + \sin^2(\theta_1)} \tag{3.37}$$
$$\times \prod_{n=1}^{N} \left(\frac{2\cos^2(\theta_2)\sin^2(\theta_1 - \frac{\pi}{4})}{2\cos^2(\theta_2)\sin^2(\theta_1 - \frac{\pi}{4}) + (\cos^2(\theta_2) + \sin^2(\theta_1))b_n} \right) d\theta_2 d\theta_1,$$

respectively. To the best of the author's knowledge, equations (3.33), (3.35),(3.36) and

(3.37) are new results.

3.5 Numerical Examples

In this section, we illustrate with numerical examples some of the results derived in the

previous sections.

3.5.1 Two-Dimensional Signalling

The SEP of H-S/MRC with MQAM and MPSK are presented in [12]. Using the results

derived in this chapter, the SEP of any other two-dimensional signaling constellation with

polygonal decision regions with SC, MRC and H-S/MRC can be evaluated from (3.28),

(3.30) and (3.32), by substituting the correct parameters w_k, η_k and $g_k(\theta)$ for $k = 1, \cdots, K$.

We consider the performance of 16-star QAM and the (8,8) constellation [13] in this

section as examples of two-dimensional signalling. Variable rate QAM constellations (e.g.

2-level star QAM to 64-level star QAM) have been proposed for use in high rate wireless

transmission systems because they have high spectral efficiency and low SEP [28]. Further,

16-star QAM has the advantage that automatic gain control (AGC) and carrier recovery are

not required when it is differentially coded, thus simplifying the structure of the receiver.

Another advantage of 16-star QAM is that each of the bits constituting a symbol has a

similar bit error probability, making speech and data mapping straightforward [29]. The performance of the (8,8) constellation is of interest in communication systems having a nonlinear power amplifier such as satellite communications. Thus, it is important to consider the performance of QAM constellations in fading channels. In ring constellations such as 16-star QAM and (8,8) the parameters, η_k, ψ_k and x_k are usually functions of the ring ratio, λ, which has to be optimized to obtain the minimum SEP. Fig. 3.1 shows the optimum values of λ for different values of SNR, for $L = 1, 2, 4, 8, 16$ and $N = 16$. It is clear from Fig. 3.1 that for very large values of SNR, the optimum value of λ is independent of L. This property holds for any other ring ratio constellation because for large values of SNR, (3.32) can be approximated as

$$P_{e,\text{H-S/MRC}} \cong \frac{N!}{\Gamma^N L^{N-L} L!} \sum_{k=1}^{K} \frac{w_k}{2\pi} \int_0^{\eta_k} g_k^N(\theta) d\theta \tag{3.38}$$

where $\eta_k = \eta_k(\lambda), \psi_k = \psi_k(\lambda)$ and $x_k = x_k(\lambda)$, in general. Hence, L has no effect when optimizing (3.38) with respect to λ for large SNR. The optimum ring ratios for (8,8) and (4,4) constellations are plotted in Figs. 3.2 and 3.3, respectively and confirm the independence of the optimum ring ratio from L, for large SNR. Fig. 3.4 shows the SEP of H-S/MRC with 16-star QAM for $N = 16$ and $L = 1, 2, 4, 8$. Note that the SEP of H-S/MRC with $(L, N) = (8, 16)$ is very close to that of 16-branch MRC. The SEP of H-S/MRC for (8,8) is plotted in Fig. 3.5 for $N = 6$ and $L = 1, \cdots, 6$. In Fig. 3.5 the ring ratio selected is equal to the optimum ring ratio for $N = 6$ at large SNR. It is clear from these figures that the SEP of H-S/MRC gets very close to that of MRC even for $L \ll N$. The notation H-L/N in these figures, is used to denote H-S/MRC in which L branches are selected and combined from the available N branches. Note that H-1/N and H-N/N correspond to SC and MRC, respectively.
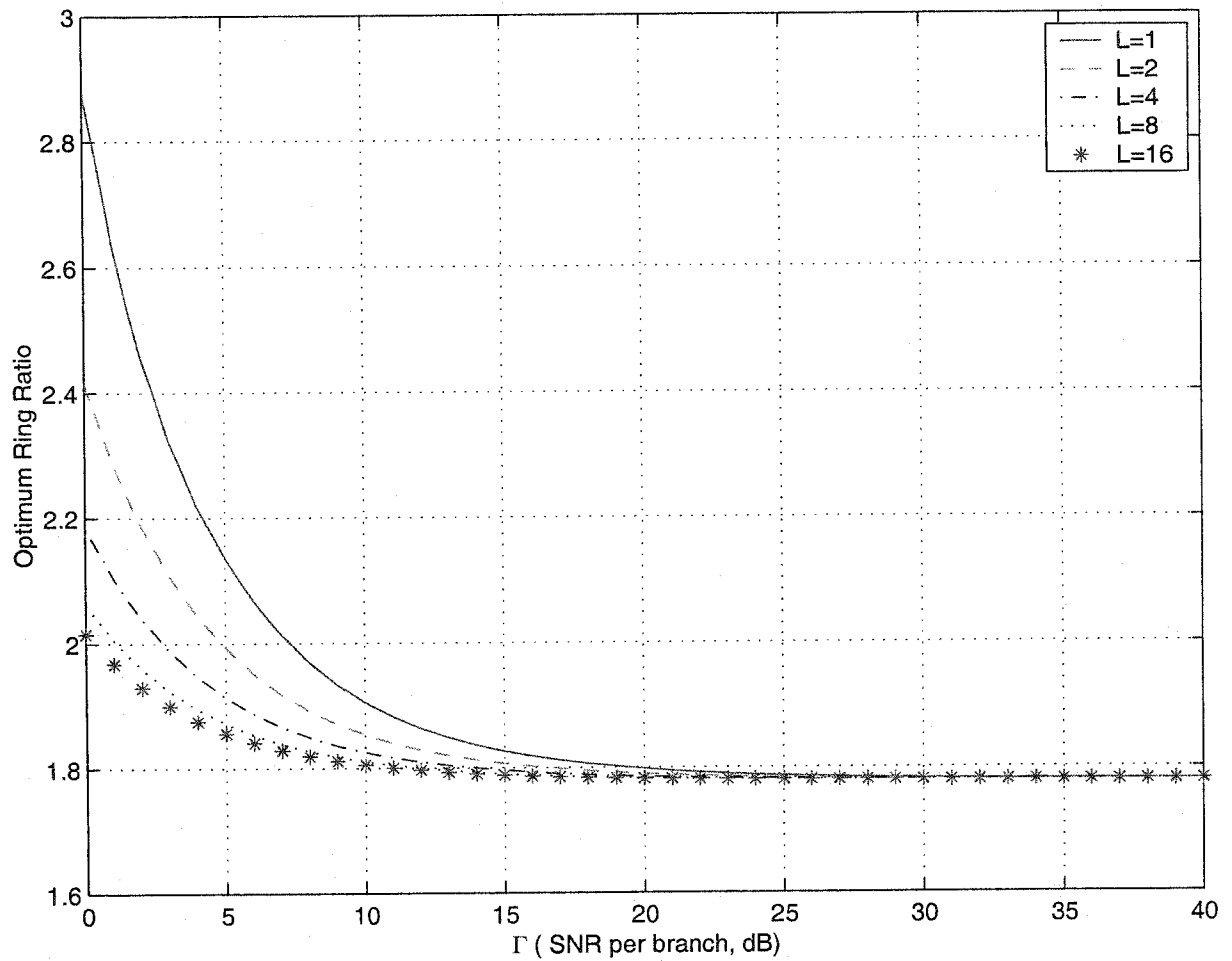
Figure 3.1. Optimum ring ratio's for the SEP of 16-star QAM constellation with H-S/MRC, as a function of average SNR per branch, for $N = 16$ and $L = 1, 2, 4, 8, 16$.
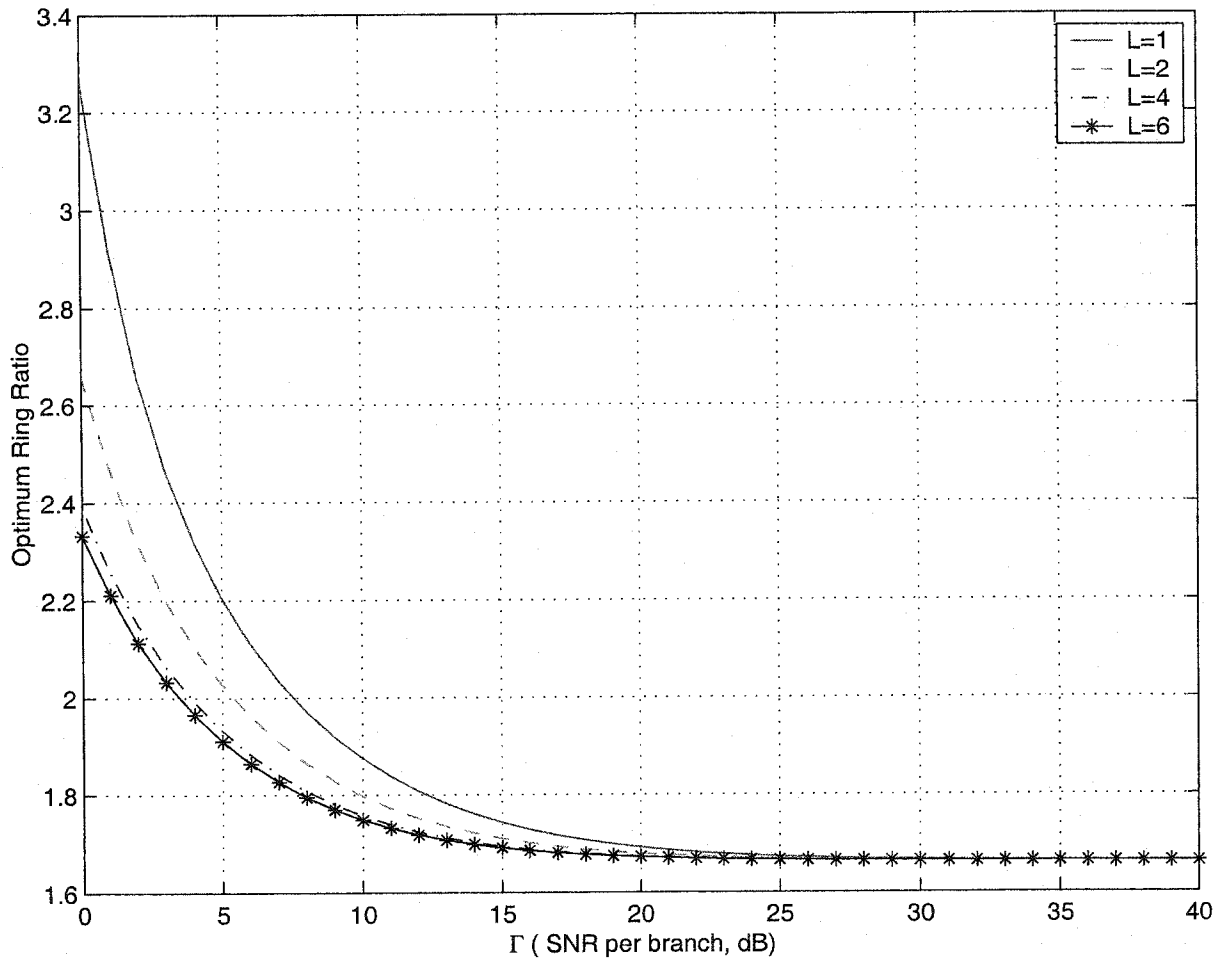
Figure 3.2. Optimum ring ratio's for the SEP of (8,8) constellation with H-S/MRC, as a function of average SNR per branch, for $N = 8$ and $L = 1, 2, 4, 8$.
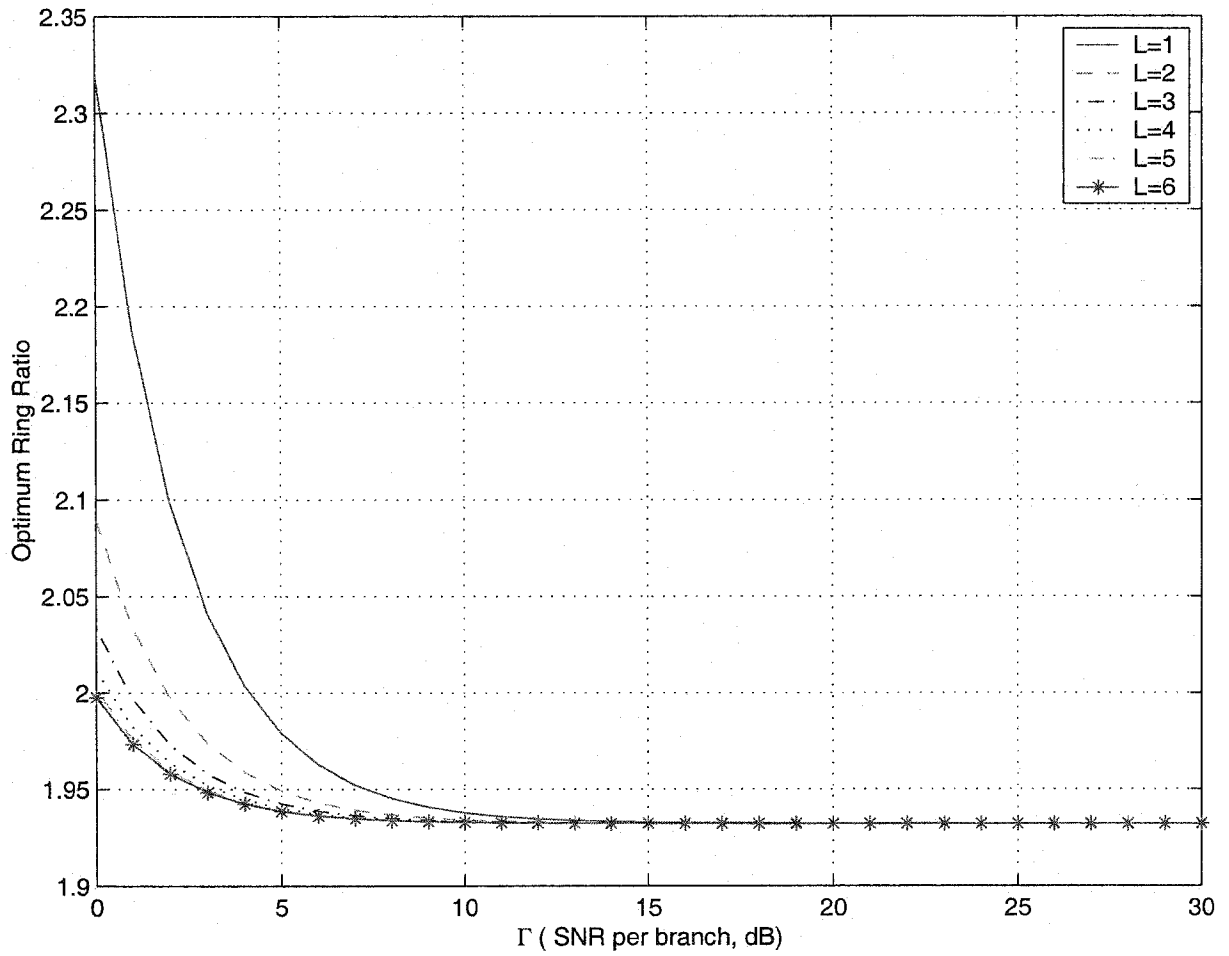
Figure 3.3. Optimum ring ratio's for the SEP of (4,4) constellation with H-S/MRC, as a function of average SNR per branch, for $N = 6$ and $L = 1, 2, 3, 4, 5, 6$.
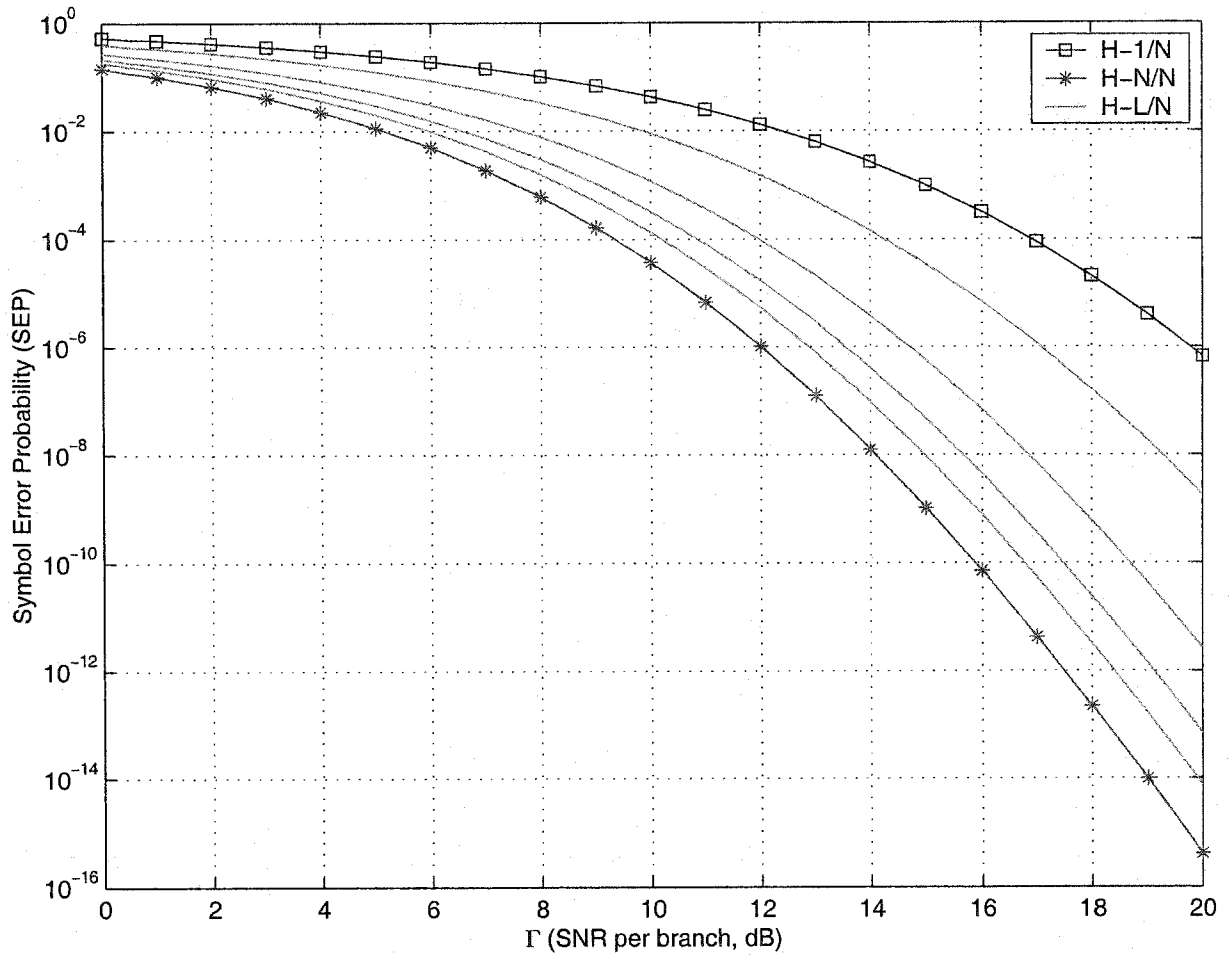
Figure 3.4. The SEP for coherent detection of 16-star QAM with H-S/MRC as a function of average SNR per branch for $L = 1, 2, 4, 6, 8$ and $N = 16$. The curves are distinguished by different $H - L/16$ starting from the highest curve representing H-1/16, and decrease monotonically to the lowest curve representing H-16/16.
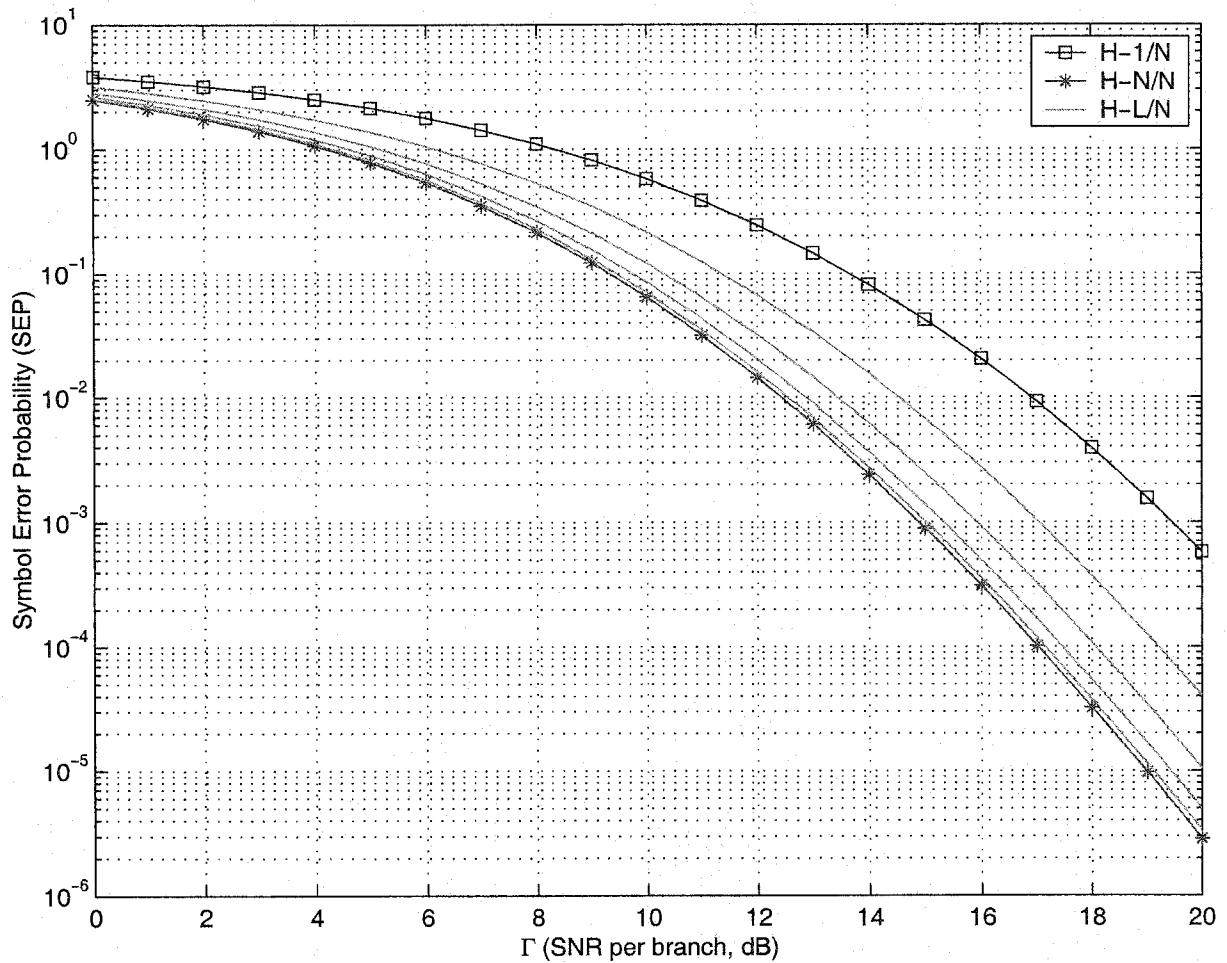
Figure 3.5. The SEP for coherent detection of (8,8) with H-S/MRC as a function of average

SNR per branch for $L = 1, \cdots, 6$ and $N = 6$. The curves are distinguished by different

$H - L/8$ starting from the highest curve representing H-1/6, and decrease monotonically to

the lowest curve representing H-6/6.

3.5.2 Orthogonal Signalling

The SEP of SC, H-S/MRC and MRC for 3-ary and 4-ary orthogonal signalling and 6-ary and 8-ary biorthogonal signalling can be derived from (3.33), (3.35), (3.36) and (3.37), by substituting the corresponding coefficients b_n^{SC}, $b_n^{\text{H-S/MRC}}$ and b_n^{MRC}, respectively. The SEP of these constellations for various L and N are plotted in Figs. 3.6-3.9. Similar to the two-dimensional signalling case, most of the gain is achieved for small L, i.e., H-S/MRC can achieve performance close to that of MRC, even for $L \ll N$.
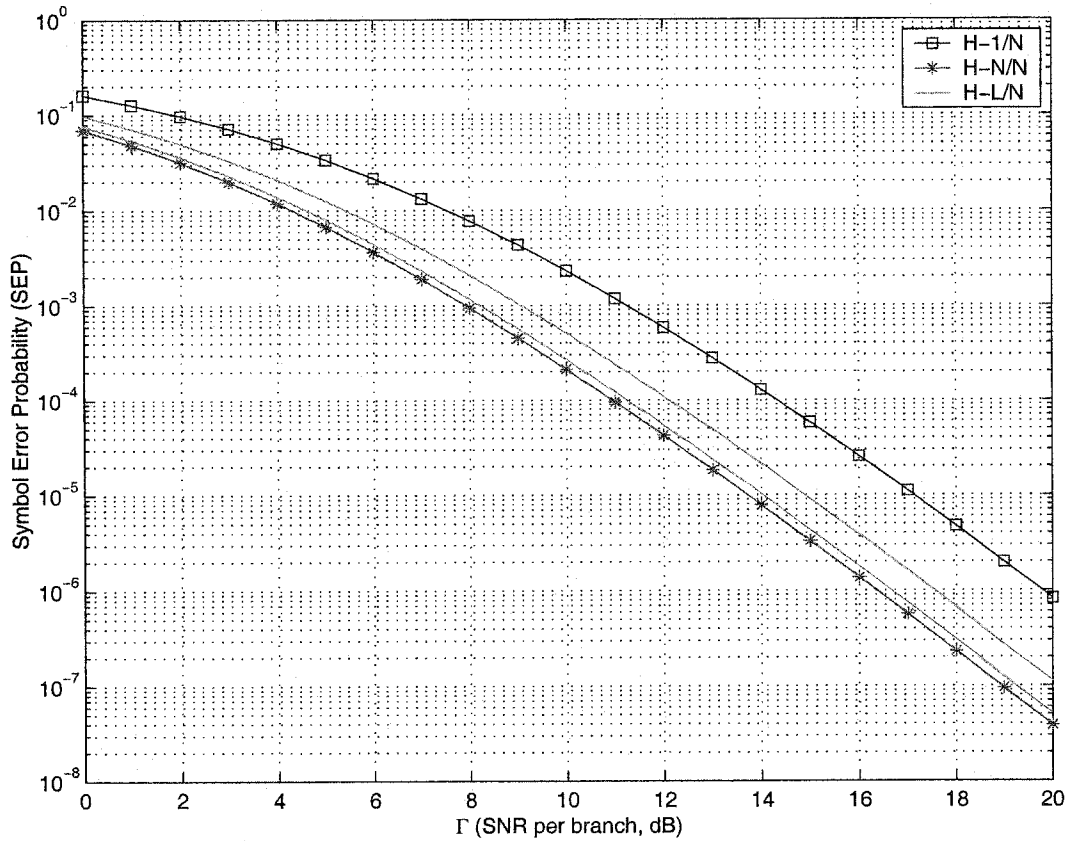
Figure 3.6. The SEP for coherent detection 3-ary orthogonal signalling with H-S/MRC as a function of average SNR per branch for $L = 1, 2, 3, 4$ and $N = 4$. The curves are distinguished by different H-L/4 starting from the highest curve representing H-1/4, and decrease monotonically to the lowest curve representing H-4/4.
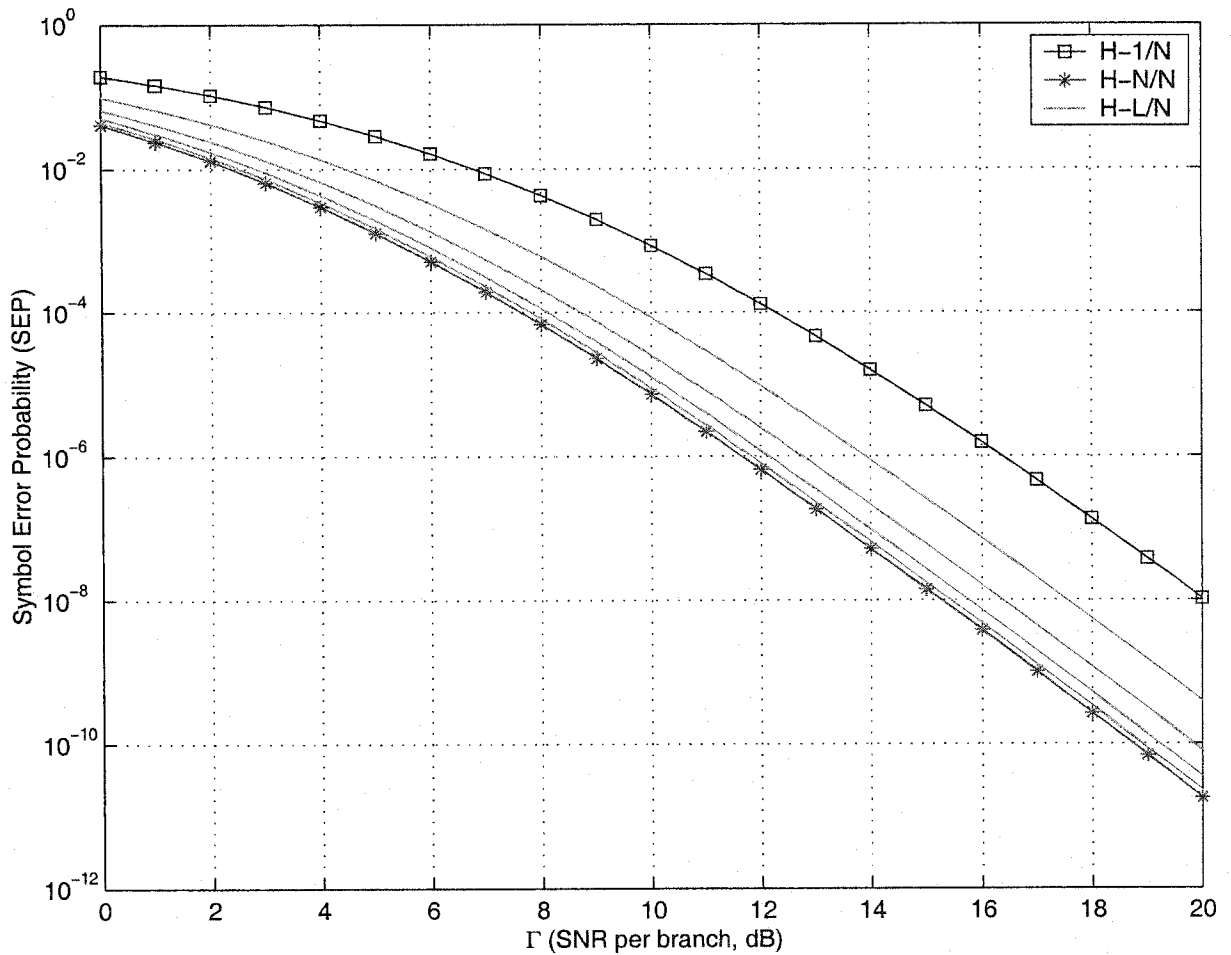
Figure 3.7. The SEP for coherent detection of 4-ary orthogonal signalling with H-S/MRC as a function of average SNR per branch for $L = 1, \cdots, 6$ and $N = 6$. The curves are distinguished by different H-L/6 starting from the highest curve representing H-1/6, and decrease monotonically to the lowest curve representing H-6/6.
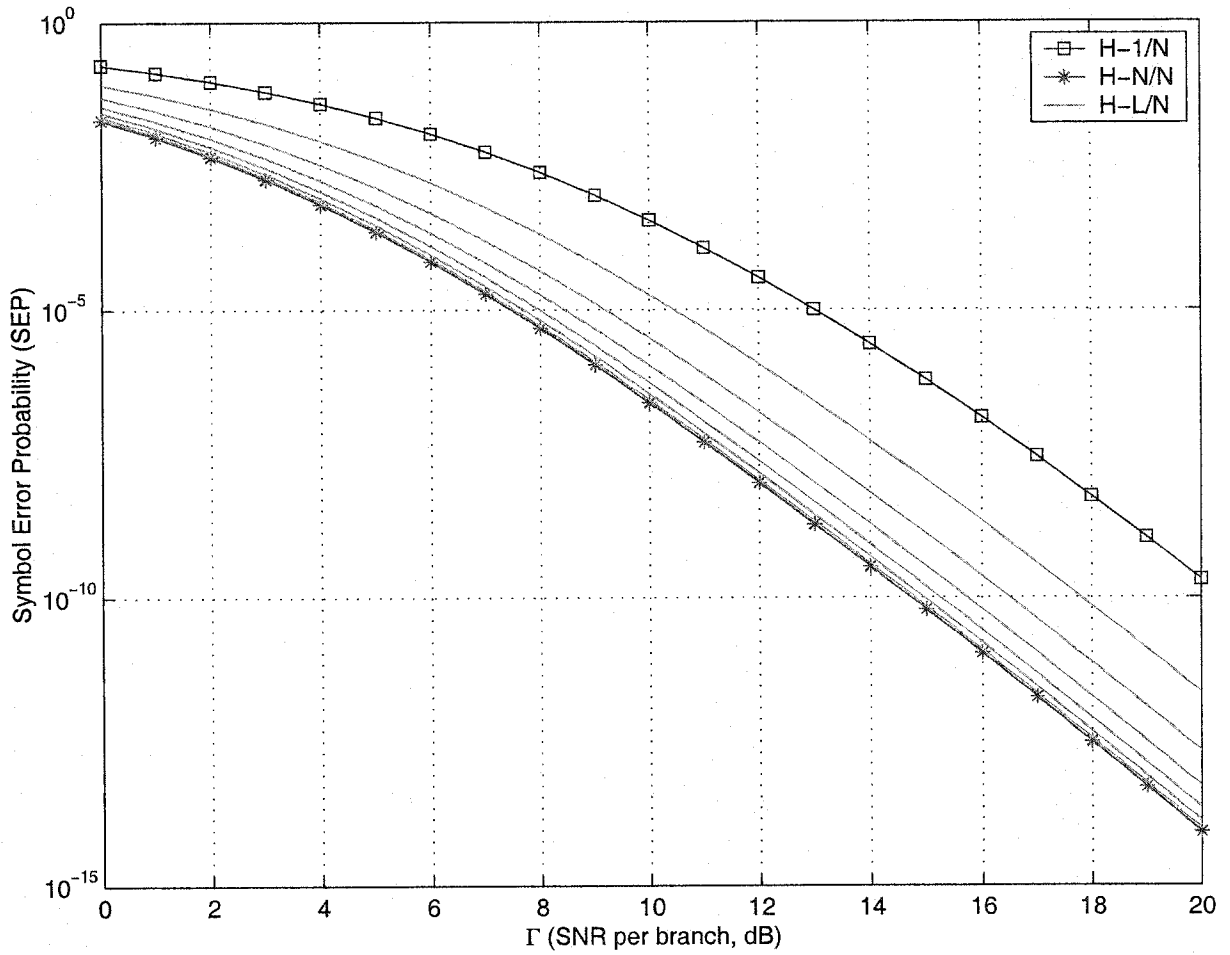
Figure 3.8. The SEP for coherent detection of 6-ary biorthogonal signalling with H-S/MRC as a function of average SNR per branch for $L = 1, \cdots, 8$ and $N = 8$. The curves are distinguished by different H-L/8 starting from the highest curve representing H-1/8, and decrease monotonically to the lowest curve representing H-8/8.
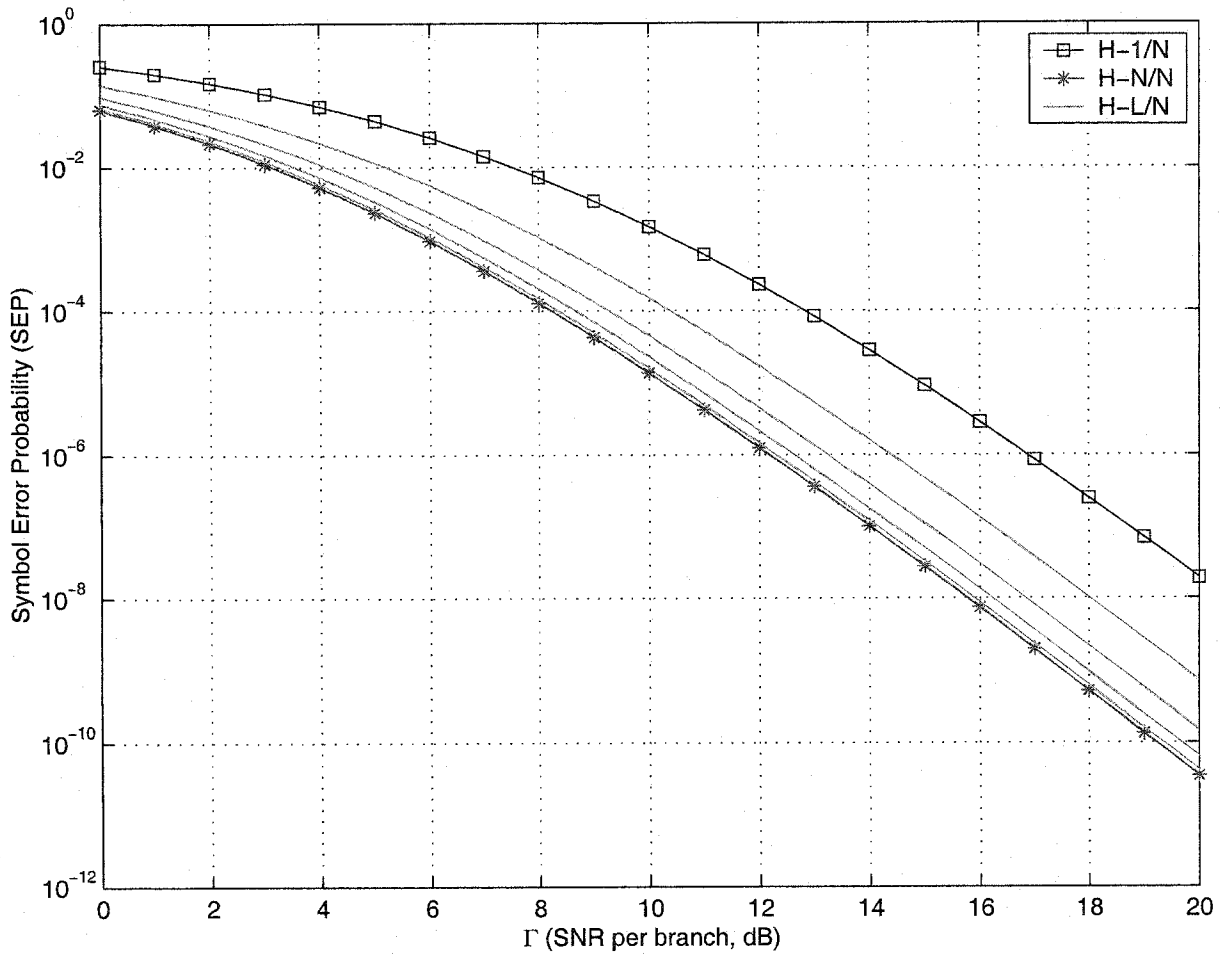
Figure 3.9. The SEP for coherent detection of 8-ary biorthogonal signalling with H-S/MRC as a function of average SNR per branch for $L = 1, \cdots, 6$ and $N = 6$. The curves are distinguished by different H-L/6 starting from the highest curve representing H-1/6, and decrease monotonically to the lowest curve representing H-6/6.

3.6 Conclusions

In this chapter, we presented a general formula for the SEP of GDC in Rayleigh fading, for two-dimensional signalling with polygonal decision regions. The SEP of GDC with two-dimensional signalling can be expressed as a summation of weighted integrals with finite limits of integration and elementary integrands. Examples of two-dimensional signalling were presented. Also new SEP's of GDC for 3-ary and 4-ary orthogonal as well as 6-ary and 8-ary biorthogonal signalling were derived. Numerical examples for the performances of these constellations for various L and N were presented. The numerical examples show that H-S/MRC, even with $L << N$, can achieve close performance to that of N-branch MRC.

Chapter 4

Hybrid-Diversity Penalty with Two-Dimensional Signalling in Rayleigh Fading

4.1 Introduction

Although MRC is known as the optimal combining technique, it may not be cost efficient in some systems. The complexity of the MRC receiver is directly proportional to the number of resolvable paths, which can be quite high, especially for multipath diversity of wideband CDMA signals. In addition MRC is sensitive to channel estimation errors, and these errors tend to be more important for the paths with small SNR. Selection combining, on the other hand, uses only one path out of the N available paths and so does not fully exploit the amount of diversity offered by the channel. Recently, there has been much interest in systems where only a subset of the N available paths are considered [30]- [40]. These schemes offer less complex receivers than the conventional MRC RAKE receivers since they have a fixed number of fingers independent of the number of multipaths. Also one can expect that these schemes are more robust towards channel estimation errors since the weakest SNR paths are excluded from the combining process. One such diversity combining scheme is H-S/MRC introduced in Chapter 1.

4.2 Penalty of H-S/MRC Relative to MRC

In H-S/MRC the receiver selects the strongest L paths from the available N paths at each instant of time and combines them using MRC. However, because only a subset of the available paths are included, a loss or penalty incurs. This loss is defined as the increase in the SNR required for H-S/MRC to achieve the same target SEP as that of MRC [15]. That is,

$$P_{e,\text{H-S/MRC}}(\beta\Gamma) = P_{e,\text{MRC}}(\Gamma). \tag{4.1}$$

In (4.1), β is the SNR penalty, Γ is the average SNR of each branch and $P_{e,\text{H-S/MRC}}(x)$ and $P_{e,\text{MRC}}(x)$ is the SEP of MRC and H-S/MRC, respectively. The definition of the SNR penalty corresponds to the widely used notion of power margin in communication systems. For example, the performance of binary orthogonal frequency shift keying is 3 dB poorer than that of binary phase shift keying [22]. The SNR penalty represents the additional transmitter power needed for H-S/MRC to achieve the same SEP as MRC. The SNR penalty is in general a function of the target SEP and hence a function of branch SNR, that is $\beta = \beta(\Gamma)$. To obtain an explicit definition of the SNR penalty, (4.1) can be written as

$$\beta(\Gamma) = \frac{1}{\Gamma} P_{e,\text{H-S/MRC}}^{-1} \left\{ P_{e,\text{MRC}}(\Gamma) \right\} \tag{4.2}$$

where $P_{e,\text{H-S/MRC}}^{-1}(x)$ is the inverse H-S/MRC SEP function. Although the inverse function may be obtained numerically if we have $P_{e,\text{H-S/MRC}}(x)$ in hand, the function $\beta(\cdot)$ is not known in closed-form. In this chapter, we give asymptotic values and bounds to the SNR penalty of H-S/MRC with any two-dimensional signalling constellation with polygonal decision regions. Previously only results for MPSK were available [15]. We also show, how to derive the bounds and the asymptotes from the diversity model. In [15], results for MPSK cases of these quantities were given without derivation and then proved.

4.3 SNR Penalty Bounds for H-S/MRC with Two-Dimensional Signalling

In this section, we derive new simple bounds to the SNR penalty of H-S/MRC with two-dimensional signalling for small and large values of SNR (β_L and β_U, respectively). As will be seen the bounds are independent of the SNR and the two-dimensional signalling constellation and depend on L and N only. The proofs for these bounds are provided in the next section.

4.3.1 Lower Bound for Small SNR

We want to derive β_L such that $P_{e,\text{H-S/MRC}}(\beta_L \Gamma) = P_{e,\text{MRC}}(\Gamma)$ or equivalently

$$P_{e,\text{H-S/MRC}}(\Gamma) = P_{e,\text{MRC}}(\beta_L^{-1}\Gamma). \tag{4.3}$$

Using (3.30) the right of (4.3) can be written as

$$
\begin{aligned}
P_{e,\text{MRC}}(\beta_L^{-1}\Gamma) &= \sum_{k \in \bar{J}_\pi} \frac{w_k}{2\pi} \int_0^{\eta_k} \left(\frac{g_k(\theta)}{g_k(\theta) + \beta_L^{-1}\Gamma} \right)^N d\theta + \sum_{k \in J_\pi} \frac{w_k}{2\pi} \int_0^{\eta_k} \left(\frac{g_k(\theta)}{g_k(\theta) + \beta_L^{-1}\Gamma} \right)^N d\theta \\
&= \sum_{k \in \bar{J}_\pi} \frac{w_k}{2\pi} \int_0^{\eta_k} \left(\frac{1}{1 + \frac{\beta_L^{-1}\Gamma}{g_k(\theta)}} \right)^N d\theta + \sum_{k \in J_\pi} \frac{w_k}{2\pi} \int_0^{\eta_k} \left(\frac{1}{1 + \frac{\beta_L^{-1}\Gamma}{g_k(\theta)}} \right)^N d\theta \tag{4.4}
\end{aligned}
$$

where

$$J_\pi = \{k | \eta_k + \psi_k = \pi\} \tag{4.5a}$$

$$\bar{J}_\pi = \{k | \eta_k + \psi_k \neq \pi\}. \tag{4.5b}$$

The first term on the right of (4.4) can be approximated as

$$\sum_{k \in \bar{J}_\pi} \frac{w_k}{2\pi} \int_0^{\eta_k} \left(\frac{1}{1 + \frac{\beta_L^{-1}\Gamma}{g_k(\theta)}} \right)^N d\theta \cong \sum_{k \in \bar{J}_\pi} \frac{w_k}{2\pi} \int_0^{\eta_k} \left(1 - \frac{N\beta_L^{-1}\Gamma}{g_k(\theta)} \right) d\theta \tag{4.6}$$

42

for small values of Γ using

$$\left(\frac{1}{1+x}\right)^N \cong (1 - Nx), \qquad (4.7)$$

since $\frac{1}{g_k(\theta)}$ is a finite value for $\theta \in (0, \eta_k)$ when $k \in \bar{J}_\pi$. The second term on the right of (4.4) can be written as

$$\sum_{k \in J_\pi} \frac{w_k}{2\pi} \int_0^{\eta_k - \varepsilon_k} \left(\frac{1}{1 + \frac{\beta_L^{-1}\Gamma}{g_k(\theta)}}\right)^N d\theta + \sum_{k \in J_\pi} \frac{w_k}{2\pi} \int_{\eta_k - \varepsilon_k}^{\eta_k} \left(\frac{1}{1 + \frac{\beta_L^{-1}\Gamma}{g_k(\theta)}}\right)^N d\theta \qquad (4.8)$$

where for each $k \in J_\pi$, ε_k is chosen such that $\frac{1}{g_k(\theta)} \ll \Gamma$ for $0 < \theta < \eta_k - \varepsilon_k$. Note that

$$\sum_{k \in J_\pi} \frac{w_k}{2\pi} \int_{\eta_k - \varepsilon_k}^{\eta_k} \left(\frac{1}{1 + \frac{\beta_L^{-1}\Gamma}{g_k(\theta)}}\right)^N d\theta < \sum_{k \in J_\pi} \frac{\varepsilon_k w_k}{2\pi} \qquad (4.9)$$

and ε_k can be made *arbitrary* small, by choosing Γ small enough, so (4.8) can be approximated as

$$\sum_{k \in J_\pi} \frac{w_k}{2\pi} \int_0^{\eta_k} \left(1 - \frac{N\beta_L^{-1}\Gamma}{g_k(\theta)}\right) d\theta \qquad (4.10)$$

using (4.7). Combining (4.6) and (4.10) one obtains

$$P_{e,\mathrm{MRC}}(\beta_L^{-1}\Gamma) \cong \sum_{k=1}^K \frac{w_k}{2\pi} \int_0^{\eta_k} \left(1 - \frac{N\beta_L^{-1}\Gamma}{g_k(\theta)}\right) d\theta. \qquad (4.11)$$

Using similar steps to those taken to derive (4.11), $P_{e,\mathrm{H\text{-}S/MRC}}(\Gamma)$ can be approximated as

$$P_{e,\mathrm{H\text{-}S/MRC}}(\Gamma) \cong \sum_{k=1}^K \frac{w_k}{2\pi} \int_0^{\eta_k} \left(1 - \frac{\Gamma}{g_k(\theta)}\right)^L \prod_{n=L+1}^N \left(1 - \frac{L\Gamma}{n g_k(\theta)}\right) d\theta \qquad (4.12a)$$

$$\cong \sum_{k=1}^K \frac{w_k}{2\pi} \int_0^{\eta_k} \left(1 - \frac{L\Gamma}{g_k(\theta)} - \sum_{n=L+1}^N \frac{L\Gamma}{n g_k(\theta)}\right) d\theta. \qquad (4.12b)$$

Substituting (4.11) and (4.12b) into (4.3) and after some mathematical manipulations, β_L is derived as

$$\beta_L = \frac{N}{L\left(1 + \sum\limits_{n=L+1}^N \frac{1}{n}\right)}. \qquad (4.13)$$

43

4.3.2 Upper Bound for Large SNR

For large values of Γ, we want to find β_U such that

$$P_{e,\text{H-S/MRC}}(\Gamma) = P_{e,\text{MRC}}(\beta_U^{-1}\Gamma). \tag{4.14}$$

Using (3.30), the right of (4.14) can be expressed as

$$P_{e,\text{MRC}}(\beta_U^{-1}\Gamma) = \sum_{k=1}^{K} \frac{w_k}{2\pi} \int_0^{\eta_k} \left(\frac{1}{1 + \frac{\beta_U^{-1}\Gamma}{g_k(\theta)}} \right)^N d\theta \tag{4.15}$$

and can be approximated as

$$P_{e,\text{MRC}}(\beta_U^{-1}\Gamma) \cong \sum_{k=1}^{K} \frac{w_k}{2\pi} \int_0^{\eta_k} \left(\frac{g_k(\theta)}{\beta_U^{-1}\Gamma} \right)^N d\theta, \tag{4.16}$$

where we have used the approximation

$$\frac{1}{1+x} \cong \frac{1}{x}, \tag{4.17}$$

valid for large x. Similarly $P_{e,\text{H-S/MRC}}(\Gamma)$ can be approximated as

$$P_{e,\text{H-S/MRC}}(\Gamma) \cong \sum_{k=1}^{K} \frac{w_k}{2\pi} \int_0^{\eta_k} \left(\frac{g_k(\theta)}{\Gamma} \right)^L \prod_{n=L+1}^{N} \left(\frac{g_k(\theta)n}{\Gamma L} \right) d\theta. \tag{4.18}$$

Substituting (4.16) and (4.18) into (4.14) and after mathematical manipulations we obtain

$$\beta_U = \left[\prod_{n=L+1}^{N} \frac{L}{n} \right]^{-\frac{1}{N}} = \left(\frac{N!}{L!L^{N-L}} \right)^{\frac{1}{N}}. \tag{4.19}$$

The following theorem establishes that (4.13) and (4.19), obtained using approximations, are indeed the lower and upper bounds for the SNR penalty of H-S/MRC relative to MRC for any two dimensional signalling constellation with polygonal decision regions.

Theorem 3: *Let β_L and β_U be as defined in (4.13) and (4.19) respectively. The SNR penalty of H-S/MRC relative to MRC is lower and upper bounded by*

$$\beta_L \leq \beta(\Gamma) \leq \beta_U. \tag{4.20}$$

44

Equivalently the SEP for any two dimensional signalling constellation is upper and lower bounded by

$$P_{e,MRC}(\beta_L^{-1}\Gamma) \leq P_{e,H\text{-}S/MRC}(\Gamma) \leq P_{e,MRC}(\beta_U^{-1}\Gamma). \tag{4.21}$$

The equivalency of (4.20) and (4.21) can be explained as below. Equation (4.20) can be written as

$$\beta_L^{-1}\Gamma \geq \beta^{-1}\Gamma \geq \beta_U^{-1}\Gamma. \tag{4.22}$$

Noting that $P_{e,\text{MRC}}(\Gamma)$ is a strict monotonically decreasing function of its argument (4.22) gives

$$P_{e,\text{MRC}}(\beta_L^{-1}\Gamma) \leq P_{e,\text{MRC}}(\beta^{-1}\Gamma) \leq P_{e,\text{MRC}}(\beta_U^{-1}\Gamma). \tag{4.23}$$

Now, using the definition of SNR penalty (4.23) can be written as

$$P_{e,\text{MRC}}(\beta_L^{-1}\Gamma) \leq P_{e,H\text{-}S/MRC}(\Gamma) \leq P_{e,\text{MRC}}(\beta_U^{-1}\Gamma). \tag{4.24}$$

4.4   Proof of the SEP bounds

In this section, we provide the proof for Theorem 3. In order to prove the bounds we will require two inequalities, which are recalled from [15]. We will first define some notations. Let $\mathbf{x} = \{x_1, x_2, \cdots, x_N\}$, and $\mathbf{p} = \{p_1, p_2, \cdots, p_N\}$ be vectors with non-negative elements. Also assume that $\mathbf{p}$ is a probability vector associated with $\mathbf{x}$ such that $\mathbb{P}\{x_n\} = p_n$ and $\sum_{n=1}^{N} p_n = 1$. The arithmetic and the geometric mean of $\mathbf{x}$ and $\mathbf{p}$ are defined as

$$\mathfrak{A}(\mathbf{x}, \mathbf{p}) \triangleq \sum_{n=1}^{N} p_n x_n \tag{4.25a}$$

and

$$\mathfrak{G}(\mathbf{x}, \mathbf{p}) \triangleq \prod_{n=1}^{N} x_n^{p_n} \tag{4.25b}$$

respectively.

Theorem 4 [15], [41]: *The arithmetic and the geometric mean satisfy the following inequality*

$$\mathfrak{A}(\mathbf{x}, \mathbf{p}) \geq \mathfrak{G}(\mathbf{x}, \mathbf{p}). \tag{4.26}$$

Proof: The Proof of Theorem 3 can be found in [41]. ∎

Theorem 5 [15]: *The following inequality holds for any non-negative vector* $\mathbf{y} = \{y_1, y_2, \cdots, y_N\}$.

$$\prod_{n=1}^{N}(y_n + 1) \geq \left[\prod_{n=1}^{N}(y_n)^{\frac{1}{N}} + 1\right]^N. \tag{4.27}$$

Proof: The proof of Theorem 5 can be found in [15]. ∎

We will now give the proof for Theorem 3. The inequalities in Theorems 4 and 5 will be used to prove the lower bound and the upper bound, respectively.

4.4.1 Proof of the Lower Bound

For each Γ and $b_k(\theta)$, define

$$x_n \triangleq \begin{cases} \dfrac{\Gamma + g_k(\theta)}{g_k(\theta)}, & n = 1, \cdots, L \\[3ex] \dfrac{\frac{L\Gamma}{n} + g_k(\theta)}{g_k(\theta)}, & n = L+1, \cdots, N. \end{cases} \tag{4.28}$$

Substituting (4.28) in (4.26) and setting $p_n = \frac{1}{N}$ for $n = 1, \cdots, N$, we obtain

$$\sum_{n=1}^{L} \frac{1}{N}\left[\frac{\Gamma + g_k(\theta)}{g_k(\theta)}\right] + \sum_{n=L+1}^{N} \frac{1}{N}\left(\frac{\frac{L\Gamma}{n} + g_k(\theta)}{g_k(\theta)}\right) \geq \tag{4.29a}$$

$$\prod_{n=1}^{L}\left(\frac{\Gamma + g_k(\theta)}{g_k(\theta)}\right)^{\frac{1}{N}} \prod_{n=L+1}^{N}\left(\frac{\frac{L\Gamma}{n} + g_k(\theta)}{g_k(\theta)}\right)^{\frac{1}{N}} \tag{4.29b}$$

which is equivalent to

$$\left[\frac{\frac{\Gamma}{N}(L + L\sum_{n=L+1}^{N}\frac{1}{n}) + g_k(\theta)}{g_k(\theta)}\right] \geq \prod_{n=1}^{L}\left(\frac{\Gamma + g_k(\theta)}{g_k(\theta)}\right)^{\frac{1}{N}} \prod_{n=L+1}^{N}\left(\frac{\frac{L\Gamma}{n} + g_k(\theta)}{g_k(\theta)}\right)^{\frac{1}{N}} \tag{4.30a}$$

$$\left[\frac{\Gamma\beta_{\mathrm{L}}^{-1}+g_k(\theta)}{g_k(\theta)}\right]^N \geq \left(\frac{\Gamma+g_k(\theta)}{g_k(\theta)}\right)^L \prod_{n=L+1}^{N}\left(\frac{\frac{L\Gamma}{n}+g_k(\theta)}{g_k(\theta)}\right). \tag{4.30b}$$

Integrating the inverse of both sides of (4.30) from 0 to η_k and scaling by $\frac{w_k}{2\pi}$ for each $k=1,..,K$ we obtain

$$\sum_{k=1}^{K}\frac{w_k}{2\pi}\int_0^{\eta_k}\left[\frac{g_k(\theta)}{\Gamma\beta_{\mathrm{L}}^{-1}+g_k(\theta)}\right]d\theta \leq \sum_{k=1}^{K}\frac{w_k}{2\pi}\int_0^{\eta_k}\left(\frac{g_k(\theta)}{\Gamma+g_k(\theta)}\right)^L \prod_{n=L+1}^{N}\left(\frac{g_k(\theta)}{\frac{L\Gamma}{n}+g_k(\theta)}\right)d\theta. \tag{4.31}$$

Therefore, for each value of Γ we have

$$P_{e,\mathrm{MRC}}(\beta_{\mathrm{L}}^{-1}\Gamma) \leq P_{e,\mathrm{H\text{-}S/MRC}}(\Gamma). \tag{4.32}$$

4.4.2 Proof of the Upper Bound

For each Γ and $b_k(\theta)$ define

$$y_n \triangleq \begin{cases} \dfrac{\Gamma}{g_k(\theta)}, & n=1,\cdots,L \\[3ex] \dfrac{\frac{L\Gamma}{n}}{g_k(\theta)}, & n=L+1,\cdots,N. \end{cases} \tag{4.33}$$

Substituting (4.33) in (4.27) we get

$$\left[\frac{\Gamma+g_k(\theta)}{g_k(\theta)}\right]^L \prod_{n=L+1}^{N}\left(\frac{\frac{L\Gamma}{n}+g_k(\theta)}{g_k(\theta)}\right) \geq \left[\frac{\Gamma}{g_k(\theta)}\prod_{n=L+1}^{N}(\frac{L}{n})^{\frac{1}{N}}+1\right]^N \tag{4.34}$$

which can be further simplified to give

$$\left(\frac{\Gamma+g_k(\theta)}{g_k(\theta)}\right)^L \prod_{n=L+1}^{N}\left(\frac{\frac{L\Gamma}{n}+g_k(\theta)}{g_k(\theta)}\right) \geq \left[\frac{\Gamma\beta_{\mathrm{U}}^{-1}+g_k(\theta)}{g_k(\theta)}\right]^N. \tag{4.35}$$

Integrating the inverse of both sides of (4.30) from 0 to η_k and scaling by $\frac{w_k}{2\pi}$ for each $k=1,..,K$ we obtain

$$\sum_{k=1}^{K}\frac{w_k}{2\pi}\int_0^{\eta_k}\left(\frac{g_k(\theta)}{\Gamma+g_k(\theta)}\right)^L \prod_{n=L+1}^{N}\left(\frac{g_k(\theta)}{\frac{L\Gamma}{n}+g_k(\theta)}\right)d\theta \leq \sum_{k=1}^{K}\frac{w_k}{2\pi}\int_0^{\eta_k}\left[\frac{g_k(\theta)}{\Gamma\beta_{\mathrm{U}}^{-1}+g_k(\theta)}\right]^N d\theta. \tag{4.36}$$

47

Therefore, for each value of Γ we have

$$P_{e,\text{H-S/MRC}}(\Gamma) \leq P_{e,\text{MRC}}(\beta_U^{-1}\Gamma). \tag{4.37}$$

4.5 Asymptotic SNR Penalties of H-S/MRC with Two-Dimensional Signalling

In the previous sections we derived bounds to the SNR penalty of hybrid diversity with two-dimensional signalling. In this section, we derive asymptotic values for the SNR penalty of hybrid diversity with two-dimensional signalling. We begin with the derivation of the asymptotic penalty for small SNR.

4.5.1 Asymptotic Penalty for Small SNR

Let $P_{e,\text{GDC}} = \sum_{k=1}^{K} w_k P_k(\Gamma)$ where

$$P_k(\Gamma) = \frac{1}{2\pi} \int_0^{\eta_k} \prod_{n=1}^{N} \left(\frac{g_k(\theta)}{g_k(\theta) + a_n\Gamma} \right) d\theta \tag{4.38}$$

and where

$$a_n = \frac{b_n}{\Gamma}. \tag{4.39}$$

If $k \in \bar{J}_\pi$, one can show that $P_k(\Gamma)$ has a Taylor series expansion around $\Gamma = 0$ and can be expressed as

$$P_k(\Gamma) = \frac{\eta_k}{2\pi} + G_k(\sum_{i=1}^{N} a_i)\Gamma + o(\Gamma) = \frac{\eta_k}{2\pi} + o(\Gamma^{1/2}) \tag{4.40}$$

where G_k is defined as

$$G_k = -\frac{1}{2\pi} \int_0^{\eta_k} \frac{1}{g_k(\theta)} d\theta \tag{4.41}$$

48

and is a finite value since $\frac{1}{g_k(\theta)}$ is defined everywhere in $\theta \in (0, \eta_k), k \in \bar{J}_\pi$. On the other hand, if $k \in J_\pi$, using Lemma 2 proved in Appendix A, we can show that

$$P_k(\Gamma) = \frac{\eta_k}{2\pi} - A_k \Gamma^{1/2} + o(\Gamma^{1/2}) \qquad (4.42)$$

where A_k is defined as

$$A_k \triangleq \frac{1}{2\pi} \int_0^\infty \left\{ 1 - \prod_{n=1}^N \left[\frac{u^2}{c_{k,n} + u^2} \right] \right\} du \qquad (4.43)$$

and $c_{k,n} = a_n x_k \sin^2(\psi_k)$. Combining (4.40) and (4.42), one obtains

$$P_{e,\text{GDC}} = \sum_{k=1}^K \frac{w_k \eta_k}{2\pi} - \left\{ \sum_{k \in J_\pi} A_k \right\} \Gamma^{1/2} + o(\Gamma^{1/2}). \qquad (4.44)$$

Consequently, for small values of SNR, $P_{e,\text{MRC}}(\Gamma)$ and $P_{e,\text{H-S/MRC}}(\Gamma)$ can be approximated as

$$P_{e,\text{MRC}} \approx \sum_{k=1}^K \frac{w_k \eta_k}{2\pi} - \left\{ \sum_{k \in J_\pi} w_k \sqrt{x_k \sin^2(\psi_k)} K(N,N) \right\} \Gamma^{1/2} \qquad (4.45a)$$

$$P_{e,\text{H-S/MRC}} \approx \sum_{k=1}^K \frac{w_k \eta_k}{2\pi} - \left\{ \sum_{k \in J_\pi} w_k \sqrt{x_k \sin^2(\psi_k)} K(L,N) \right\} \Gamma^{1/2} \qquad (4.45b)$$

where $K(L,N)$ is defined as

$$K(L,N) \triangleq \frac{1}{2\pi} \int_0^\infty \left\{ 1 - \left[\frac{u^2}{u^2 + 1} \right]^L \prod_{n=L+1}^N \left[\frac{u^2}{\frac{L}{n} + u^2} \right] \right\} du. \qquad (4.46)$$

Substituting (4.45a) and (4.45b) in (4.1) and solving for the SNR penalty β we get the asymptotic SNR penalty, β_L^A, valid for small values of SNR as

$$\beta_L^A = \left[\frac{K(N,N)}{K(L,N)} \right]^2. \qquad (4.47)$$

As can be seen from (4.47), β_L^A depends only on L and N and is independent of the two dimensional signalling constellation and the value of SNR, Γ.

4.5.2 Asymptotic Penalty for Large SNR

To obtain the asymptotic penalty for large SNR, we obtain the asymptotic expansion of (3.30) and (3.32). A series of the form

$$c_0 + \frac{c_1}{x} + \frac{c_2}{x^2} + \cdots, \quad (c_0, c_1, \cdots \text{constant}) \tag{4.48}$$

is called an asymptotic expansion of a function $f(x)$ which is defined for every sufficiently large value of x if, for every fixed $n = 0, 1, 2, \cdots$

$$[f(x) - (c_0 + \frac{c_1}{x} + \frac{c_2}{x^2} + \cdots + \frac{c_n}{x^n})]x^n \to 0 \tag{4.49}$$

as $x \to \infty$ [42]. If $f(x)$ has an asymptotic expansion, its coefficients are unique and are given by [42]

$$c_0 = \lim_{x \to \infty} f(x) \tag{4.50a}$$

$$c_1 = \lim_{x \to \infty} (f(x) - c_0)x \tag{4.50b}$$

$$\vdots \tag{4.50c}$$

Let $c_{n,\text{MRC}}$ and $c_{n,\text{H-S/MRC}}$ denote the coefficients of the asymptotic expansions for (3.30) and (3.32), respectively. The first non-zero coefficients in the asymptotic expansions of (3.30) and (3.32) are

$$c_{N,\text{MRC}} = \sum_{k=1}^{K} \frac{w_k}{2\pi} \int_0^{\eta_k} g_k^N(\theta) d\theta \tag{4.51}$$

and

$$c_{N,\text{H-S/MRC}} = \left[\frac{N!}{L!L^{N-L}} \right] \sum_{k=1}^{K} \frac{w_k}{2\pi} \int_0^{\eta_k} g_k^N(\theta) d\theta \tag{4.52}$$

respectively. So for large SNR, (3.30) and (3.32) can be well approximated by

$$P_{e,\text{asy}}^{\text{MRC}} = \sum_{k=1}^{K} \frac{w_k}{2\pi\Gamma^N} \int_0^{\eta_k} g_k^N(\theta) d\theta \tag{4.53a}$$

50

and

$$P_{e,asy}^{\text{H-S/MRC}} = \left[\frac{N!}{L!L^{N-L}}\right] \sum_{k=1}^{K} \frac{w_k}{2\pi\Gamma^N} \int_0^{\eta_k} g_k^N(\theta)d\theta. \tag{4.53b}$$

Substituting (4.53a) and (4.53b) in (4.1) and solving for the SNR penalty β we get the asymptotic SNR penalty, β_U^A, valid for large values of SNR as

$$\beta_U^A = \left(\frac{N!}{L!L^{N-L}}\right)^{\frac{1}{N}}. \tag{4.54}$$

Note that (4.54), is equal to the upper bound derived in (4.19).

4.6 Numerical Examples

Table 4.1 gives some representative values of the lower and upper bounds on the SNR penalty. One can see that the maximum difference between the bounds is less than 0.85 dB. As one can expect for fixed values of L, the penalty increases as N increases. Fig. 4.1 [15] shows that the difference between β_L and β_U becomes negligible as N is increased. This is also shown in Fig. 4.2 in which the ratio β_U/β_L is plotted as a function of N, for various L [15]. One can see that the ratio approaches one (0 dB), for values of L close to N. Table 4.2 shows β_L and β_L^A for all values of $(L,N) \leq 12$. The difference between the β_L and β_L^A is typically in the second or third significant digit. Hence, β_L is an excellent approximation to β_L^A and little is lost in assessing the performance of a practical system using the rigorous bound, β_L. In the following, we show that the SEP of H-S/MRC can be easily estimated using the results of Theorem 3. We consider the performance of several 8-ary and 16-ary two-dimensional signalling constellations.

4.6.1 8-ary Modulation Formats

The 8-ary signal sets considered are 8PSK, the 8-ary optimum in AWGN, rectangular, triangular, (4,4) and (1,7) [18]. Fig. 4.3 shows the SEP for coherent detection of these

51

constellations with 4 branch MRC and 2-8/MRC. Note that the order of performance in H-S/MRC is the same as that of MRC. The exact SNR penalty as a function of SNR, obtained by numerically inverting the curves in Fig. 4.3 is depicted in Fig. 4.4 together with β_L, β_U and β_L^A for $(L,N) = (2,8)$. Fig. 4.4 confirms the validity of Theorem 3.

4.6.2 16-ary and Higher Order Modulation Formats

The 16-ary signal sets considered are 16-QAM, 16-star QAM, rotated (8,8) and the 16-ary optimum in AWGN. In Chapter 3 we found optimum ring ratios for the performance of ring constellations such as (4,4), (8,8) and 16-star QAM. Fig. 4.5 shows the exact SEP and the lower and upper bounds to the SEP for coherent detection of 16 star-QAM with $L = 1,4,8$ and $N = 16$. The lower and upper bounds are obtained from the SEP of 16-branch MRC operating at $\beta_L^{-1}\Gamma$ and $\beta_U^{-1}\Gamma$ respectively. The exact SNR penalty as a function of SNR, obtained by numerically inverting the curves in Fig. 4.5, is depicted in Fig. 4.6 together with β_L, β_U and β_L^A for $(L,N) = (4,16)$. Fig. 4.7 shows the the exact SNR penalty versus the SEP for $(L,N) = (4,16)$. In Fig. 4.8, the SEP's of the signalling constellations mentioned above, are plotted for $(L,N) = (2,6)$. It can be seen that again the relative performance of the constellations with H-S/MRC is the same as for MRC. The SNR penalty for these constellations for $(L,N) = (2,6)$ is plotted in Fig. 4.9.

Finally, we consider the SEP performance of MQAM for different values of M. The exact SEP for coherent detection of MQAM, for $(L,N) = (4,8)$ and $M = 4,16,64$ is depicted in Fig. 4.10. For each value of M, the lower and upper bounds are obtained from the SEP of 8-branch MRC operating at $\beta_L^{-1}\Gamma$ and $\beta_U^{-1}\Gamma$, respectively. In Fig. 4.11, the exact SNR penalty obtained by numerically inverting the curves in Fig. 4.10 together with β_L, β_L^A and β_U is depicted as a function of SNR. Note that Fig. 4.11 clearly shows that the SNR penalty is not, in general, a monotonic function of the SNR, Γ.

Table 4.1. Lower Bounds and Upper Bounds $\{\beta_L, \beta_U\}$ of the SNR Penalty in dB

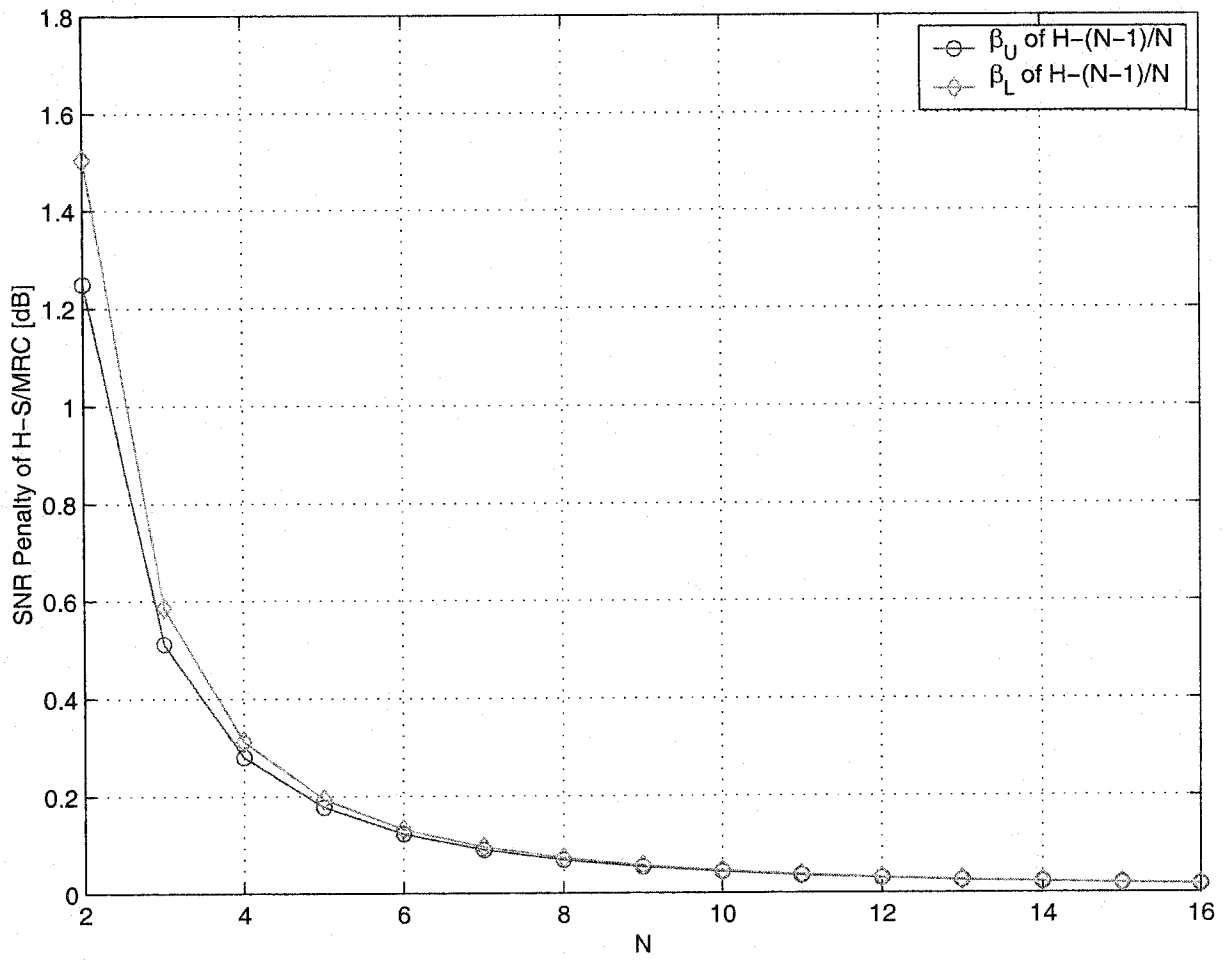| L	N									
	3	4	5	6	7	8	9	10	11	12
2	0.5115 0.5870	1.0146 1.1928	1.4671 1.7501	1.8709 2.2536	2.2333 2.7089	2.5613 3.1229	2.8605 3.5017	3.1355 3.8505	3.3898 4.1735	3.6264 4.4742
3	0 0	0.2803 0.3123	0.6048 0.6936	0.9241 1.0797	1.2258 1.4511	1.5077 1.8022	1.7704 2.1321	2.0156 2.4418	2.2451 2.7327	2.4606 3.0067
4		0 0	0.1773 0.1938	0.4043 0.4550	0.6420 0.7372	0.8764 1.0213	1.1023 1.2992	1.3179 1.5672	1.5230 1.8241	1.7180 2.0697
5			0 0	0.1223 0.1320	0.2901 0.3219	0.4741 0.5368	0.6616 0.7608	0.8470 0.9857	1.0274 1.2074	1.2017 1.4236
6				0 0	0.0895 0.0956	0.2187 0.2398	0.3654 0.4089	0.5189 0.5898	0.6737 0.7755	0.8270 0.9617
7					0 0	0.0684 0.0725	0.1709 0.1857	0.2906 0.3220	0.4186 0.4712	0.5500 0.6270
8						0 0	0.0539 0.0568	0.1373 0.1481	0.2368 0.2603	0.3453 0.3854
9							0 0	0.0436 0.0457	0.1127 0.1208	0.1969 0.2149
10								0 0	0.0360 0.0376	0.0942 0.1005
11									0 0	0.0303 0.0315
12										0 0

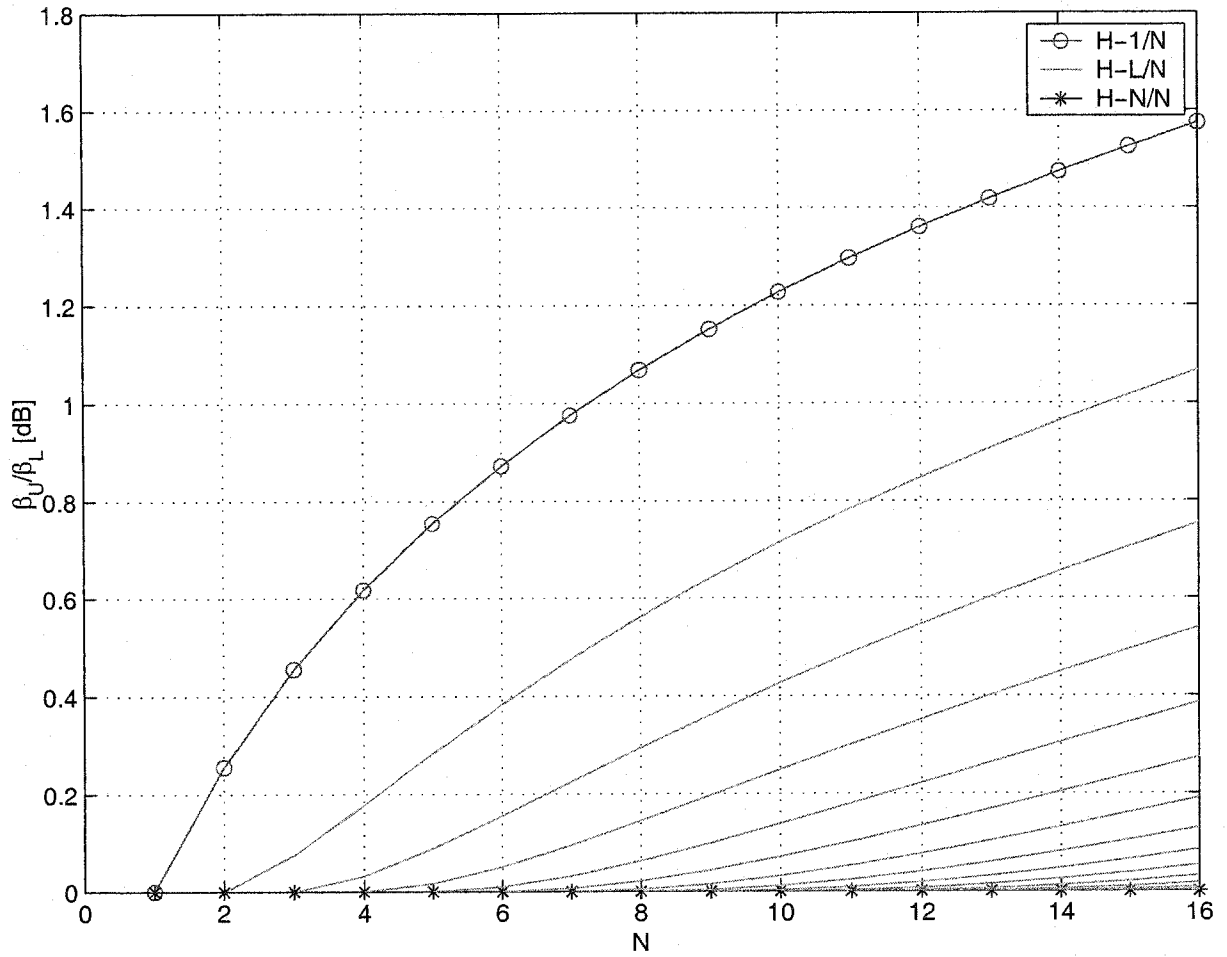Figure 4.1. The penalty incurred by dropping one branch in an H-S/MRC diversity system.

Figure 4.2. The ratio β_U/β_L in dB as a function of N for various L. The highest curve is for $L = 1$, and L decreases monotonically to the lowest curve with $L = 16$.

Table 4.2. Lower Bounds and Asymptotic values $\{\beta_L, \beta_L^A\}$ of the SNR Penalty in dB

					N					
L	3	4	5	6	7	8	9	10	11	12
2	0.5115	1.0146	1.4671	1.8709	2.2333	2.5613	2.8605	3.1355	3.3898	3.6264
	0.5203	1.0312	1.4894	1.8973	2.2628	2.5930	2.8938	3.1701	3.4254	3.6627
3	0	0.2803	0.6048	0.9241	1.2258	1.5077	1.7704	2.0156	2.2451	2.4606
	0	0.2832	0.6116	0.9342	1.2388	1.5230	1.7876	2.0343	2.2650	2.4815
4		0	0.1773	0.4043	0.6420	0.8764	1.1023	1.3179	1.5230	1.7180
		0	0.1786	0.4076	0.6473	0.8837	1.1112	1.3283	1.5347	1.7307
5			0	0.1223	0.2901	0.4741	0.6616	0.8470	1.0274	1.2017
			0	0.1230	0.2919	0.4773	0.6661	0.8526	1.0341	1.2094
6				0	0.0895	0.2187	0.3354	0.5189	0.6737	0.8270
				0	0.0899	0.2198	0.3673	0.5218	0.6775	0.8316
7					0	0.0684	0.1709	0.2906	0.4186	0.5500
					0	0.0686	0.1715	0.2919	0.4206	0.5527
8						0	0.0539	0.1373	0.2368	0.3453
						0	0.0541	0.1377	0.2377	0.3467
9							0	0.0436	0.1127	0.1969
							0	0.0437	0.1130	0.1975
10								0	0.0360	0.0942
								0	0.0361	0.0944
11									0	0.0303
									0	0.0303
12										0
										0

Figure 4.3. The symbol error probability as a function of average SNR per branch for coherent detection of six 8-ary constellations with H-S/MRC for $N = 8$ and $L = 2$.
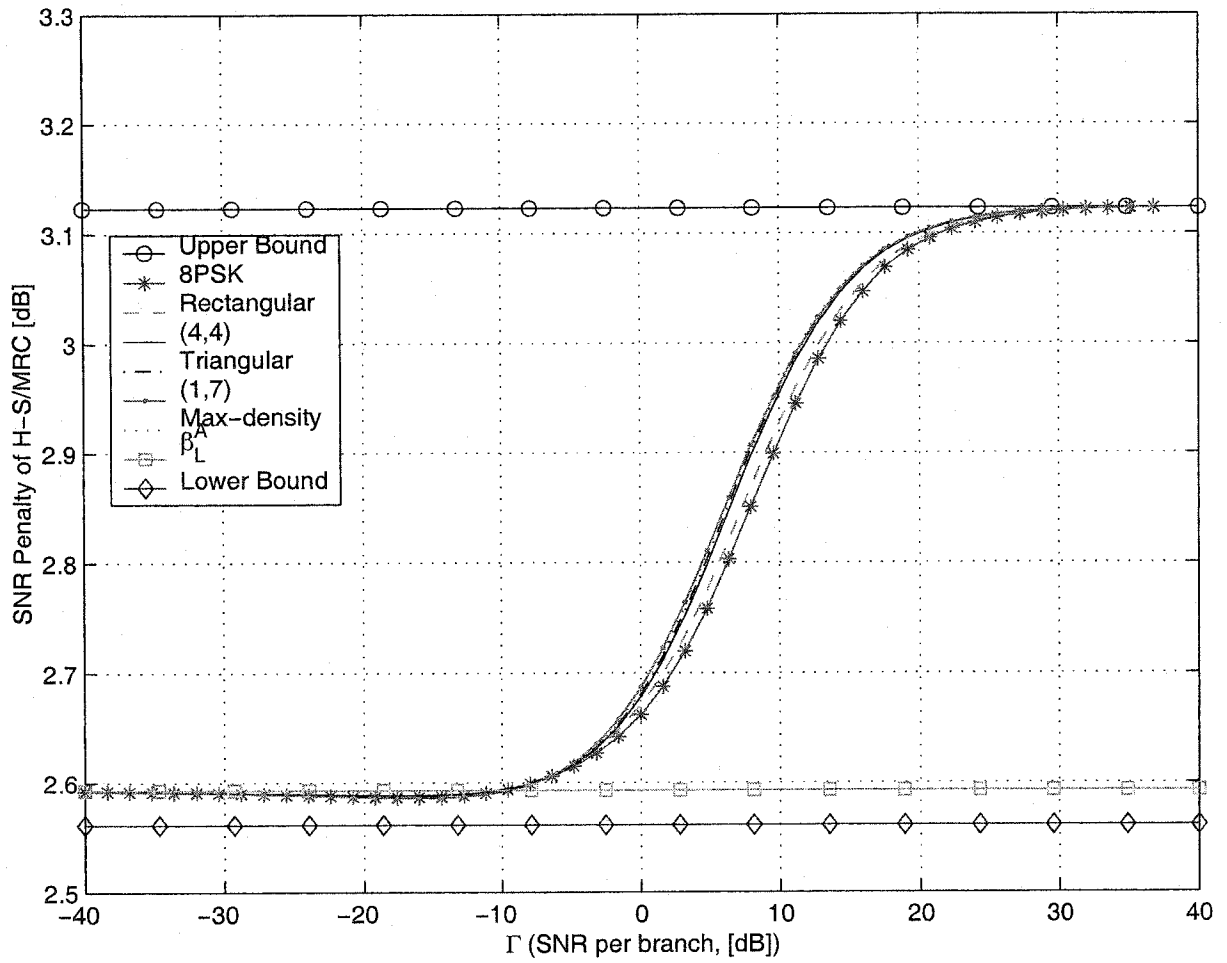
Figure 4.4. The SNR penalty as a function of SNR of six 8-ary constellations with H-S/MRC for $(L, N) = (2, 8)$.
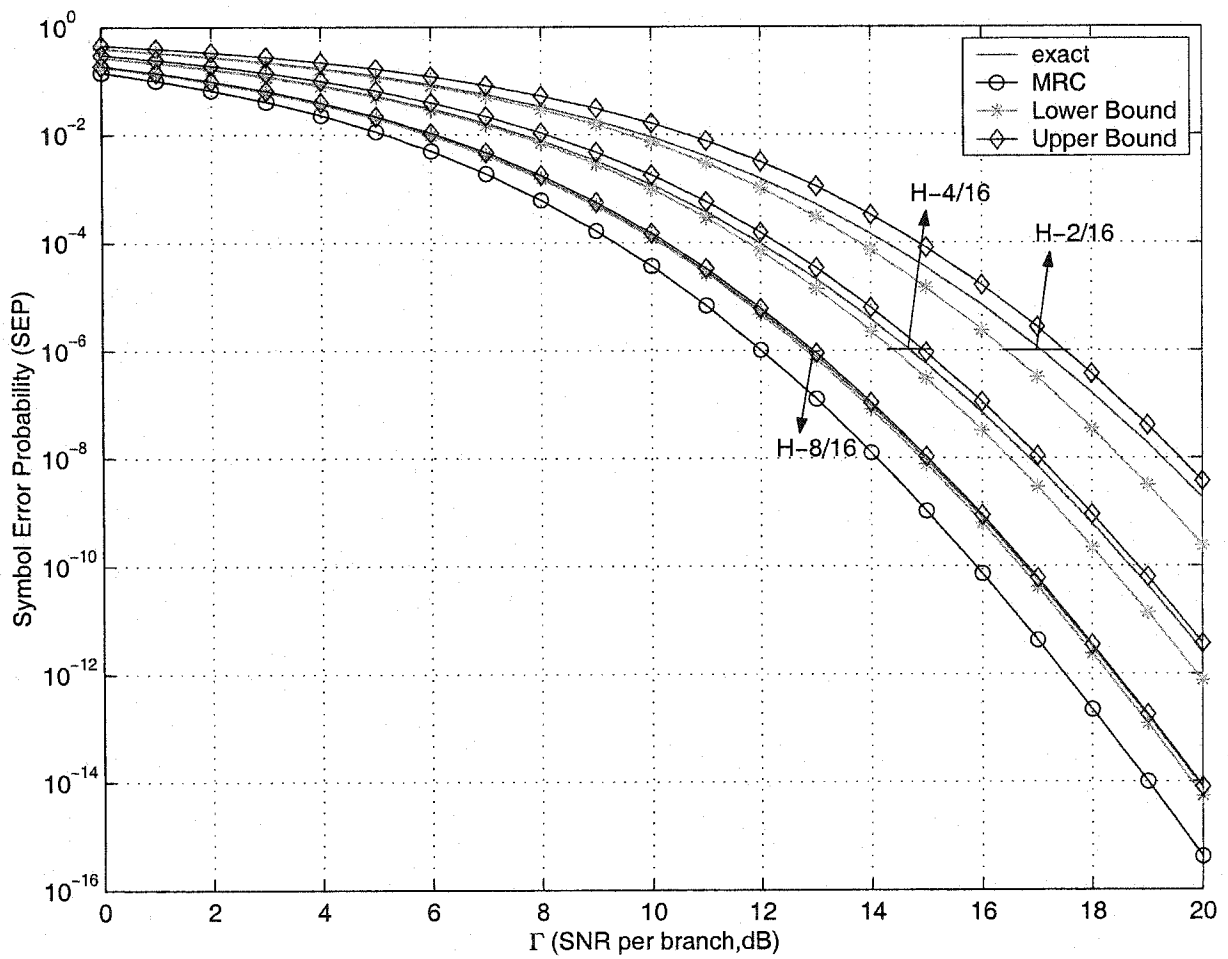
Figure 4.5. The symbol error probability as a function of average SNR per branch for coherent detection of 16-star QAM with H-S/MRC for $N = 16$ and $L = 1, 4, 8$. The upper and lower bounds are obtained from MRC results according to Theorem 3.

Figure 4.6. The SNR penalty as a function of SNR of 16-star QAM with H-S/MRC for $(L,N) = (4,16)$.
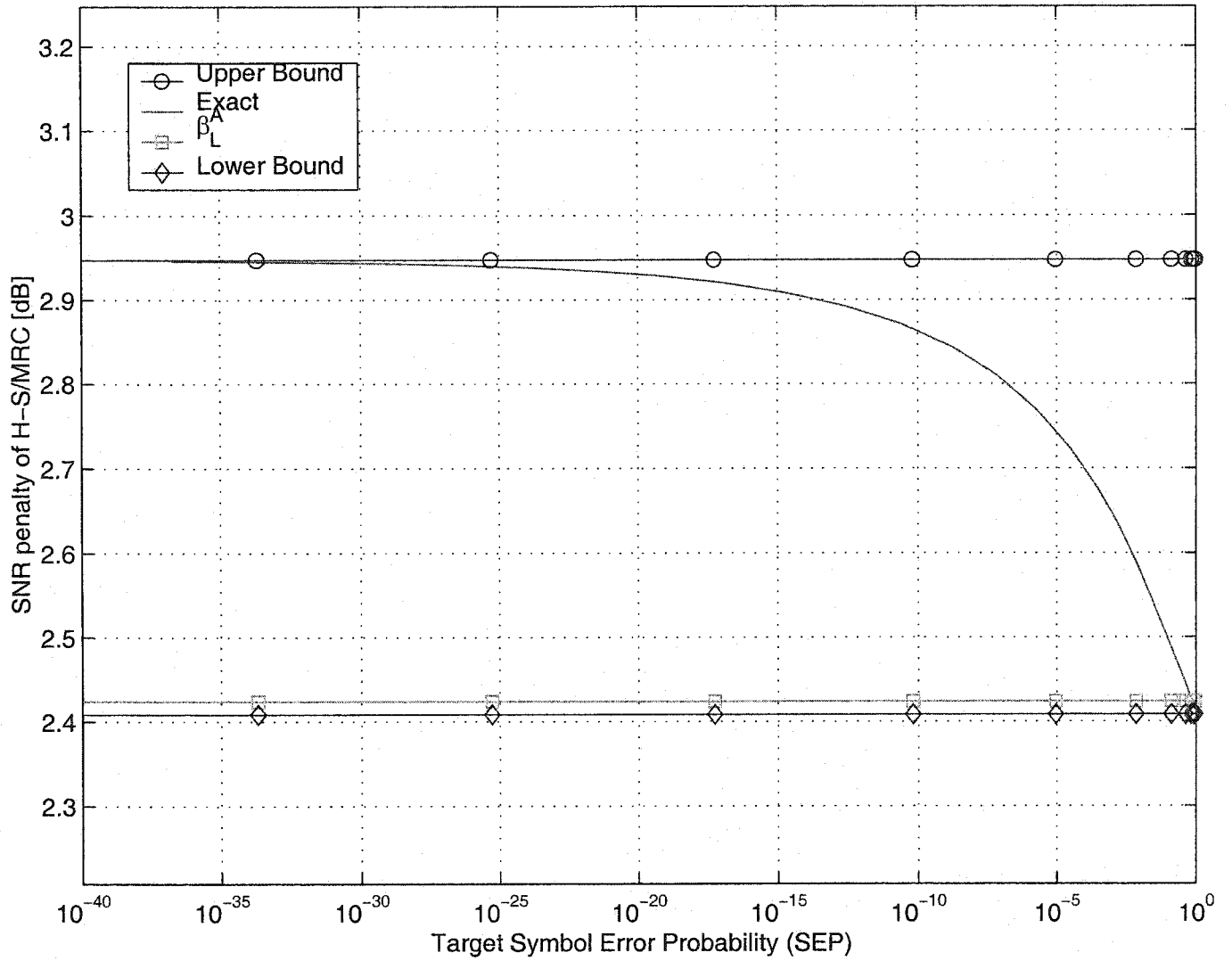
Figure 4.7. The SNR penalty as a function of SEP of 16-star QAM with H-S/MRC for $(L,N) = (4,16)$.
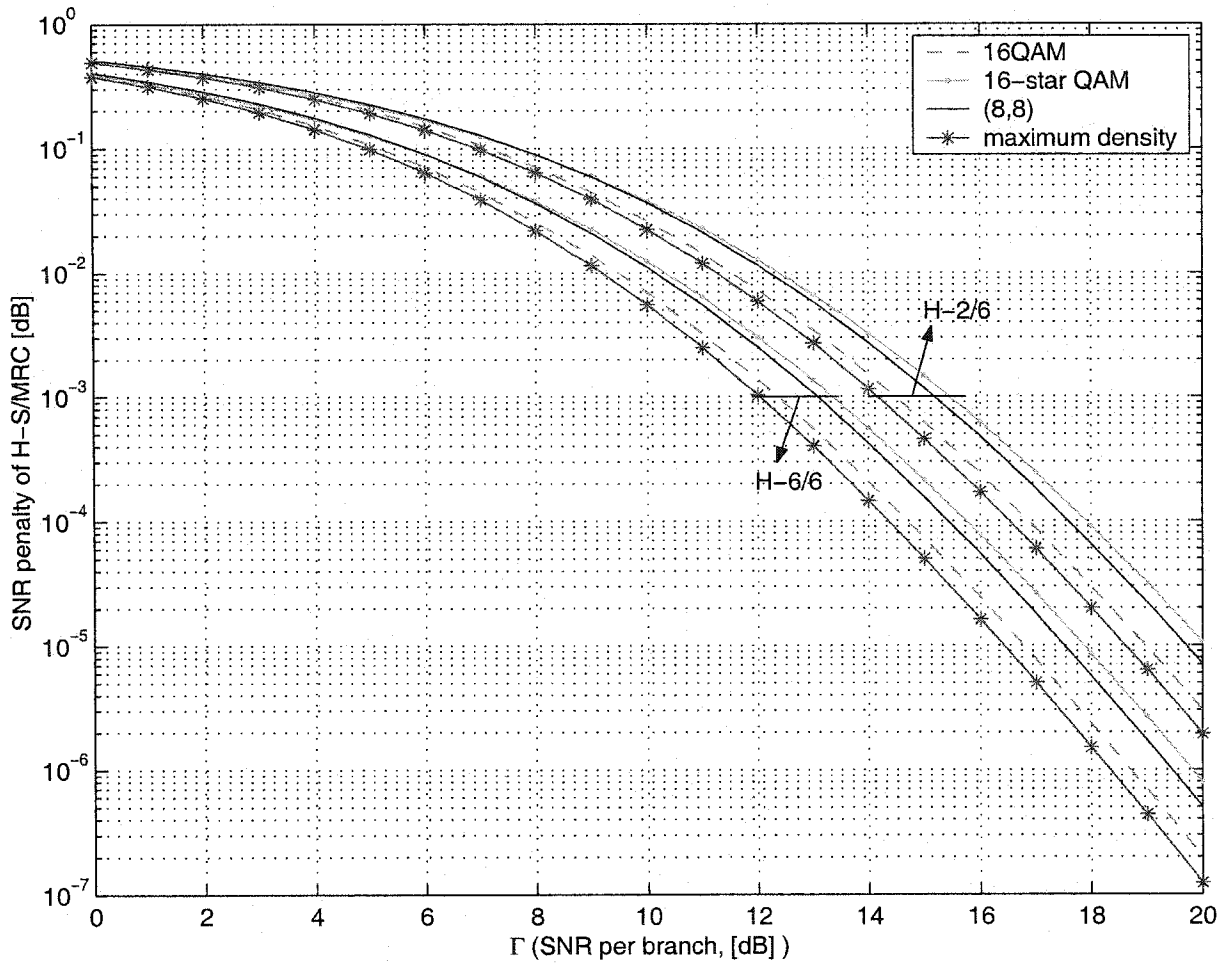
Figure 4.8. The symbol error probability as a function of average SNR per branch for coherent detection of 16-star QAM, 16QAM, (8,8) and 16-ary maximum density with H-S/MRC for $N = 6$ and $L = 2,6$. The upper and lower bounds are obtained from MRC results according to Theorem 3.
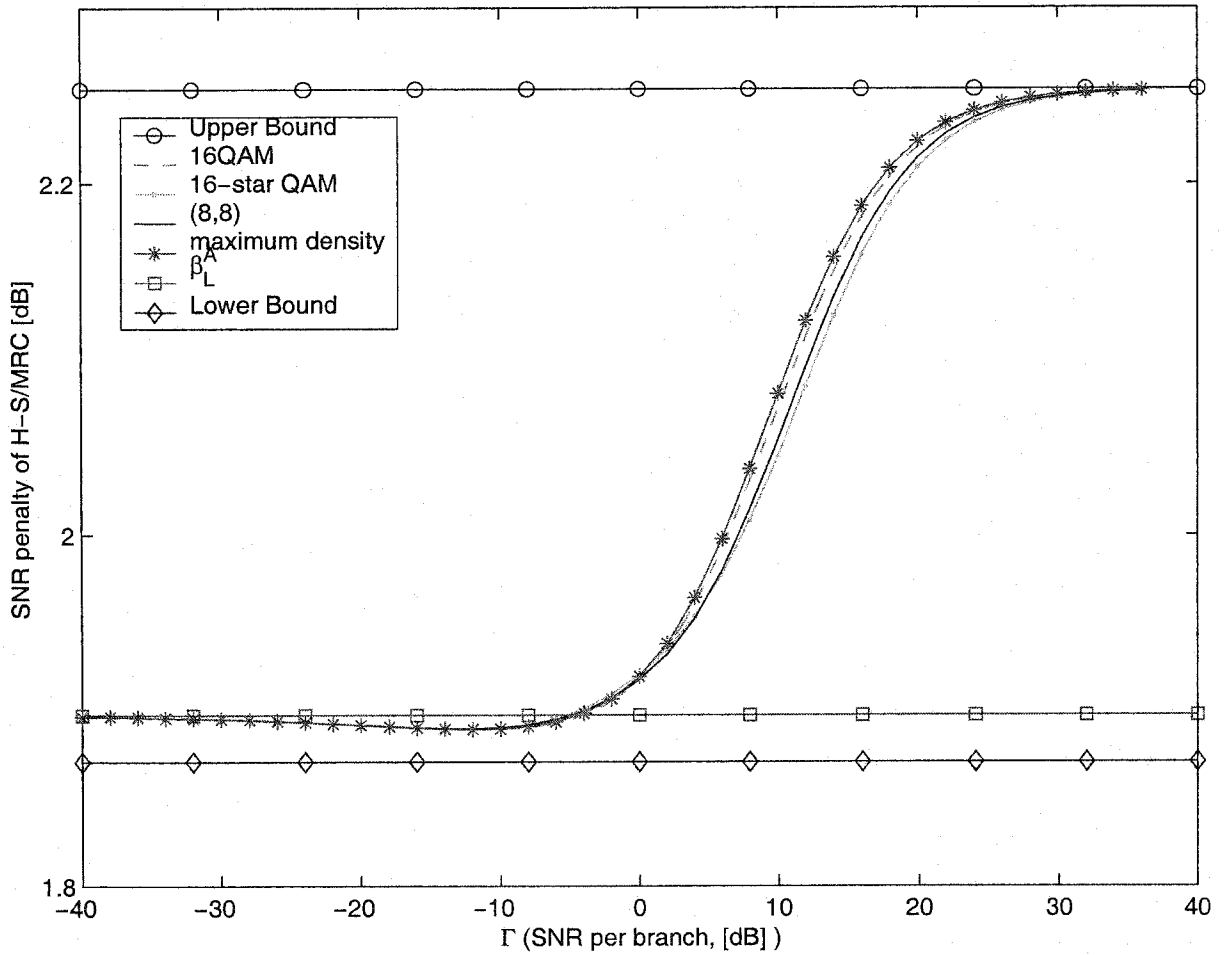
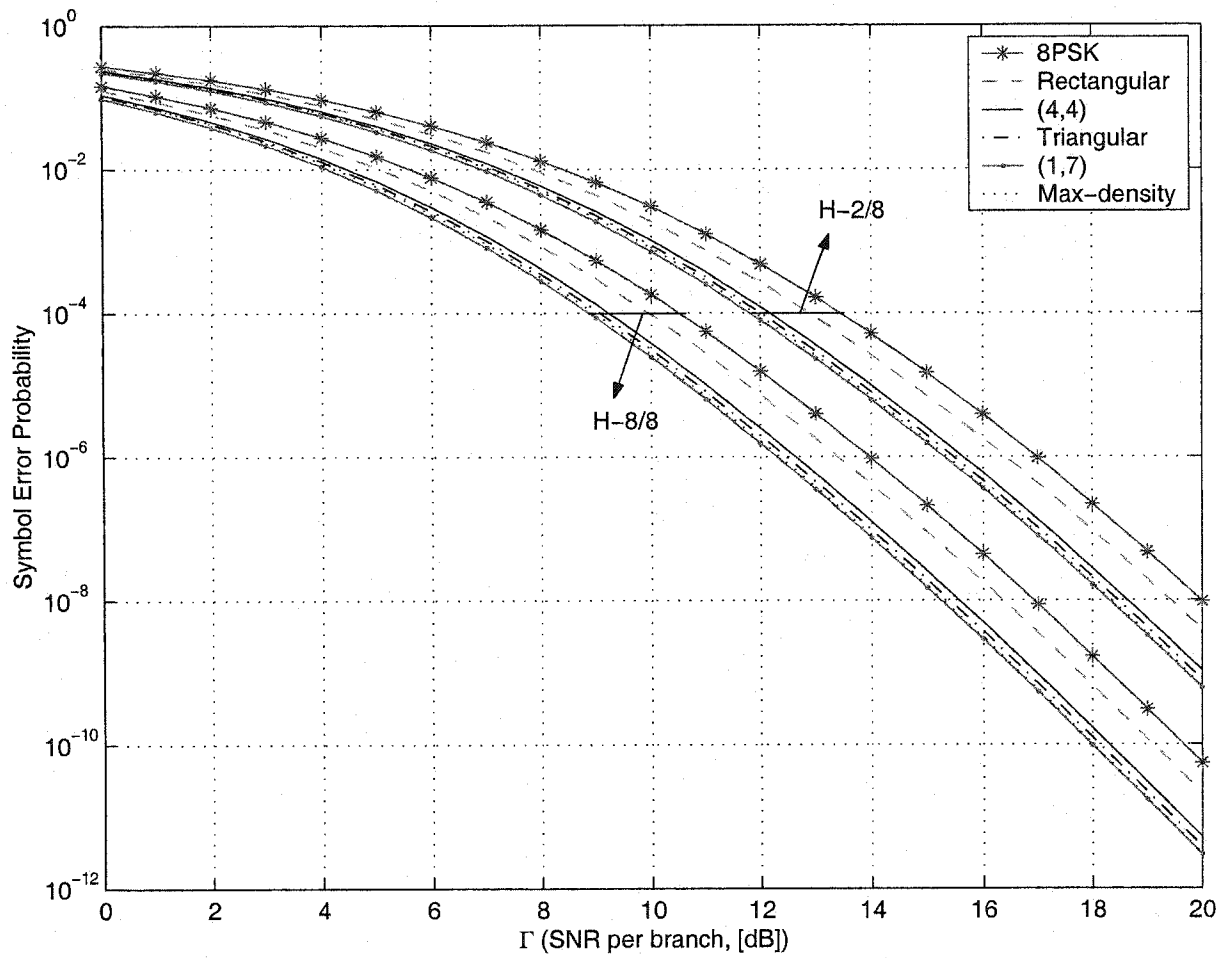Figure 4.9. The SNR penalty as a function of SNR of 16-star QAM, 16QAM, (8,8) and 16-ary maximum density with H-S/MRC for $(L,N) = (2,6)$.
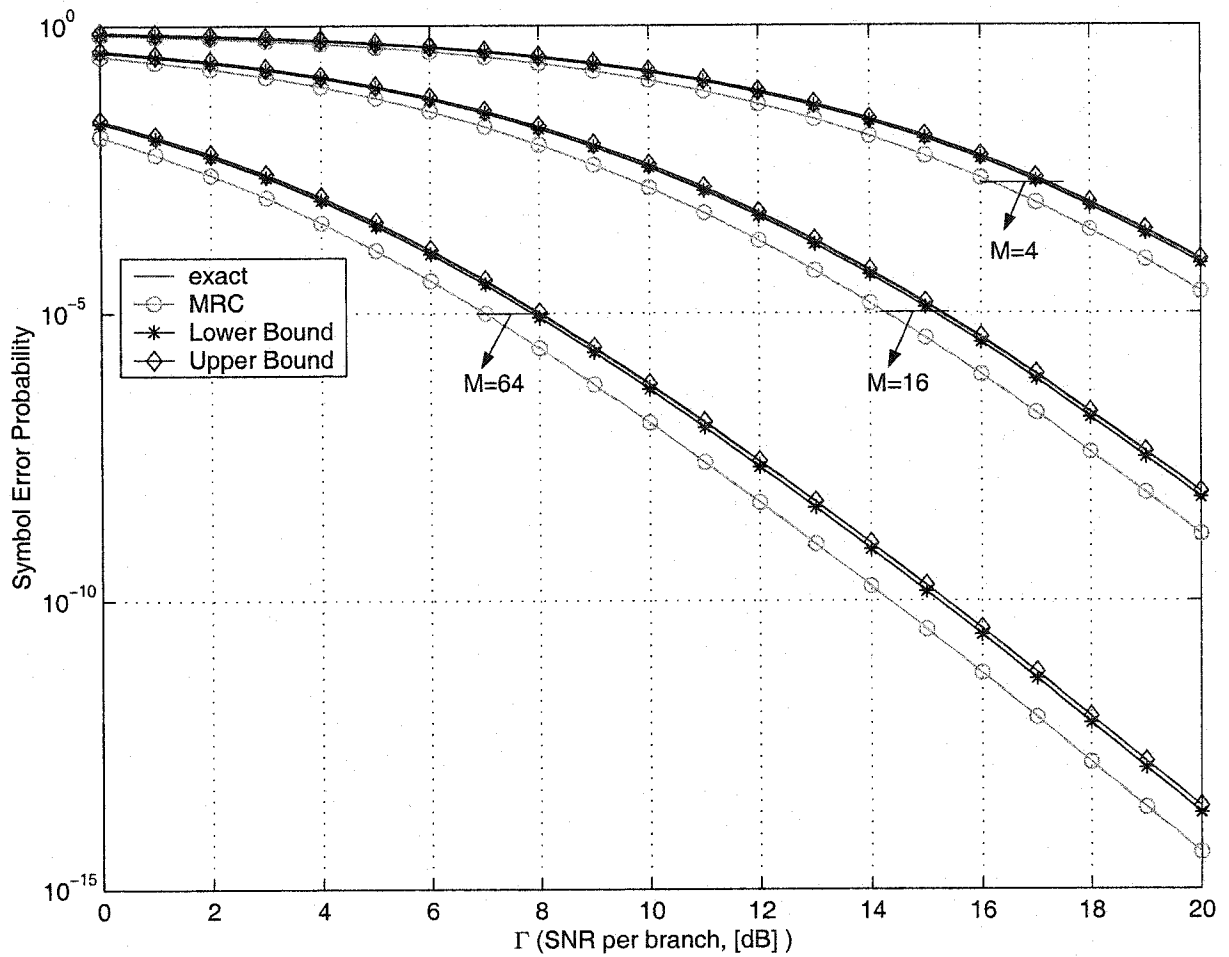
Figure 4.10. The symbol error probability as a function of average SNR per branch for coherent detection of QAM with H-S/MRC and $M = 4, 16, 64$ and for $(L, N) = (4, 8)$. The upper and lower bounds are obtained from MRC results according to Theorem 3.
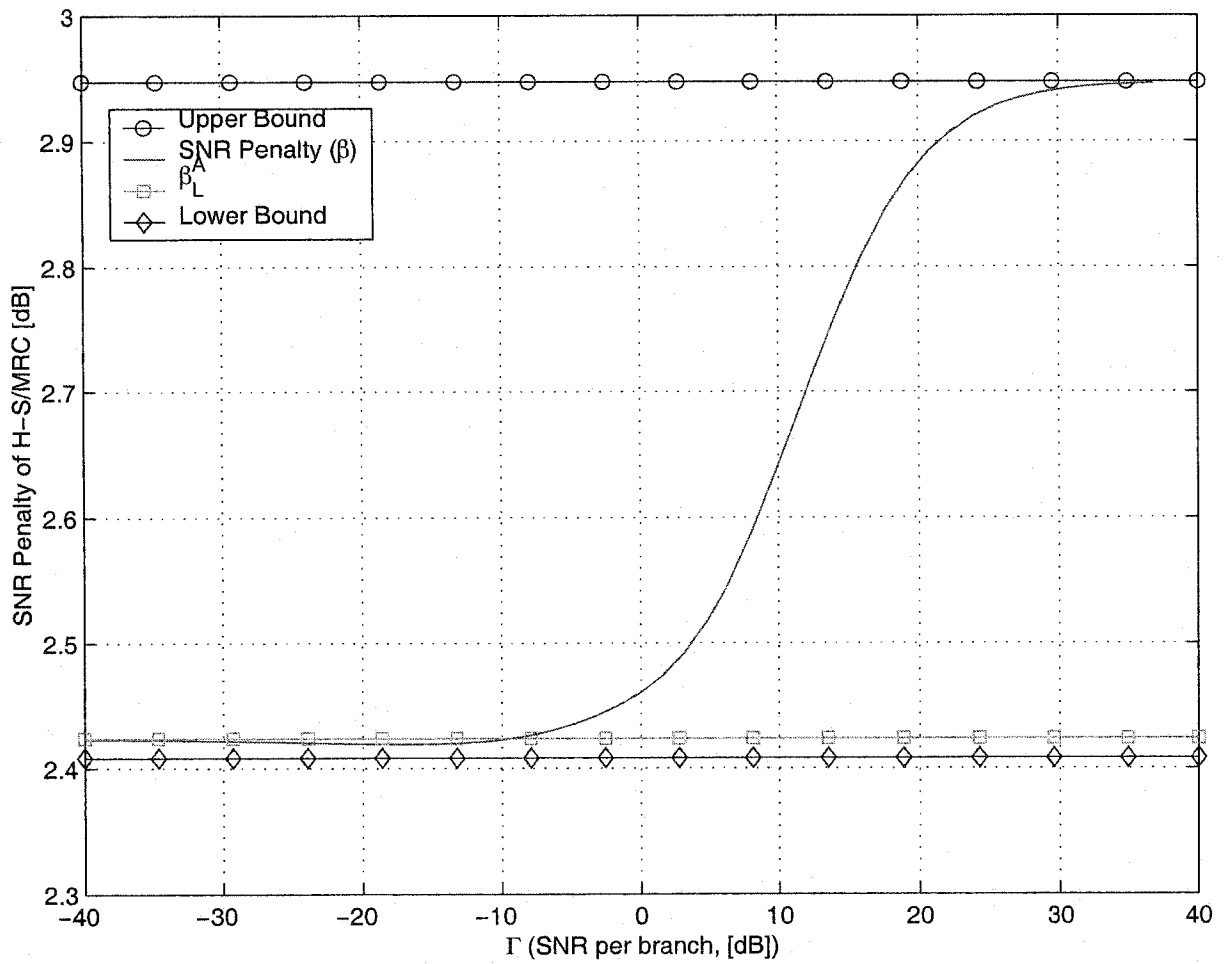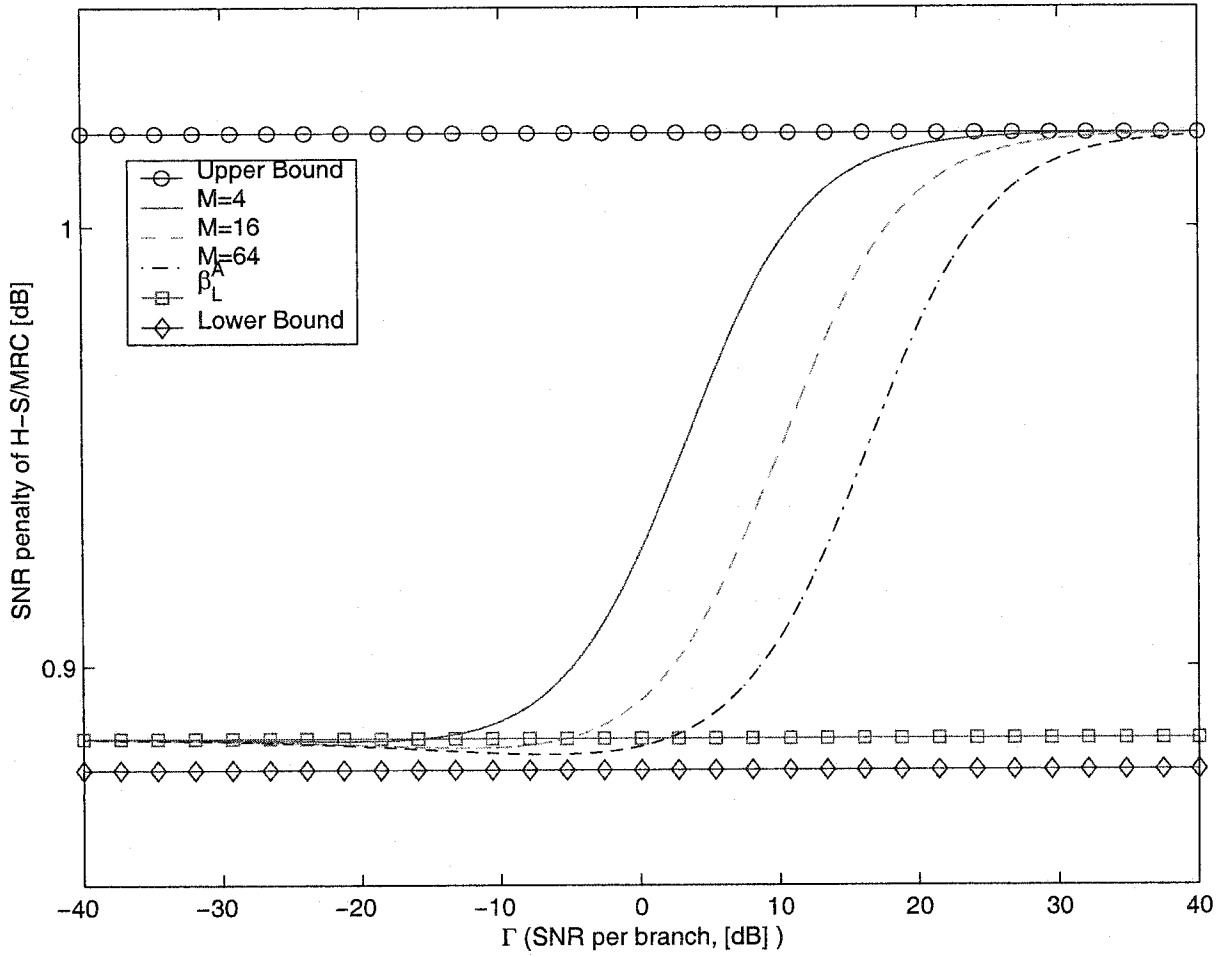
Figure 4.11. The SNR penalty as a function of SNR of MQAM with H-S/MRC for $(L, N) = (4, 8)$ and $M = 4, 16, 64$.

4.7 Conclusions

In this chapter, we derived new simple lower and upper bounds to the SNR penalty of H-S/MRC used with any two-dimensional signalling constellations with polygonal decision regions. The bounds are expressed as closed-form expressions and are only dependent of L and N. Using these bounds the SEP of H-S/MRC, $P_{e,\text{H-S/MRC}}(\Gamma)$, can be approximated to a high degree of accuracy using the SEP of MRC operating at $P_{e,\text{MRC}}(\beta_L^{-1}\Gamma)$ and $P_{e,\text{MRC}}(\beta_U^{-1}\Gamma)$, for small and large values of SNR, respectively. Analytical expressions for the SNR penalties of H-S/MRC were derived for small and large values of SNR, respectively. We showed that the difference between the asymptotic SNR for small SNR and the lower bound are typically in the second or third significant digit, so little is lost by assessing the performance of a system using the lower bound for small SNR. The asymptote for large SNR was shown to be equal to the upper bound.

Chapter 5

Penalty of Hybrid Diversity with Arbitrary Modulation in Rayleigh Fading

In the previous chapter, we derived the asymptotes for the SNR penalty for small and large SNR, respectively. In this chapter we generalize the results of Chapter 5 to arbitrary modulations.

5.1 Asymptotic Penalty for Small SNR

In the following, we find the asymptotic SNR penalty for small values of SNR for arbitrary modulations. Recall that the SEP of the GDC system is given by

$$P_{e,\text{GDC}} = \mathbb{E}_{\gamma_{\text{GDC}}}\{\Pr(e|\gamma_{\text{GDC}})\} = \int_0^\infty \Pr(e|\gamma_{\text{GDC}})f_{\gamma_{GDC}}(\gamma)d\gamma \tag{5.1}$$

where $\Pr(e|\gamma_{\text{GDC}})$ is the conditional SEP in an additive white Gaussian noise (AWGN) channel (no fading). We assume that $\Pr(e|\Gamma\sum_{n=1}^N a_n V_n)$ in (3.25) has a series expansion in terms of $\sqrt{\Gamma}$, so it can be written as

$$\Pr(e|\Gamma\sum_{n=1}^N a_n V_n) = \sum_{i=0}^\infty c_i(\sqrt{\Gamma(a_1 v_1 + \cdots + a_n v_n)})^i. \tag{5.2}$$

67

Substituting (5.2) in (3.25) and using (3.22) and (3.29), one obtains formally

$$P_{e,\text{GDC}} = \sum_{i=0}^{\infty} c_i \left\{ \int_0^\infty \int_0^\infty \cdots \int_0^\infty \sqrt{(a_1 v_1 + \cdots + a_N v_N)^i} e^{-(v_1 + \cdots + v_N)} dv_1 \cdots dv_N \right\} \sqrt{\Gamma^i}.$$

$$(5.3)$$

For small values of SNR, Γ, (5.3) can be approximated as

$$P_{e,\text{GDC}} \cong c_0 + c_1 \left\{ \int_0^\infty \int_0^\infty \cdots \int_0^\infty \sqrt{a_1 v_1 + \cdots + a_N v_N} e^{-(v_1 + \cdots + v_N)} dv_1 \cdots dv_N \right\} \sqrt{\Gamma}. \quad (5.4)$$

Using the results of Lemma 3 and Lemma 4 in Appendix B we can show that

$$\int_0^\infty \cdots \int_0^\infty \sqrt{a_1 v_1 + \cdots + a_N v_N} e^{-(v_1 + \cdots + v_N)} dv_1 \cdots dv_N =$$
$$\frac{1}{\sqrt{\pi}} \int_0^\infty \left(1 - \frac{u^{2N}}{(u^2 + a_1) \cdots (u^2 + a_N)} \right) du.$$

$$(5.5)$$

Substituting (5.5) in (5.4), we obtain a simplified expression for the SEP of the GDC system

for small values of SNR as

$$P_{e,\text{GDC}} \cong c_0 + \frac{c_1 \sqrt{\Gamma}}{\sqrt{\pi}} \int_0^\infty \left(1 - \frac{u^{2N}}{(u^2 + a_1) \cdots (u^2 + a_N)} \right) du. \quad (5.6)$$

Consequently, by substituting (3.29) and (3.31) in (5.6) we obtain the SEP for MRC and

H-S/MRC for small values of SNR, as

$$P_{e,\text{MRC}} \cong c_0 + \left[\frac{c_1}{\sqrt{\pi}} \int_0^\infty \left\{ 1 - \left[\frac{u^2}{u^2 + 1} \right]^N \right\} du \right] \sqrt{\Gamma} \quad (5.7)$$

and

$$P_{e,\text{H-S/MRC}} \cong c_0 + \left[\frac{c_1}{\sqrt{\pi}} \int_0^\infty \left\{ 1 - \left[\frac{u^2}{u^2 + 1} \right]^L \prod_{n=L+1}^N \left[\frac{u^2}{\frac{L}{n} + u^2} \right] \right\} du \right] \sqrt{\Gamma}, \quad (5.8)$$

respectively. Substituting (5.7) and (5.8) in (4.1) and solving for the SNR penalty β, one

obtains the asymptotic SNR penalty for small values of SNR, β_L^A, as

$$\beta_L^A = \left[\frac{K(N,N)}{K(L,N)} \right]^2 \quad (5.9)$$

where $K(L,N)$ is defined in (4.46). Note that asymptotic SNR penalty derived in (5.9) is

equal to the asymptotic SNR penalty derived in Chapter 4. Our derivation here proves that

the same low SNR penalty is incurred for all modulation formats, depending only on L and

N.

5.2 Asymptotic Penalty for Large SNR

In this section, we derive the asymptotic SNR penalty for large values of SNR. The asymptotic SEP for the GDC system can be expressed as [43]

$$P_{e_{asy}}^{\text{GDC}}(\Gamma) = \frac{\lambda_N}{\Gamma^N} \tag{5.10}$$

where

$$\lambda_N = \lim_{\Gamma \to \infty} [\Gamma^N P_{e,\text{GDC}}] \tag{5.11}$$

and $P_{e,\text{GDC}}$ is given in (3.25) and can be written as

$$P_{e,\text{GDC}} = \frac{1}{\Gamma^N \prod\limits_{n=1}^{N} a_n} \int_0^\infty \int_0^\infty \cdots \int_0^\infty \Pr(e|\sum_{n=1}^N u_n) \prod_{n=1}^N e^{-\frac{u_n}{\Gamma a_n}} du_1 \cdots du_N \tag{5.12}$$

using the change of variables $u_n = \Gamma v_n a_n$ in (3.25). Using Theorem 1 of [43] one can show that λ_N can be expressed as

$$\lambda_N = \frac{1}{\prod\limits_{n=1}^{N} a_n} \int_0^\infty \int_0^\infty \cdots \int_0^\infty \Pr(e|\sum_{n=1}^N u_n) du_1 \cdots du_N. \tag{5.13}$$

Substituting (5.13) in (5.10) one obtains

$$P_{e_{asy}}^{\text{GDC}} = \frac{1}{\Gamma^N \prod\limits_{n=1}^{N} a_n} \int_0^\infty \int_0^\infty \cdots \int_0^\infty \Pr(e|\sum_{n=1}^N u_n) du_1 \cdots du_N. \tag{5.14}$$

Consequently, the asymptotic SEP for MRC and H-S/MRC can be expressed as

$$P_{e_{asy}}^{\text{MRC}} = \frac{1}{\Gamma^N} \int_0^\infty \int_0^\infty \cdots \int_0^\infty \Pr(e|\sum_{n=1}^N u_n) du_1 \cdots du_N \tag{5.15}$$

and

$$P_{e_{asy}}^{\text{H-S/MRC}} = \frac{N!}{L! L^{N-L} \Gamma^N} \int_0^\infty \int_0^\infty \cdots \int_0^\infty \Pr(e|\sum_{n=1}^N u_n) du_1 \cdots du_N, \tag{5.16}$$

respectively. Substituting (5.15) and (5.16) in (4.1) and solving for β, the asymptotic SNR penalty for large SNR, β_U^A, is obtained as

$$\beta_U^A = \left(\frac{N!}{L! L^{N-L}} \right)^{\frac{1}{N}}. \tag{5.17}$$

69

Note that the asymptotic SNR penalty for large values of SNR, derived in (5.17) is the same as the asymptotic SNR penalty derived in Chapter 4 for two-dimensional signalling with polygonal decision regions. The derivation of the SNR penalty for large SNR presented here, is independent of the modulation format and depends on L and N only.

5.3 Numerical Examples

In this section, some numerical examples are presented. Based on the examples, we also conjecture that previously published lower and upper bounds valid for two-dimensional signalling with polygonal decision regions are also valid for other modulation formats. In Chapter 4, a lower bound was derived to the SNR penalty of hybrid diversity with two-dimensional signalling as

$$\beta_L = \frac{N}{L\left(1 + \sum\limits_{n=L+1}^{N} \frac{1}{n}\right)}. \tag{5.18}$$

In the examples, we will see that (5.18) appears also to be a bound to the SNR penalty of hybrid diversity with higher order modulation formats. Also, we found an upper bound to the SNR penalty of H-S/MRC with two-dimensional signalling as

$$\beta_U = \left(\frac{N!}{L!L^{N-L}}\right)^{\frac{1}{N}}. \tag{5.19}$$

Note that (5.19) is equal to the asymptotic penalty for large SNR, derived in (5.17) and as we will see in the examples it appears to be a tight upper bound to the SNR penalty. Figs. 5.1-5.4 show the SEP of coherent detection of 3-ary and 4-ary orthogonal signalling and 6-ary and 8-ary biorthognal signalling for various L and N. The SEP's are calculated using new analytical expressions for the error probability of these constellations in AWGN channels [14]. Also the SEP of MRC operating at SNR values scaled by β_L and β_U^A are plotted for each value of L and N. One can see in Figs. 5.1-5.4 that the SEP of hybrid

diversity, $P_{e,\text{H-S/MRC}}(\Gamma)$, is lower and upper bounded by $P_{e,\text{MRC}}(\beta_L^{-1}\Gamma)$ and $P_{e,\text{MRC}}(\beta_U^{A-1}\Gamma)$, respectively. Note also that as L approaches N the differences between the SEP of H-S/MRC, and the conjectured bounds become smaller. While the 4-ary and 8-ary schemes are more practical, the 3-ary and 6-ary schemes represent tests of our conjectures on more "unconventional" modulation formats. In Fig. 5.5, the exact penalty of 3-ary orthogonal signalling is plotted together with β_L^A, β_L and β_U^A, for $(L, N) = (8, 16)$. The exact SNR penalty is obtained by numerically inverting the curves in Fig. 5.1. The exact SNR penalty of 4-ary signalling, 6-ary biorthogonal and 8-ary biorthogonal signalling are obtained in a manner similar to that of 3-ary signalling for various L and N and are plotted in Figs. 5.6, 5.7 and 5.8, respectively. Note that in Figs. 5.5-5.8, (5.9) is the asymptotic penalty for small SNR and (5.18) is a lower bound to the SNR penalty for these examples. The asymptotic penalty for large SNR (5.19) appears to be an upper bound to the SNR penalty.
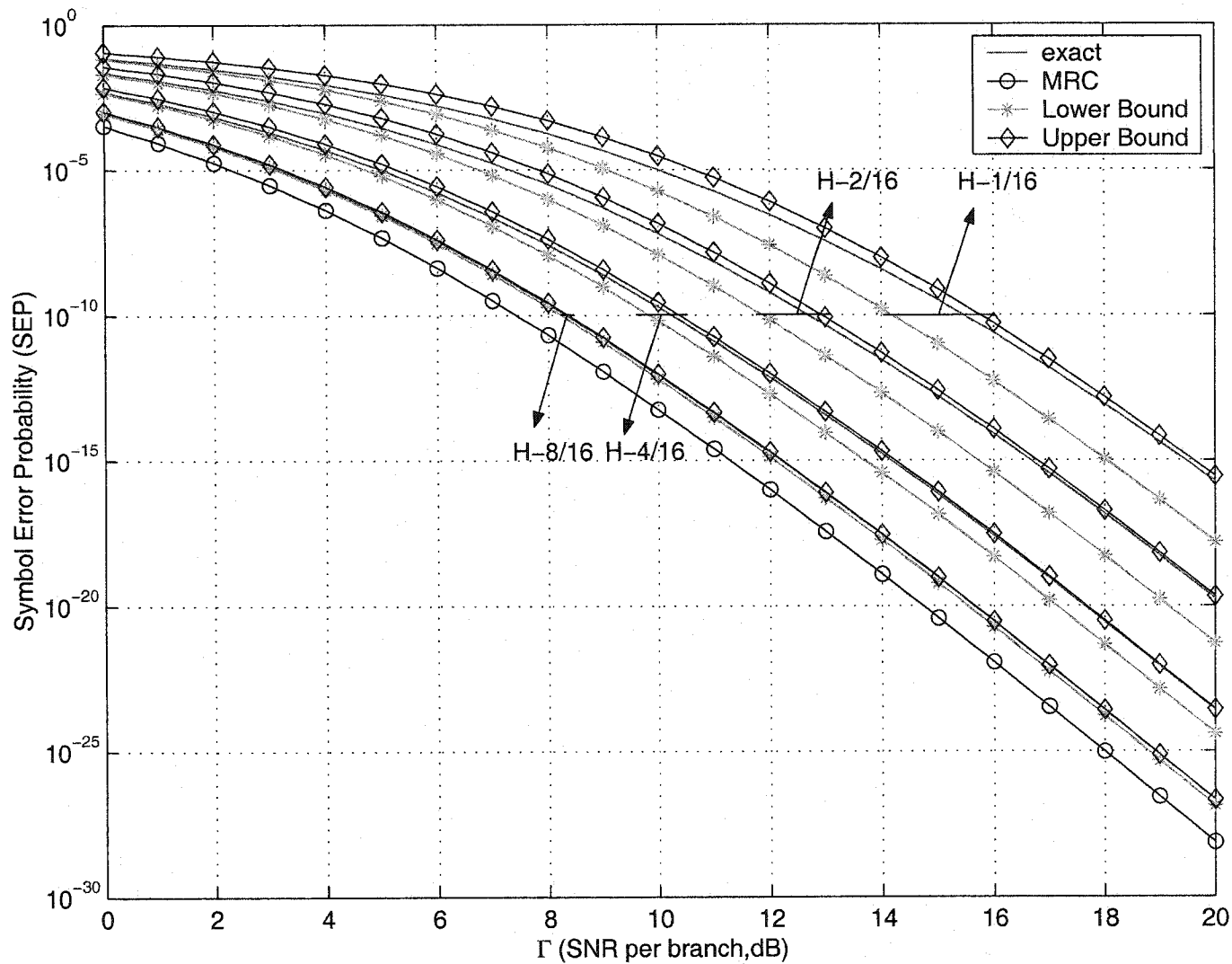
Figure 5.1. The symbol error probability as a function of average SNR per branch for coherent detection of 3-ary orthogonal signalling with H-S/MRC for $L = 1, 2, 4, 8$ and $N = 16$. The conjectured lower and upper bounds are plotted for comparison.
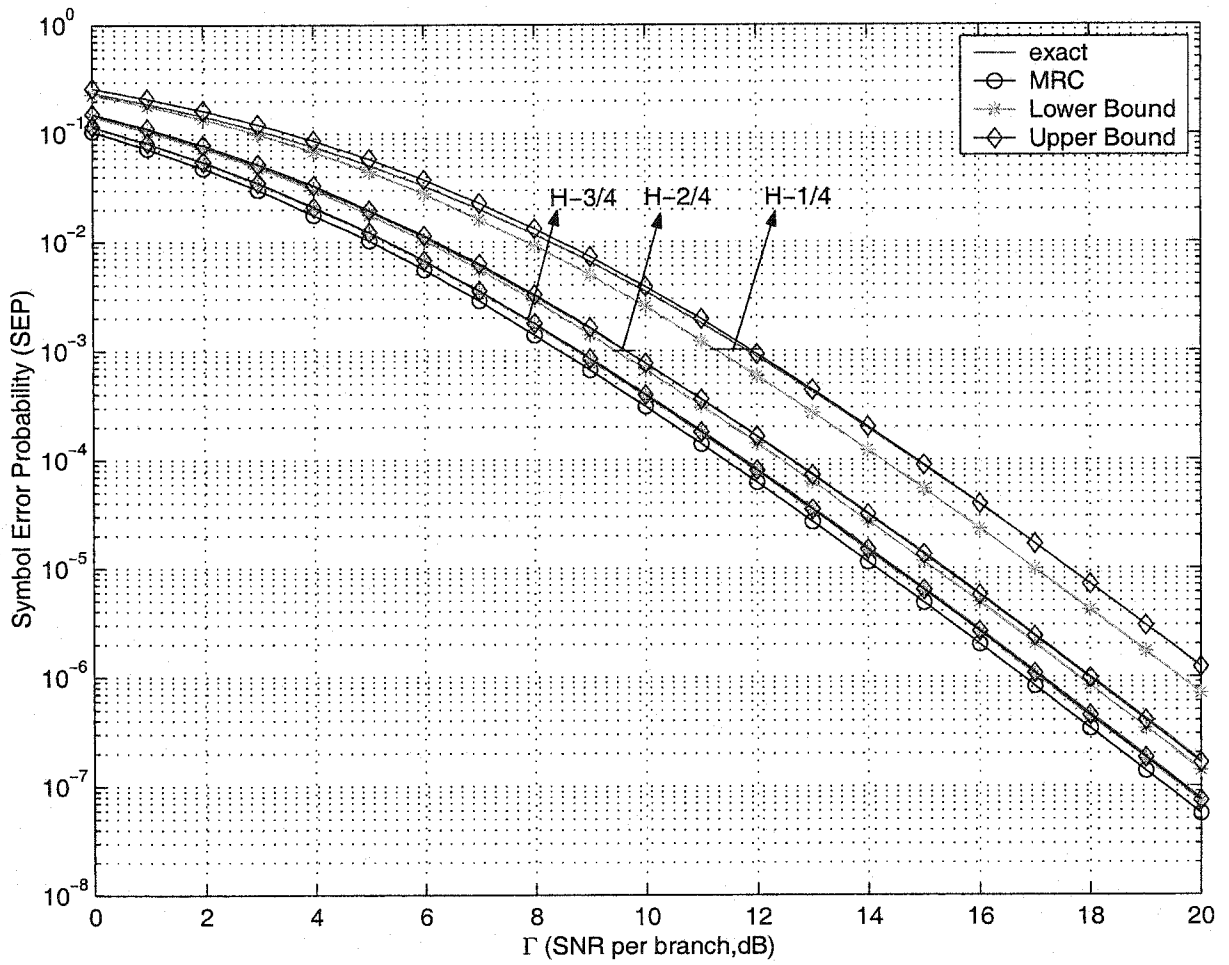
Figure 5.2. The symbol error probability as a function of average SNR per branch for coherent detection of 4-ary orthogonal signalling with H-S/MRC for $L = 1, 2, 3$ and $N = 4$. The conjectured lower and upper bounds are plotted for comparison.
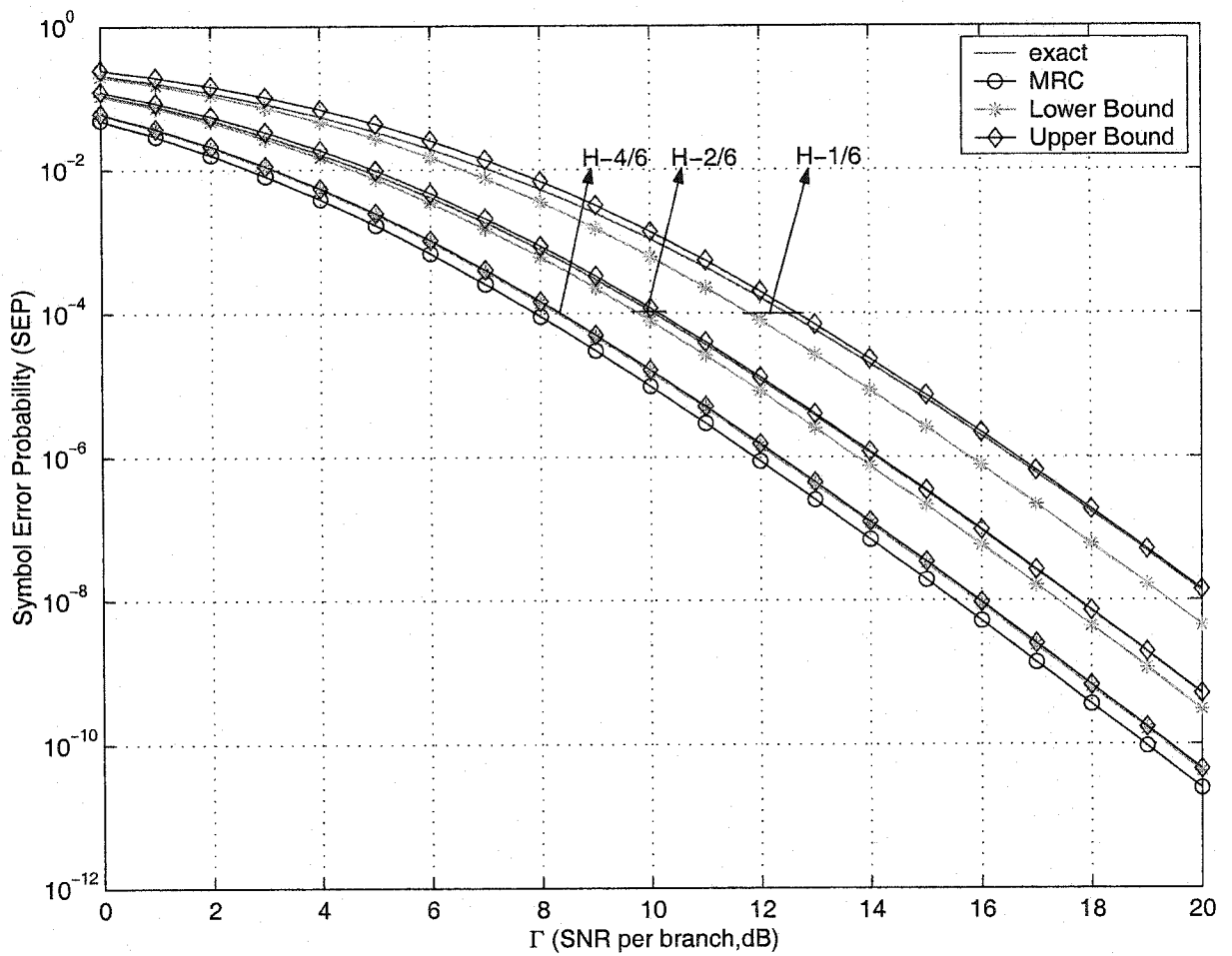
Figure 5.3. The symbol error probability as a function of average SNR per branch for coherent detection of 6-ary biorthogonal signalling with H-S/MRC for $L = 1, 2, 4$ and $N = 6$. The conjectured lower and upper bounds are plotted for comparison.
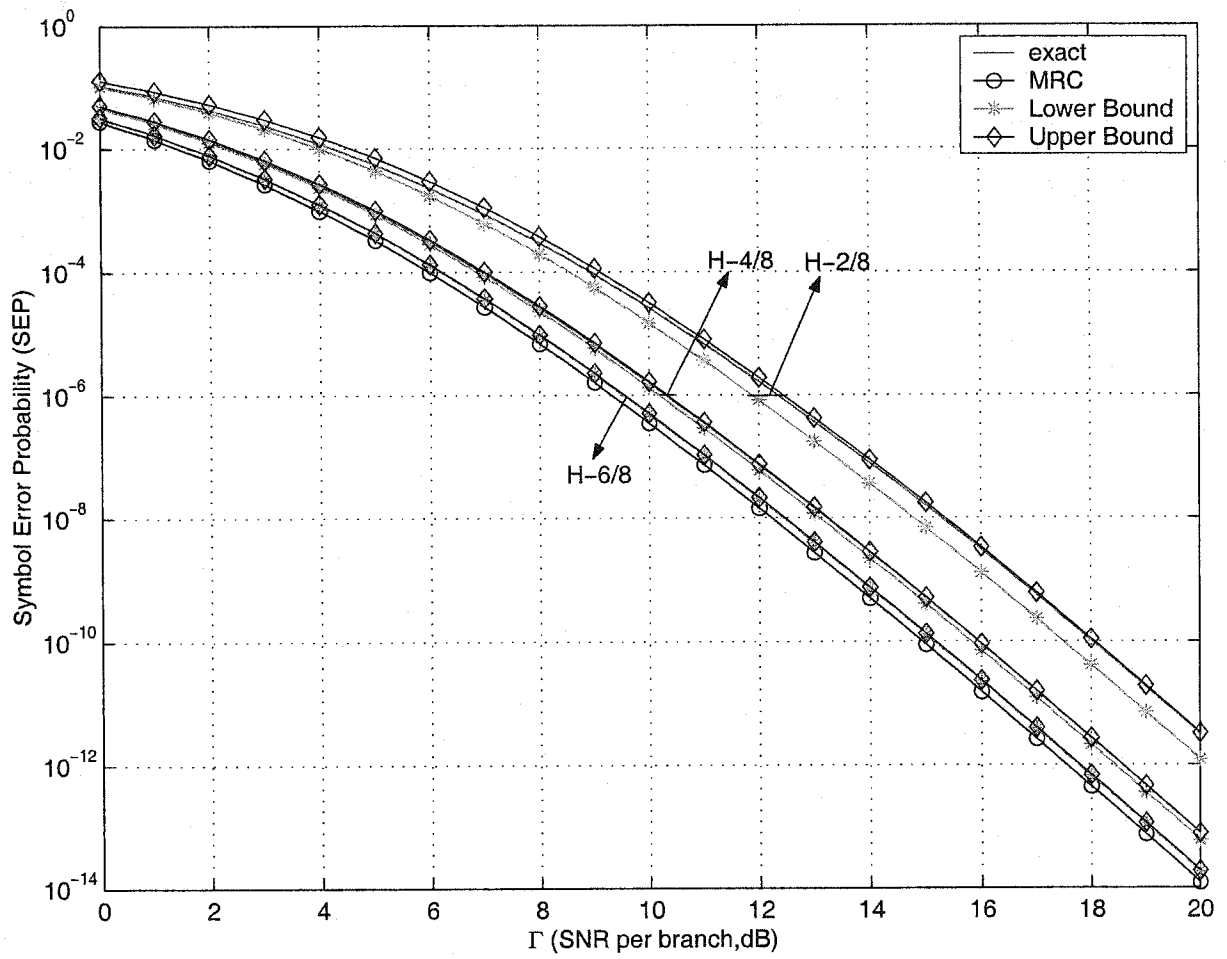
Figure 5.4. The symbol error probability as a function of average SNR per branch for coherent detection of 8-ary biorthogonal signalling with H-S/MRC for $L = 1, 2, 4$ and $N = 8$. The conjectured lower and upper bounds are plotted for comparison.
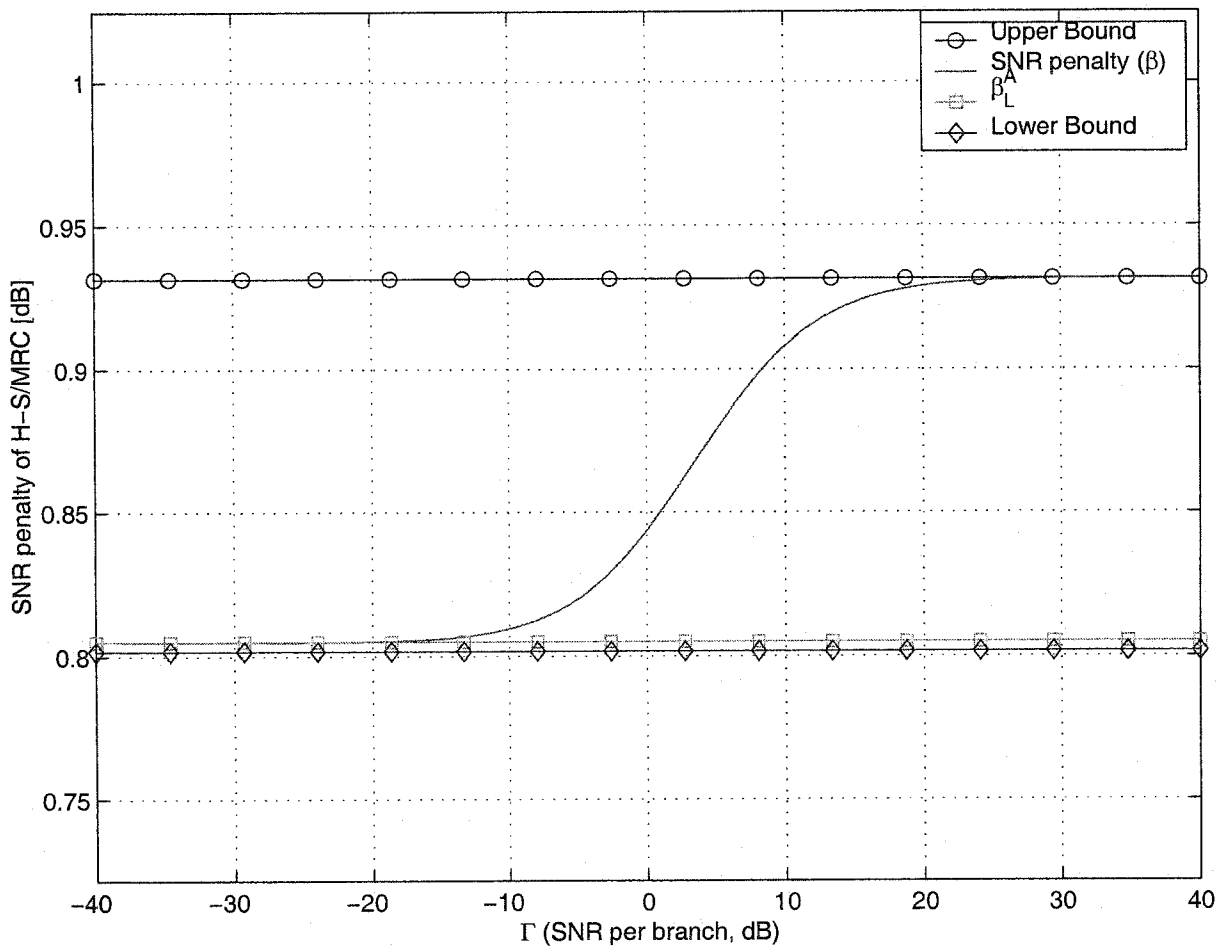
Figure 5.5. The SNR penalty as a function of SNR for 3-ary orthogonal signalling with H-S/MRC for $(L,N) = (8,16)$. The conjectured lower and upper bounds are plotted for comparison.
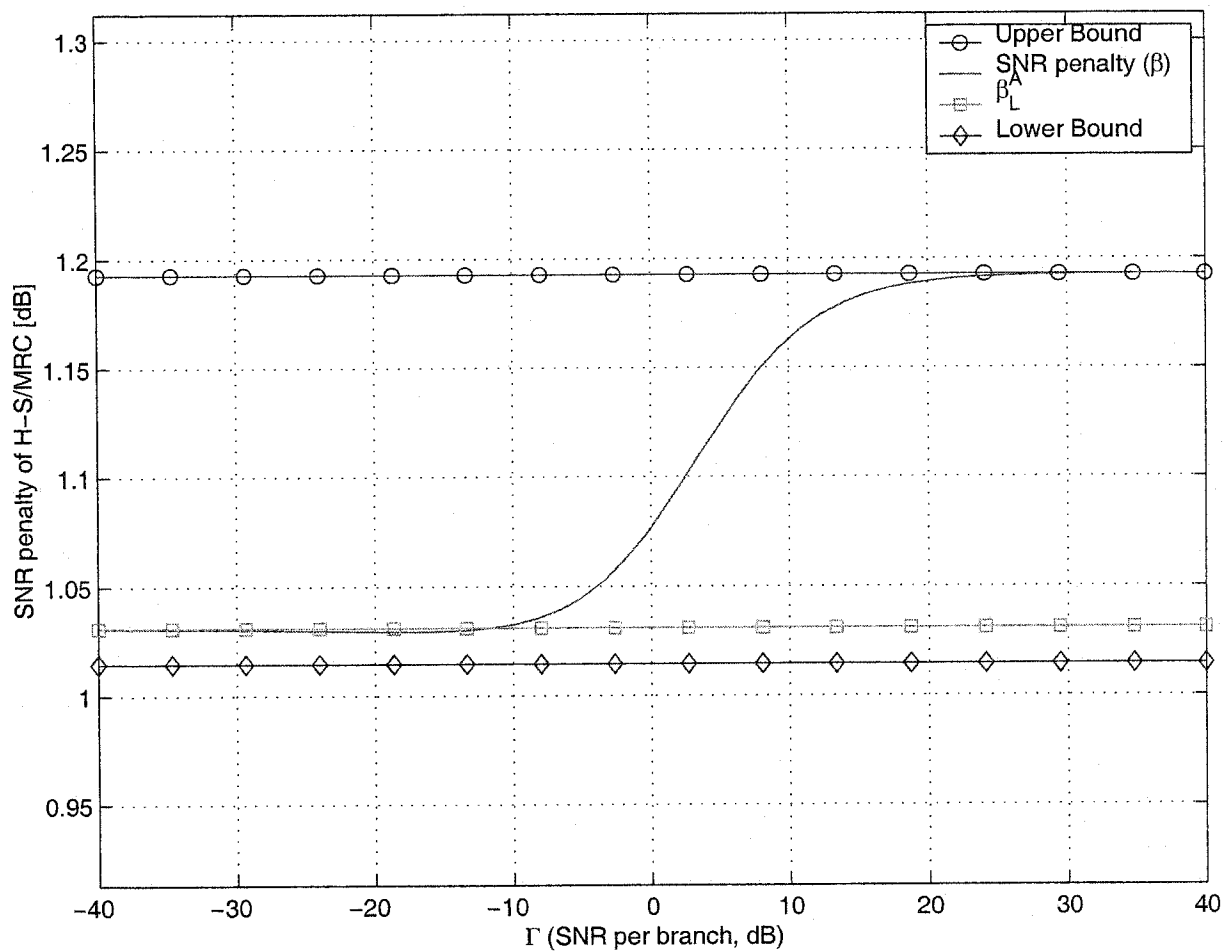
Figure 5.6. The SNR penalty as a function of SNR for 4-ary orthogonal signalling with H-S/MRC for $(L,N) = (2,4)$. The conjectured lower and upper bounds are plotted for comparison.
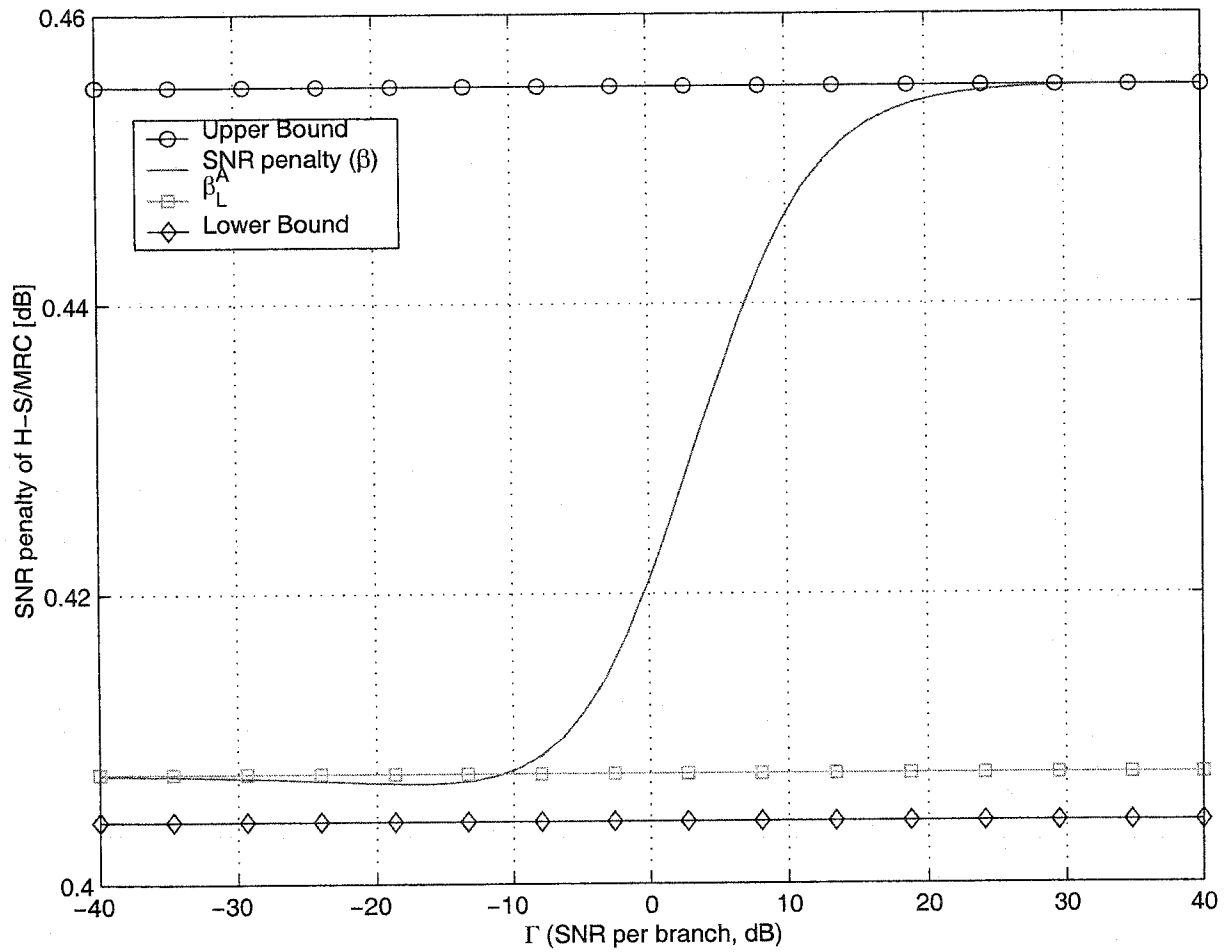
Figure 5.7. The SNR penalty as a function of SNR for 6-ary biorthogonal signalling with H-S/MRC for $(L,N) = (4,6)$. The conjectured lower and upper bounds are plotted for comparison.
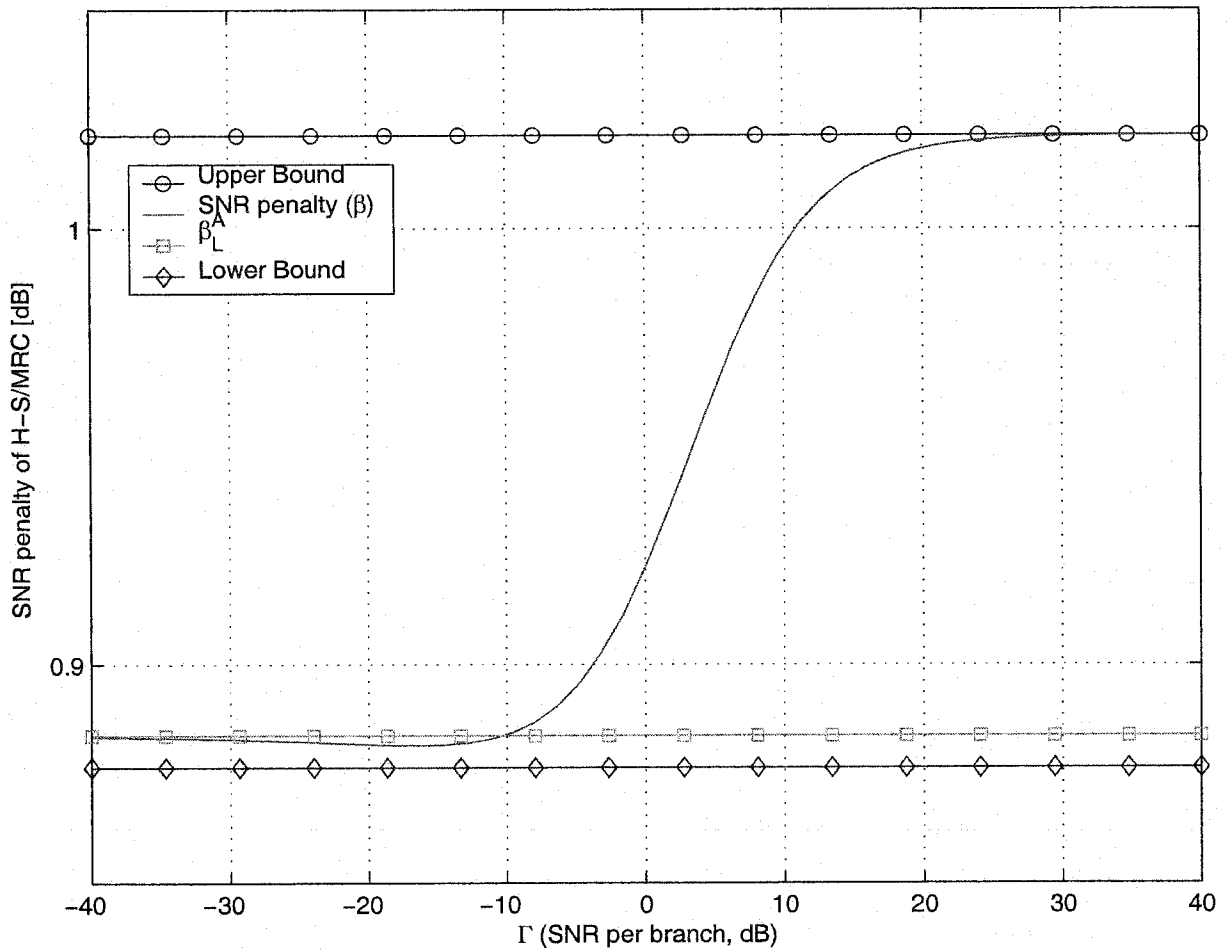
Figure 5.8. The SNR penalty as a function of SNR for 8-ary biorthogonal signalling with H-S/MRC for $(L,N) = (4,8)$. The conjectured lower and upper bounds are plotted for comparison.

5.4 Conclusions

In this chapter, we have established that the SNR penalties of H-S/MRC relative to MRC in Rayleigh fading have small SNR and large SNR asymptotes. Analytical expressions for the asymptotes have been derived. The asymptotic SNR penalties depend only on L and N, and are independent of the modulation format and the average SNR. Based on several numerical examples, we conjecture that the SNR bounds derived in Chapter 4 for two-dimensional signalling constellations are also valid for arbitrary modulation formats. Using the results of this chapter, the SEP of hybrid diversity, $P_{e,\text{H-S/MRC}}(\Gamma)$ operating at small and large SNR, can be easily approximated to a high degree of accuracy, using the SEP of MRC operating at $\beta_L^{A^{-1}}\Gamma$ and $\beta_U^{A^{-1}}\Gamma$, respectively.

Chapter 6

Conclusion

To mitigate the effect of fading in wireless communication systems, we use diversity methods. Well known diversity methods include SC and MRC. It is well known that MRC is the optimal linear diversity combining technique. However, MRC may not be cost efficient in some systems. The complexity of the MRC receiver is directly proportional to the number of resolvable paths, which could be quite high. In addition, MRC is sensitive to channel estimation errors, and these errors tend to be more important in paths with small SNR. On the other hand, SC is very simple and uses only one path out of the N available paths and so does not fully exploit the amount of diversity which is offered by the system. Recently there has been much interest in systems in which only a subset of paths are considered. One of these schemes is H-S/MRC where the systems selects at each instant of time the L paths with the largest SNR's among the N available paths. Since H-S/MRC selects the paths with the largest SNR's it is less sensitive to the channel estimation error. Also the system complexity reduces compared to that of MRC because only a subset of the paths are selected and combined. However, a loss or penalty is incurred when using H-S/MRC instead of MRC, for not using all the available paths. This penalty was defined as the increase in SNR needed for H-S/MRC to get the same target SEP as that of MRC. The SEP

of SC, H-S/MRC and MRC were analyzed using a unified approach, by first finding the SEP of a GDC system. In this thesis, we have given a relatively complete discussion on the SNR penalty of H-S/MRC relative to MRC in Rayleigh fading channels.

In summary,

1. New, analytical expressions for the SEP of GDC with 3-ary and 4-ary orthogonal signalling and 6-ary and 8-ary biorthogonal signalling were obtained. The SEP of MRC and SC, as well as H-S/MRC can be derived from the SEP of GDC for these constellations. The SEP's are expressed as a summation of single or double integrals with finite integration integrals and elementary function integrands. It was shown that even for small L compared to N, H-S/MRC gets close SEP performance to that of MRC.

2. New, simple lower and upper bounds to the SNR penalty of H-S/MRC used with any two-dimensional signalling constellation with polygonal decision regions were derived. The bounds are expressed in closed-form and only depend on L and N and are independent of the SNR. Using these bounds the SEP of H-S/MRC, $P_{e,\text{H-S/MRC}}(\Gamma)$, can be approximated to a high degree of accuracy using the SEP of MRC operating at $P_{e,\text{MRC}}(\beta_L^{-1}\Gamma)$ and $P_{e,\text{MRC}}(\beta_U^{-1}\Gamma)$, for small and large values of SNR, respectively.

3. New, analytical expressions for the asymptotic values for the SNR penalty of H-S/MRC used with any two-dimensional signalling, for small and large values of SNR, were derived. The asymptotes depend only on L and N and are independent of the SNR. It was shown that the penalty asymptote for large SNR is equal to the upper bound and the difference between the asymptotic SNR for small SNR and the lower bound are typically in the second or third significant digit.Hence, little is lost by assessing the performance of a system using the lower bound for small SNR.

4. New, analytical expressions for the asymptotic values of the SNR penalty of H-S/MRC

used with arbitrary modulations, were obtained. The expressions for these asymptotes depend only on L and N and are independent of the modulation format and the SNR. Using the asymptotes the SEP of H-S/MRC with arbitrary modulation, can be approximated using that of MRC operating at $P_{e,\mathrm{MRC}}(\beta_L^{A^{-1}}\Gamma)$ and $P_{e,\mathrm{MRC}}(\beta_U^{A^{-1}}\Gamma)$, for small and large values of SNR, respectively.

5. Based on several examples we conjectured that the penalty bounds valid for two-dimensional signalling are also valid for *arbitrary* modulation.

References

[1] D. G. Brennan, "Linear Diversity Combining Techniques," *Proc. of the IRE*, vol. 46, pp. 1075–1102, June 1959.

[2] B. Sklar, "Rayleigh Fading Channels in mobile Digital communication systems part I : Characterization," *IEEE Commun. Magazine*, vol. 35, pp. 90–100, July 1997.

[3] B. Sklar, "Rayleigh Fading Channels in mobile Digital Communication Systems Part II : Mitigation," *IEEE Commun. Magazine*, vol. 35, pp. 102–109, July 1997.

[4] G. L. Stuber, *Principles of Mobile Communication*, 2nd ed. Norwell, MA: Kluwer Academic Publishers, 2001.

[5] J. D. Parsons, *The Mobile Radio Propagation Channel*, 2nd ed. New York: McGraw-Hill, 2000.

[6] T. S. Rappaport, *Wireless Communications Principles and Practice*, 2nd ed. New Jersey: Prentice Hall PTR, 2002.

[7] W. C. Jakes, *Microwave Mobile Communications*. New York: IEEE press, reprint, 1974.

[8] M. J. Gans, "A Power-Spectral Theory of Propagation in the mobile radio environment," *IEEE Trans. Veh. Tech.*, vol. 80, no. VT-16, pp. 27–38, February 1972.

[9] S. O. Rice, "Mathematical Analysis of Random Noise," *Bell System Tech. J.*, vol. 23, pp. 282–332, July 1944.

[10] L. R. Kahn, "Ratio Squarer," *Proc. IRE (Corresp.)*, vol. 42, pp. 1954, November 1954.

[11] M. K. Simon and M.-S. Alouini, *Digital Communication over Fading Channels: A Unified Approach to Performance Analysis*. New York: Wiley, 2000.

[12] M. Z. Win and J. H. Winters, "Virtual branch analysis of symbol error probability for hybrid selection/maximal-ratio combining in Rayleigh fading," *IEEE Trans. Commun.*, vol. 49, pp. 1926–1934, November 2001.

[13] J. W. Craig, "A new simple and exact result for calculating the probability of error for two-dimensional signaling constellation," in *Proc. IEEE Military Conf. MILCOM 91*, May 1991, vol. Boston, MA, pp. 25.5.1–25.5.5.

[14] X. Dong and N. C. Beaulieu, "New Analytical Expressions for Probability of Error for classes of orthogonal signals in Rayleigh fading," in *Globecom'99*, December 1999, vol. Rio de Janeiro, Brazil, pp. 2528–2533.

[15] M. Z. Win, N. C. Beaulieu, L. A. Shepp, B. F. Logan, and J. K. Winters, "On the SNR Penalty of MPSK with Hybrid Selection/Maximal Ratio Combining over IID Rayleigh Fading Channels," *submitted to IEEE Trans. Commun.*, 2001.

[16] J. M. Wozencraft and I. M. Jacobs, *Principles of Communication Engineering*. New York: John Wiley and Sons, 1965.

[17] M. K. Simon, S. M. Hinedi, and W. C. Lindsey, *Digital Communication Techniques: Signal Design and Detection*. Upper Saddle River, NJ: Prentice Hall, 1995.

[18] X. Dong, N. C. Beaulieu, and P. H. Wittke, "Signaling constellations for fading channels," *IEEE Trans. Commun.*, vol. 47, pp. 703–714, May 1999.

[19] F. Xiong, *Digital Modulation Techniques*. 685 Canton St. MA 02062: Artech House Inc., 2000.

[20] X. Dong, N. C. Beaulieu, and P. H. Wittke, "Error probabilities of two-dimensional *m*-ary signaling in fading," *IEEE Trans. Commun.*, vol. 47, pp. 352–355, March 1999.

[21] J. G. Proakis, *Digital Communications*, 4th ed. New York: McGraw-Hill, 2001.

[22] B. P. Lahti, *Modern Digital and Analog Communication System*, 3rd ed. Oxford: Oxford University Press, 1998.

[23] S. Ross, *A First Course in Probability*, 6th ed. Upper Saddle River, NJ: Prentice Hall, 2002.

[24] A. Annamalai, C. Tellambura, and V. K. Bhargava, "Exact evaluation of maximal-ratio and equal-gain diversity receivers for M-ary QAM on Nakagami fading channels," *IEEE Trans. Commun.*, vol. 47, pp. 1335–1344, September 1999.

[25] M. K. Simon and D. Divsalar, "Some new twists to problems involving the Gaussian probability integral," *IEEE Trans. Commun.*, vol. 46, pp. 200–210, February 1998.

[26] P. V. Sukhatme, "Tests of significance for samples of the χ^2 population with two degrees of freedom ," *Ann. of Eugen.*, vol. 8, pp. 52–56, 1937.

[27] M.-S. Alouini and M. K. Somon, "An MGF-based performance analysis of generalized selection combining over Rayleigh fading channels," *IEEE Trans. Commun.*, vol. 48, pp. 401–415, March 2000.

[28] W. T. Webb, "Spectrum efficiency of Multilevel Modulation Schemes in Mobile Radio Communications," *IEEE Trans. Commun.*, vol. 43, pp. 2344–2349, August 1995.

[29] W. T. Webb and R. Steele, "Variable rate QAM for Mobile Radio," *IEEE Trans. Commun.*, vol. 43, pp. 2223–2230, July 1995.

[30] T. Eng, N. Kong, and L. B. Milstein, "Comparison of diversity combining techniques for Rayleigh-fading channels," *IEEE Trans. Commun.*, vol. 44, pp. 1117–1129, September 1996.

[31] N. Kong and L. B. Milstein, "Combined average SNR of a generalized diversity selection combining scheme," in *Proc. IEEE Int. Conf. on Commun.*, Atlanta, GA, June 1998, vol. 3, pp. 1556–1560.

[32] N. Kong and L. B. Milstein, "Average SNR of a generalized diversity selection combining scheme," *IEEE Commun. Lett.*, vol. 3, pp. 57–59, March 1999.

[33] M. Z. Win and J. H. Winters, "Analysis of hybrid selection/maximal-ratio combining of diversity branches with unequal SNR in Rayleigh fading," in *Proc. 49th Annual Int. Veh. Technol. Conf.*, Houston, TX, May 1999, vol. 1, pp. 215–220.

[34] M. Z. Win and J. H. Winters, "Analysis of hybrid selection/maximal-ratio combining in Rayleigh fading," in *Proc. IEEE Int. Conf. on Commun.*, Vancouver, Canada, June 1999, vol. 1, pp. 6–10.

[35] M. Z. Win and J. H. Winters, "Analysis of hybrid selection/maximal-ratio combining in Rayleigh fading," *IEEE Trans. Commun.*, vol. 47, pp. 1773–1776, December 1999.

[36] H. Erben, S. Zeisberg, and H. Nuszkowski, "BER performance of a hybrid SC/MRC 2DPSK RAKE receiver in realistic mobile channels," in *Proc. Annual Int. Veh. Tech. Conf.*, Stockhom, Sweden, June 1994, vol. 2, pp. 738–741.

[37] M. Z. Win and R. A. Schultz, "On the energy capture of ultra-wide bandwidth signals in dense multipath environments," *IEEE Commun. Lett.*, vol. 2, pp. 245–247, September 1998.

[38] M. Z. Win and Z. A. Kostić, "Impact of spreading bandwidth on Rake reception in dense multipath channels," in *Proc. 8th Comm. Theory Mini Conf.*, Vancouver, Canada, June 1999, vol. 2, pp. 78–82.

[39] M. Z. Win and Z. A. Kostić, "Virtual path analysis of selective Rake receiver in dense multipath channels," *IEEE Commun Lett.*, vol. 3, pp. 308–310, November 1999.

[40] M. Z. Win, G. Chrisikos, and N. R. Sollenberger, "Performance of Rake reception in dense multipath channels: Implications of spreading bandwidth and selection diversity order," *IEEE J. Select. Areas Commun.*, vol. 18, pp. 1516–1525, August 2000.

[41] G. Hardy, J. Littlewood, and G.Pólya, *Inequalities*, 2nd ed. Cambridge, UK: Cambridge University Press, 1952.

[42] E. Kreyszig, *Advanced Engineering Mathematics*, 4th ed. New York, USA: John Wiley & Sons, 1979.

[43] H. A. Abdel-Ghaffar and S. Pasupathy, "Asymptotic Performance of M-ary and Binary Signals over Multipath/Multichannel Rayleigh and Ricean Fading," *IEEE Trans. Commun.*, vol. 48, November 1995.

[44] T. M. Apostol, *Mathematical Analysis*, 2nd ed. Reading, Massachusettes: Addison-Wesley, 1974.

[45] L. Hanzo, T. Webb, and T. Keller, *Single- and Multi-carrier Quadrature Amplitude Modulation: Principles and Applications for Personal Communications, WLANs and Broadcasting*. Chinchester, UK: Wiley, 2002.

[46] J. Lu, T. Tjhung, and C. Chai, "Error Probability Performance of L-Branch Diversity Reception of MQAM in Rayleigh Fading," *IEEE Trans. Commun.*, vol. 46, February 1998.

[47] M.-S. Alouini and A. Goldsmith, "A unified approach for calculating error rates of linearly modulated signals over generalized fading channels," *Proc. Int. Conf. on Commun.*, vol. 1, pp. 459–463, June 1998.

Appendix A

In this appendix, we give a proof of (4.42) in Lemma 2. We will use the result of Lemma 1 to prove Lemma 2.

Lemma 1: *For any real number $p \leq 1$ and integer N,*

$$1 - (1-p)^N \leq Np. \tag{A.1}$$

Proof: The proof is by induction. For $N = 1$, both sides of the inequality in (A.1) are equal to p. Now assume that (A.1) is valid for $N = k$. For $N = K + 1$ the right of (A.1) can be written as

$$1 - (1-p)^{k+1} = 1 - (1-p)(1-p)^k \leq 1 - (1-p)(1-kp) = (k+1)p - kp^2 \leq (k+1)p. \tag{A.2}$$

Hence, the proof is complete. ∎

Lemma 2: *Define*

$$p(\Gamma) = \frac{1}{2\pi} \int_0^{\eta_k} \prod_{n=1}^{N} \left(\frac{\sin^2(\theta)}{\sin^2(\theta) + c_{k,n}\Gamma} \right) d\theta \tag{A.3}$$

where $c_{k,n} = a_n x_k \sin^2(\psi_k)$. Then

$$p(\Gamma) = \frac{\eta_k}{2\pi} - A_k \Gamma^{1/2} + o(\Gamma^{1/2}) \tag{A.4}$$

where

$$A_k = \frac{1}{2\pi} \int_0^{\infty} \left\{ 1 - \prod_{n=1}^{N} \left[\frac{u^2}{c_{k,n} + u^2} \right] \right\} du. \tag{A.5}$$

90

Proof: Define

$$g(\Gamma) \triangleq \frac{\eta_k}{2\pi} - \frac{1}{2\pi} \int_0^{\eta_k} \prod_{n=1}^{N} \left(\frac{\sin^2(\theta)}{\sin^2(\theta) + c_{k,n}\Gamma} \right) d\theta \qquad \text{(A.6a)}$$

$$= \frac{1}{2\pi} \int_0^{\eta_k} \left\{ 1 - \prod_{n=1}^{N} \left(\frac{\sin^2(\theta)}{\sin^2(\theta) + c_{k,n}\Gamma} \right) \right\} d\theta. \qquad \text{(A.6b)}$$

Note that $g(\Gamma) = \frac{\eta_k}{2\pi} - p(\Gamma)$. For every $\varepsilon \geq 0$ there exists $\delta(\varepsilon)$ such that

$$\frac{1}{1+\varepsilon} \leq \frac{\sin(\theta)}{\theta} \leq \frac{1}{1-\varepsilon}. \qquad \text{(A.7)}$$

This is true because $h(\theta) = \frac{\theta}{\sin(\theta)}$ is a continuous function around $\theta = 0$ and $h(0) = 1$, so

for every $\varepsilon \geq 0$ there exists a $\delta(\varepsilon)$ such that $\mid \theta - 0 \mid \leq \delta(\varepsilon) \longrightarrow \mid \frac{\theta}{\sin\theta} - 1 \mid \leq \varepsilon$. Now define

$$I_1(\Gamma, \varepsilon) \triangleq \frac{1}{2\pi} \int_0^{\delta(\varepsilon)} \left\{ 1 - \prod_{n=1}^{N} \left(\frac{\sin^2(\theta)}{\sin^2(\theta) + c_{k,n}\Gamma} \right) \right\} d\theta \qquad \text{(A.8a)}$$

$$I_2(\Gamma, \varepsilon) \triangleq \frac{1}{2\pi} \int_{\delta(\varepsilon)}^{\eta_k} \left\{ 1 - \prod_{n=1}^{N} \left(\frac{\sin^2(\theta)}{\sin^2(\theta) + c_{k,n}\Gamma} \right) \right\} d\theta. \qquad \text{(A.8b)}$$

Note that $g(\Gamma) = I_1(\Gamma, \varepsilon) + I_2(\Gamma, \varepsilon)$. In the following we will show that

$$I_1(\Gamma, \varepsilon) = A_k \Gamma^{1/2} \qquad \text{(A.9)}$$

and

$$I_2(\Gamma, \varepsilon) = o(\Gamma^{1/2}). \qquad \text{(A.10)}$$

Let $C_k = \max\{c_{k,n}\}_{n=1}^{N}$. Using the result of Lemma 1 one can find an upper bound to

$I_2(\Gamma, \varepsilon)$ as follows

$$I_2(\Gamma, \varepsilon) \leq \frac{1}{2\pi} \int_{\delta(\varepsilon)}^{\eta_k} \left\{ 1 - \left(1 - \frac{C_k\Gamma}{\sin^2(\theta) + C_k\Gamma} \right)^N \right\} d\theta \qquad \text{(A.11a)}$$

$$\leq \frac{1}{2\pi} \int_{\delta(\varepsilon)}^{\eta_k} \left(\frac{NC_k\Gamma}{C_k\Gamma + \sin^2(\theta)} \right) d\theta \qquad \text{(A.11b)}$$

$$\leq \frac{1}{2\pi} \int_{\delta(\varepsilon)}^{\eta_k} \left(\frac{NC_k\Gamma}{C_k\Gamma + \sin^2(\delta(\varepsilon))} \right) d\theta \qquad \text{(A.11c)}$$

$$= \frac{1}{2\pi} \frac{NC_k\Gamma}{NC_k + \sin^2(\delta(\varepsilon))} [\eta_k - \delta(\varepsilon)]. \qquad \text{(A.11d)}$$

91

Dividing both sides of the inequalities in (A.11) by $\Gamma^{1/2}$ and taking the limits as Γ approaches zero one obtains

$$\limsup_{\Gamma \to 0} \frac{1}{\Gamma^{1/2}} I_2(\Gamma, \varepsilon) \leq \limsup_{\Gamma \to 0} \frac{1}{2\pi} \frac{NC_k[\eta_k - \delta(\varepsilon)]}{NC_k + \sin^2(\delta(\varepsilon))} \Gamma^{1/2} = 0. \qquad (A.12)$$

But from the definition of $I_2(\Gamma, \varepsilon)$ one can clearly see that $I_2(\Gamma, \varepsilon) \geq 0$. So

$$\lim_{\Gamma \to 0} \frac{1}{\Gamma^{1/2}} I_2(\Gamma, \varepsilon) = 0 \qquad (A.13)$$

which is equivalent to (A.10). Now consider $I_1(\Gamma, \varepsilon)$; We claim that for any $\varepsilon' \geq 0$

$$\limsup_{\Gamma \to 0} \left| \frac{1}{\Gamma^{1/2}} I_1(\Gamma, \varepsilon) - \frac{1}{2\pi} \int_0^\infty \left\{ 1 - \prod_{n=1}^{N} \left[\frac{u^2}{c_{k,n} + u^2} \right] \right\} du \right| \leq \varepsilon'. \qquad (A.14)$$

To show (A.14), we first prove that

$$\limsup_{\Gamma \to 0} \left[\frac{1}{\Gamma^{1/2}} I_1(\Gamma, \varepsilon) - \frac{1}{2\pi} \int_0^\infty \left\{ 1 - \prod_{n=1}^{N} \left(\frac{u^2}{c_{k,n} + u^2} \right) \right\} \right] du \leq \varepsilon'. \qquad (A.15)$$

Using the left inequality in (A.7) we can find an upper bound for $I_1(\Gamma, \varepsilon)$ as

$$I_1(\Gamma, \varepsilon) \;=\; \frac{1}{2\pi} \int_0^{\delta(\varepsilon)} \left\{ 1 - \prod_{n=1}^{N} \left(1 - \frac{c_{k,n}\Gamma}{c_{k,n}\Gamma + \sin^2(\theta)\frac{\theta^2}{\theta^2}} \right) \right\} d\theta \qquad (A.16a)$$

$$\leq \frac{1}{2\pi} \int_0^{\delta(\varepsilon)} \left\{ 1 - \prod_{n=1}^{N} \left(1 - \frac{c_{k,n}\Gamma}{c_{k,n}\Gamma + \frac{\theta^2}{(1+\varepsilon)^2}} \right) \right\} d\theta \qquad (A.16b)$$

$$= \frac{1}{2\pi} \int_0^{\frac{\delta(\varepsilon)}{(1+\varepsilon)} \frac{1}{\Gamma^{1/2}}} \left\{ 1 - \prod_{n=1}^{N} \left[\frac{u^2}{c_{k,n} + u^2} \right] \right\} \Gamma^{1/2}(1+\varepsilon) du \qquad (A.16c)$$

where the change of variable $u = \frac{1}{\Gamma^{1/2}} \frac{\theta}{1+\varepsilon}$ has been used. Now taking the limits of both sides of (A.16) when Γ approaches zero one obtains

$$\limsup_{\Gamma \to 0} \left[\frac{1}{\Gamma^{1/2}} I_1(\Gamma, \varepsilon) - \frac{1}{2\pi} \int_0^\infty \left\{ 1 - \prod_{n=1}^{N} \left(\frac{u^2}{c_{k,n} + u^2} \right) \right\} du \right] \leq \varepsilon' \qquad (A.17)$$

where $\varepsilon' = A_k \varepsilon$. Similar to the steps taken to derive (A.15) and using the right inequality in (A.7), one can show that

$$\liminf_{\Gamma \to 0} \left[\frac{1}{\Gamma^{1/2}} I_1(\Gamma, \varepsilon) - \frac{1}{2\pi} \int_0^\infty \left\{ 1 - \prod_{n=1}^{N} \left(\frac{u^2}{c_{k,n} + u^2} \right) \right\} du \right] \geq -\varepsilon'. \qquad (A.18)$$

92

Combining (A.17) and (A.18) one obtains (A.14). Recall that $I_1(\Gamma, \varepsilon) = g(\Gamma) - I_2(\Gamma, \varepsilon)$.

Substituting this in (A.14), one obtains

$$\limsup_{\Gamma \to 0} \left| \frac{1}{\Gamma^{1/2}} g(\Gamma) - \frac{1}{2\pi} \int_0^\infty \left\{ 1 - \prod_{n=1}^{N} \left[\frac{u^2}{c_{k,n} + u^2} \right] \right\} du \right| \leq \varepsilon' \qquad (A.19)$$

which is equivalent to

$$\lim_{\Gamma \to 0} \frac{g(\Gamma)}{\Gamma^{1/2}} = A_k. \qquad (A.20)$$

Finally, combining (A.10) and (A.20) gives (A.4). ∎

Appendix B

In this appendix, we state two lemmas. The proof of (5.5) follows by combining the results of Lemma 3 and Lemma 4.

Lemma 3: *Define*

$$I_1(x_1,\cdots,x_N) \triangleq \int_0^\infty \cdots \int_0^\infty \sqrt{x_1 v_1 + \cdots + x_N v_N}\, e^{-(v1+\cdots+v_N)} dv_1 \cdots dv_N \qquad (B.21)$$

and

$$
\begin{aligned}
I_2(x_1,\cdots,x_N) \triangleq\; & \frac{\sqrt{x_1}}{\sqrt{\pi}} \int_0^\infty \Big(\frac{x_1}{x_1+x_2 u^2}\Big)\Big(\frac{x_1}{x_1+x_3 u^2}\Big)\cdots\Big(\frac{x_1}{x_1+x_N u^2}\Big)\Big(\frac{1}{1+u^2}\Big)du \\
+\; & \frac{\sqrt{x_2}}{\sqrt{\pi}} \int_0^\infty \Big(\frac{x_2}{x_2+x_3 u^2}\Big)\Big(\frac{x_2}{x_2+x_4 u^2}\Big)\cdots\Big(\frac{x_2}{x_2+x_N u^2}\Big)\Big(\frac{1}{1+u^2}\Big)du \\
+\; & \cdots + \frac{\sqrt{x_N}}{\sqrt{\pi}} \int_0^\infty \frac{1}{1+u^2}du.
\end{aligned}
\qquad (B.22)
$$

Then

$$I_1(x_1,\cdots,x_N) = I_2(x_1,\cdots,x_N) \qquad (B.23)$$

for any integer $N \geq 2$ and for all $x_i > 0$, $\quad i = 1,\cdots,N$.

Proof: The proof is by induction. We first prove (B.23) for $N = 2$. We can write $I_1(x_1,x_2)$ as

$$
\begin{aligned}
I_1(x_1,x_2) &= \int_0^\infty \int_0^\infty \sqrt{x_1 v_1 + x_2 v_2}\, e^{-(v1+v2)} dv_1 dv_2 & (B.24a) \\
&= \frac{\sqrt{x_1 \pi}}{2} \int_0^\infty e^{\frac{x_2 v_2}{x_1}-v_2}\mathrm{erfc}\left(\sqrt{\frac{x_2 v_2}{x_1}}\right) dv_2 & (B.24b) \\
&+ \int_0^\infty \sqrt{x_2 v_2}\, e^{-v_2} dv_2.
\end{aligned}
$$

94

Using Craig's alternative representation of the complementary error function [13], and changing the order of integration in (B.24) one obtains

$$
\begin{aligned}
I_1(x_1, x_2) &= \sqrt{\frac{x_1 \pi}{2}} \int_0^\infty e^{\frac{x_2 v_2}{x_1} - v2} \left\{ \frac{2}{\pi} \int_0^{\pi/2} e^{-\frac{x_2 v_2}{x_1 \sin^2(\theta)}} d\theta \right\} dv_2 \\
&\quad + \int_0^\infty \sqrt{x_2 v_2} e^{-v_2} dv_2 \qquad\qquad\qquad\qquad\qquad\qquad\qquad\text{(B.25a)} \\
&= \sqrt{\frac{x_1}{\pi}} \int_0^{\pi/2} \frac{x_1 \sin^2(\theta)}{x_1 \sin^2(\theta) + x_2 \cos^2(\theta)} d\theta \\
&\quad + \sqrt{\frac{x_2}{\pi}} \int_0^\infty \frac{1}{1 + u^2} du \qquad\qquad\qquad\qquad\qquad\qquad\text{(B.25b)} \\
&= \sqrt{\frac{x_1}{\pi}} \int_0^\infty \frac{x_1}{(x_1 + x_2 u^2)(1 + u^2)} du + \sqrt{\frac{x_2}{\pi}} \int_0^\infty \frac{1}{1 + u^2} du \quad \text{(B.25c)} \\
&= I_2(x_1, x_2) \qquad\qquad\qquad\qquad\qquad\qquad\qquad\qquad\qquad\text{(B.25d)}
\end{aligned}
$$

where we have used the change of variable $u = \cot(\theta)$. The interchange of the order of integration is valid because the integrand in (B.24) is a continuous function in the region of integration [44, Fubini's Theorem, p. 394].

Now assume that (B.23) holds for $N = k - 1$, that is

$$
I_1(x_1, \cdots, x_{k-1}) = I_2(x_1, \cdots, x_{k-1}). \qquad\qquad\qquad\qquad\text{(B.26)}
$$

We now show that (B.23) is also valid for $N = k$. One has

$$
\begin{aligned}
I_1(x_1, \cdots, x_k) &= \int_0^\infty \int_0^\infty \cdots \int_0^\infty \sqrt{x_1 v_1 + \cdots + x_k v_k} e^{-(v_1 + \cdots + v_k)} dv_1 \cdots dv_k \\
&= \frac{\sqrt{x_1 \pi}}{2} \int_0^\infty \int_0^\infty \cdots \int_0^\infty e^{\frac{x_2 v_2 + \cdots + x_k v_k}{x_1} - (v_2 + \cdots + v_k)} \\
&\quad \times \operatorname{erfc}\left(\sqrt{\frac{x_2 v_2 + \cdots + x_k v_k}{x_1}} \right) dv_2 \cdots dv_k \\
&\quad + \int_0^\infty \int_0^\infty \cdots \int_0^\infty \sqrt{x_2 v_2 + \cdots + x_k v_k} e^{-(v_2 + \cdots + v_k)} dv_2 \cdots dv_k \\
&= G_1 + I_1(x_2, \cdots, x_k) = G_1 + I_2(x_2, \cdots, x_k) \qquad\qquad\text{(B.27)}
\end{aligned}
$$

where G_1 is defined as

$$G_1 = \frac{\sqrt{x_1\pi}}{2} \int_0^\infty \int_0^\infty \cdots \int_0^\infty e^{\frac{x_2v_2+\cdots+x_kv_k}{x_1}-(v_2+\cdots+v_k)} \operatorname{erfc}\left(\sqrt{\frac{x_2v_2+\cdots+x_kv_k}{x_1}}\right) dv_2\cdots dv_k$$

$$= \frac{\sqrt{x_1\pi}}{2} \int_0^\infty \int_0^\infty \cdots \int_0^\infty e^{\frac{x_2v_2+\cdots+x_kv_k}{x_1}-(v_2+\cdots+v_k)} \left\{\frac{2}{\pi}\int_0^{\pi/2} e^{-\frac{x_2v_2+\cdots+x_kv_k}{x_1\sin^2(\theta)}} d\theta\right\} dv_2\cdots dv_k.$$

$$(B.28)$$

Changing the order of integration and using the change of variables $u = \cot(\theta)$ in (B.28) yields

$$G_1 = \sqrt{\frac{x_1}{\pi}} \int_0^{\pi/2} \int_0^\infty e^{-\frac{x_1\sin^2(\theta)+x_2\cos^2(\theta)}{x_1\sin^2(\theta)}v_2} dv_2\cdots$$

$$\times \int_0^\infty e^{-\frac{x_1\sin^2(\theta)+x_k\cos^2(\theta)}{x_1\sin^2(\theta)}v_k} dv_k d\theta \qquad (B.29a)$$

$$= \sqrt{\frac{x_1}{\pi}} \int_0^{\pi/2} \frac{x_1\sin^2(\theta)}{x_1\sin^2(\theta)+x_2\cos^2(\theta)} \cdots \frac{x_1\sin^2(\theta)}{x_1\sin^2(\theta)+x_k\cos^2(\theta)} d\theta \quad (B.29b)$$

$$= \sqrt{\frac{x_1}{\pi}} \int_0^\infty \frac{x_1}{(x_1+x_2u^2)} \cdots \frac{x_1}{(x_1+x_ku^2)} \frac{1}{(1+u^2)} du. \qquad (B.29c)$$

Substituting (B.29) in (B.27) gives $I_1(x_1,\cdots,x_k) = I_2(x_1,\cdots,x_k)$ and, hence, the proof is complete. ∎

Lemma 4: *Define*

$$I_3(x_1,\cdots,x_N) \triangleq \frac{1}{\sqrt{\pi}} \int_0^\infty \left(1 - \frac{u^{2N}}{(u^2+x_1)\cdots(u^2+x_N)}\right) du. \qquad (B.30)$$

Then

$$I_3(x_1,\cdots,x_N) = I_2(x_1,\cdots,x_N) \qquad (B.31)$$

where $I_2(x_1,\cdots,x_N)$ is defined in (B.22) and $x_i > 0$ for all $i = 1,\cdots,N$.

Proof: We use induction to prove (B.31). For $N = 2$, it is easy to verify that $I_3(x_1,x_2) = I_2(x_1,x_2)$. We assume that (B.31) is valid for $N = k - 1$. That is

$$I_3(x_1,\cdots,x_{k-1}) = I_2(x_1,\cdots,x_{k-1}). \qquad (B.32)$$

We now show that (B.31) is also valid for $N = k$. That is

$$I_3(x_1,\cdots,x_k) = I_2(x_1,\cdots,x_k). \qquad (B.33)$$

96

The left of (B.33) can be written as

$$I_3(x_1, \cdots, x_k) = \frac{1}{\sqrt{\pi}} \int_0^\infty \left(1 - \frac{u^{2k}}{(u^2 + x_1)(u^2 + x_2) \cdots (u^2 + x_k)} \right) du \quad \text{(B.34a)}$$

$$= \frac{1}{\sqrt{\pi}} \int_0^\infty \left(1 - \frac{u^{2(k-1)}}{(u^2 + x_2)(u^2 + x_3) \cdots (u^2 + x_k)} \right) du$$

$$+ \frac{1}{\sqrt{\pi}} \int_0^\infty \frac{x_1 u^{2(k-1)}}{(x_1 + u^2)(x_2 + u^2) \cdots (x_k + u^2)} du \quad \text{(B.34b)}$$

$$= I_3(x_2, \cdots, x_k)$$

$$+ \frac{1}{\sqrt{\pi}} \int_0^\infty \frac{x_1 u^{2(k-1)}}{(x_1 + u^2)(x_2 + u^2) \cdots (x_k + u^2)} du. \quad \text{(B.34c)}$$

We can write the right of (B.33) as

$$I_2(x_1, \cdots, x_k) = I_2(x_2, \cdots, x_k)$$

$$+ \sqrt{\frac{x_1}{\pi}} \int_0^\infty \frac{x_1}{(x_1 + x_2 u^2)} \frac{x_1}{(x_1 + x_3 u^2)} \cdots \frac{x_1}{(x_1 + x_k u^2)} \frac{1}{(1 + u^2)} du. \quad \text{(B.35)}$$

Using the change of variable $u = \frac{\sqrt{x_1}}{v}$ in (B.35) we obtain

$$I_2(x_1, \cdots, x_k) = I_2(x_2, \cdots, x_k) + \frac{1}{\sqrt{\pi}} \int_0^\infty \frac{x_1 v^{2(k-1)}}{(x_1 + u^2)(x_2 + v^2) \cdots (x_k + v^2)} dv. \quad \text{(B.36)}$$

Comparing (B.34c) with (B.36) and using (B.32) gives (B.33) and, hence, the proof is complete. ∎

Vita

Sasan Haghani

EDUCATION

University of Alberta	M.Sc. Candidate	Electrical and Computer Engineering
		September 2000 – Present
Isfahan University of Technology	B.Sc.(First Class)	Electrical and Computer Engineering
		September 1995 – June 2000

WORK EXPERIENCE

Research Assistant, University of Alberta,

Department of Electrical and Computer Engineering, 2000-present

Teaching Assistant, University of Alberta,

Department of Electrical and Computer Engineering, 2000-present

AWARDS

First Class Undergraduate Award, Isfahan University of Technology, 2000.

PUBLICATIONS

Sasan Haghani, Moe Z. Win and Norman C. Beaulieu "Penalty of Hybrid Diversity for Generalized Two-Dimensional Signaling in Rayleigh Fading", Submitted to *IEEE Transactions on Communications*.

Sasan Haghani, Moe Z. Win and Norman C. Beaulieu "Penalty of Hybrid Diversity with Arbitrary Modulation in Rayleigh Fading", Submitted to *IEEE Transactions on Communications*.

Sasan Haghani, Moe Z. Win and Norman C. Beaulieu "Bounds to the Error Probability of Hybrid Diversity Two-Dimensional Signaling", Submitted to *IEEE GLOBECOM Conference 2002*.